TRACE V5.0
ASSESSMENT MANUAL

Appendix A: Fundamental Validation Cases

Division of Risk Assessment and Special Projects
Office of Nuclear Regulatory Research
U. S. Nuclear Regulatory Commission
Washington, DC 20555-0001

This page intentionally left blank

Structural Heat Conduction

A.1. Radial and Axial Heat Conduction Test

Author(s): David L. Caraher

Affiliation: Information Systems Laboratories, Inc.

Code Version: TRACE V5.0

Platform and Operating System: Intel x86, Windows XP

A.1.1. Introduction

The purpose of this assessment is to compare TRACE's finite difference solution of the heat conduction equations with analytical solutions. Two simulations are presented. One evaluates the radial heat conduction equations and the other evaluates the 2-D axial-radial heat conduction equations.

A.1.2. Test Problem Description

A.1.2.1. Radial Conduction in a Cylinder with Insulated Ends

The 1-D radial steady-state conduction equation was solved for a generic 10 cm long fuel rod, as illustrated in Figure A.1-1 For this test problem the inner material is representative of fuel surrounded by a gap that is surrounded by cladding. The material from r = 0 to r = r_1 has a uniform source of 1000 W. From r = r_1, to r = r_2, a gap exists with a gap heat transfer coefficient of 1000 W/m^2-K. From r = r_2 to r = r_3, the conductivity is 13.8 W/m-K. The cladding's surface heat-transfer coefficient is 2836 W/m^2-K. The rod is surrounded by water at a temperature of 300 K.

The governing differential equation is

$$\frac{1}{r}\frac{d}{dr}\left(rk\frac{dT}{dr}\right) = q''' \tag{1-1}$$

The boundary conditions are

$$\left.\frac{dT}{dr}\right|_{r=0} = 0 \text{ and} \tag{1-2}$$

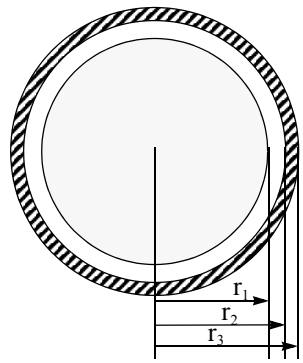

Figure A.1-1. 1-D Conduction Test Problem Geometry

$$q_3'' = h_3(T_3 - T_f) \tag{1-3}$$

where h_3 is the rod's outside surface heat transfer coefficient, T_3 is the rod's outside surface temperature, q'' is the rod's outside surface heat flux, and T_f is the constant temperature of the fluid surrounding the rod.

For steady state

$$q_3'' = \frac{q'''}{(2\pi r_3 L)} \quad \text{is the outer clad surface heat flux and} \tag{1-4}$$

$$q_1'' = \frac{q'''}{(2\pi r_1 L)} \quad \text{is the heat flux at the fuel pellet surface.} \tag{1-5}$$

L is the rod's length and q''' is the interior heat source.

The solution for this problem is

$$T = T_3 - q_3'' r_3 \ln\left(\frac{r}{r_3}\right) / k_3 \qquad \text{for } r_2 < r < r_3 \tag{1-6}$$

$$T = T_1 + q_1''(r_1^2 - r^2)/(2k_1 r_1) \qquad \text{for } r < r_1 \tag{1-7}$$

Let q''' = 1000 Watts, L = 0.1 m, r_1 = 6.35 mm, r_2 = 6.426 mm, and r_3 = 7.239 mm. Further, let k_1 = 2 W/m-K, k_3 = 13.8 W/m-K, h_{gap} = 1000 W/m^2-K, h_3 = 2836 W/m^2-K, and T_f = 300 K. Note that

$$T_3 = \frac{q_3''}{h_3} + T_f\,, \tag{1-8}$$

$$T_2 = T_3 - q_3'' r_3 \ln\left(\frac{r_2}{r_3}\right) / k_3 \quad \text{and,} \tag{1-9}$$

$$T_1 = \frac{q_1''}{h_{gap}} + T_2 \tag{1-10}$$

A.1.2.2. Radial and Axial Conduction in a Cylinder with Insulated Ends

The analytical solution was calculated for the case of a solid 5 mm diameter rod, 20 cm in length standing in a pool of water having a constant temperature of 300 K in the bottom 10 cm and 500 K in the top 10 cm. A constant heat transfer coefficient of 1000 W/m^2-K is applied to the outer surface of the rod and a uniform heat source of 1000 W is distributed within the rod. The relevant governing equations for this problem are from Reference 1. These equations were solved and the solution tabulated for the TRAC-PF1/MOD2 developmental assessment documented in Reference 2. The tabulated solution values from Tables 3-1 and 3-2 of Reference 2 are used here in Table A.1.1 and Table A.1.2 for comparison to the temperatures calculated by TRACE.

A.1.3. TRACE Model Description

Two TRACE models were constructed, one for the radial conduction problem and another for the axial-radial conduction problem.

A.1.3.1. Radial Conduction Model

The TRACE model (Figure A.1-2) for this problem consists of a 10 cm long PIPE containing 314 m^3 of water at 300 K. A BREAK component is connected to the upper end of the PIPE (only because TRACE would not run without junctions connected to the PIPE). A HTSTR which simulates a nuclear fuel rod is immersed in the PIPE's liquid. This HTSTR is 10 cm long and consists of an 11.7 mm OD pellet with a thermal conductivity of 2 W/m-K inside of a 10 cm long cladding of 12.852 mm ID and 14.478 mm OD with a thermal conductivity of 13.8 W/m-K. The annular region (gas gap) between the pellet and the cladding has a constant heat transfer coefficient of 1000 W/m^2-K while the outer surface of the cladding has an constant HTC of 2836 W/m^2-K. The density and the specific heat of both the pellet and the cladding are 1 kg/m^3 and 1 J/kg-K. Having such small values for density and specific heat ensures that a steady state temperature is reached very rapidly. The pellet is heated uniformly by a 1000 W power source. Initially, the fuel rod is at temperature of 300 K.

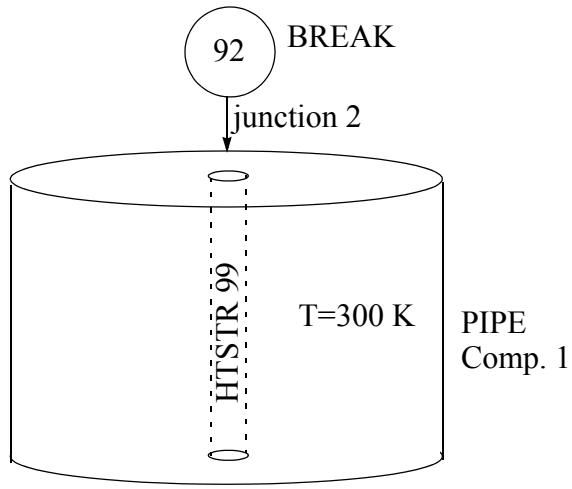

Figure A.1-2. TRACE Nodalization for the Steady State Radial Heat Conduction Problem

A.1.3.2. Axial-Radial Conduction Model

The TRACE model (Figure A.1-3) for this problem consists of a 20 cm long PIPE containing 628 m^3 of water. The water in the lower half of the tank is at 300 K while the water in the upper half is at 500 K. A BREAK component is attached to the top of the PIPE. A HTSTR is immersed in the water. It simulates a 5 mm OD cylindrical rod 20 cm long. It has a power of 1000 W distributed uniformly in the radial and axial directions. The HTSTR consists of 8 axial nodes, each 25 mm longer. TRACE's fine mesh renodalization model is active in this simulation. This results in axial nodes of 5 mm along most of the rod. The rod's thermal conductivity, density, and specific heat are 2 W/m-K, 1 kg/m^3, and 1 J/kg-K, respectively. The rod's initial temperature is 300 K. Its outer surface's HTC is fixed at 1000 W/m^2-K.

A.1.4. Tests Simulated with TRACE

A.1.4.1. Simulation of Radial Heat Conduction Problem

The TRACE simulation was run for 1 second. Steady state was attained by 0.0005 s. The calculated and analytical solution axial temperature distributions are compared in Table A.1.1 for rod temperatures along the centerline of the rod.

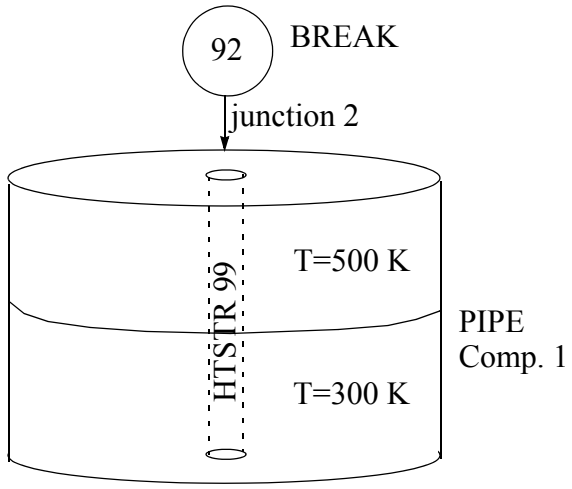

Figure A.1-3. TRACE Nodalization for the Axial-Radial Heat Conduction Problem

Table A.1.1. Comparison of TRACE and Analytical Solutions for a 1-D Steady State Radial Heat Conduction Problem

Node Location (mm)	Analytical Solution (K)	TRACE Solution (K)	Error (K)
0.000	1039.8	1038.3	-1.5
1.830	1006.7	1005.3	-1.4
2.590	973.6	972.1	-1.5
3.175	940.3	938.8	-1.5
3.670	906.9	905.4	-1.5
4.100	873.9	872.4	-1.5
4.490	840.9	839.4	-1.5
4.850	807.7	806.2	-1.5
5.185	774.5	773.0	-1.5
5.500	741.3	739:8	-1.5
5.800	707.8	706.4	-1.4
6.080	675.0	673.5	-1.5
6.350	641.9	640.4	-1.5
6.426	391.3	391.3	0.0
6.670	387.0	387.0	0.0
6.840	384.1	384.1	0.0
7.040	380.7	380.7	0.0
7.239	377.5	377.5	0.0

The results given in Table A.1.1 demonstrate that the finite-difference solutions to the radial heat-conduction equation are accurate.

A.1.4.2. Simulation of the Radial-Axial Heat Conduction Problem

The TRACE simulation was run for one second. Steady state conditions were achieved within 0.005 s. The calculated and analytical solution radial temperature distributions are compared in Table A.1.2 and shown in Figure A.1-4

Table A.1.2. Comparison of TRACE and Analytical Solutions for the Steady State Axial-Radial Heat Conduction Problem

Node Location (mm)	Analytical Solution (K)	TRACE Solution (K)	Error (K)
0	658.1	658.1	0.0
10	658.1	658.1	0.0
20	658.1	658.1	0.0
30	658.1	658.1	0.0
40	658.1	658.1	0.0
50	658.1	658.1	0.0
60	658.1	658.1	0.0
70	658.1	658.1	0.0
80	658.2	658.4	+0.2
90	662.7	664.8	+2.1
100	758.1	758.0	-0.1
110	853.9	851.4	-2.5
120	857.9	857.8	+0.3
130	858.1	858.1	0.0
140	858.1	858.1	0.0
150	858.1	858.1	0.0
160	858.1	858.1	0.0
170	858.1	858.1	0.0
180	858.1	858.1	0.0
190	858.1	858.1	0.0

The results given in Table A.1.2 demonstrate that the TRACE finite-difference solutions to the 2-D heat-conduction equation are accurate. The largest errors are where temperature profile is steepening. These errors can be reduced by increasing the axial noding of the HTSTR in TRACE.

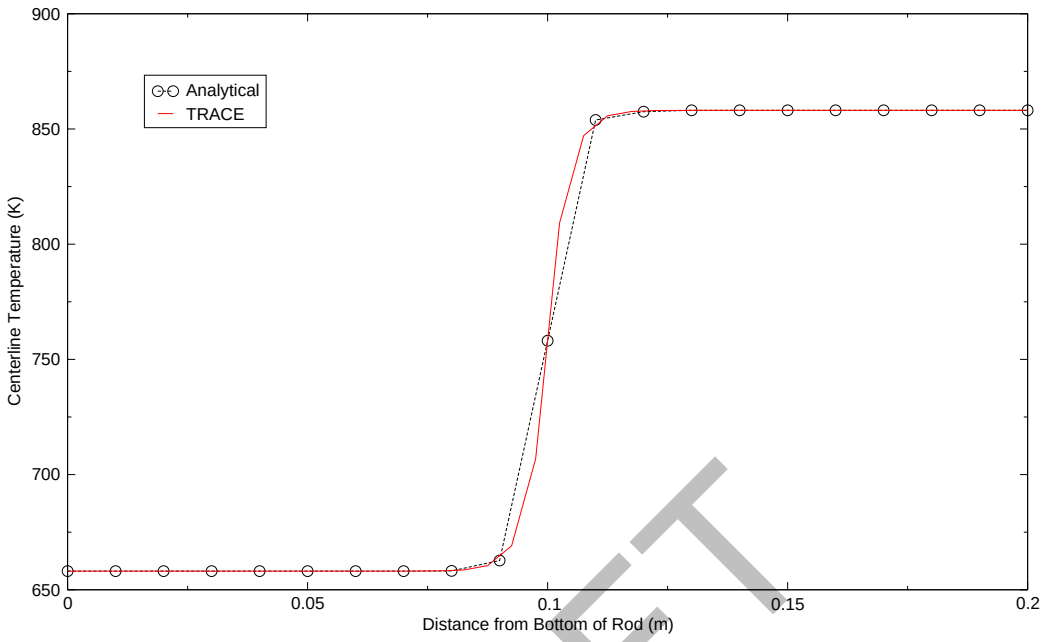

Figure A.1-4. TRACE and Analytical Axial Centerline Temperatures.

By doubling the number of axial nodes in the 80 - 120 mm range the difference between TRACE and the analytical solution can be reduced to less than 0.5 KAssessment Results Summary

Radial and Radial-Axial heat conduction problems were simulated with TRACE version 5.0 and found to be in excellent agreement with the analytical solutions for the problems, demonstrating that the finite-difference conduction equations in TRACE are accurate.

A.1.5. References

1 H.S. Carslaw and J.C. Jaeger, "Conduction of Heat in Solids", Oxford University Press, 1959.

2 J.C. Lin, V. Marinez, J.W. Spore, "TRAC-PF1/MOD2 Developmental Assessment Manual, Los Alamos National Laboratory, August 1993.

Basic Hydraulics

A.2. Drain - Fill Problem

Author(s): Dean Wang, Vesselin Palazov

Affiliation: Information Systems Laboratories, Inc.

Code Version: TRACE V5.0

Platform and Operating System: Intel x86, Windows XP

A.2.1. Introduction

The ability of TRACE to predict the motion of a water level can be assessed by the 1D drain and fill test problem. The purpose of this test problem is to verify that TRACE has the ability to track liquid level across node boundaries and to determine the accuracy of calculating the gravity head as the cells slowly drain and fill.

In this section, the TRACE predictions with the 1D level tracking model turned on globally or locally were analyzed and compared to the exact analytical solution. Comparisons are presented for predicted void fraction, mass flow rate, and pressure for selected cells. In addition, the code predictions with the level tracking feature turned off globally or locally are compared against the calculational results obtained with the level tracking model being active in order to assess the model performance and its effect on the code predictive capabilities.

The 1D drain and fill test problem was included in the TRAC-P test matrix (Ref. 1) and it was also a sample case used by Aktas in his thesis work (Ref. 2) that documents the development of the level tracking model.

A.2.2. TRACE Model Description

The TRACE model of the drain and fill test problem consists of a vertical PIPE component that is partially filled with water, a FILL component connected to the bottom end of the pipe, and a BREAK component connected to the top pipe end. The BREAK component provides a constant pressure boundary condition (1.0E+05 Pa) at the top of the pipe. The FILL component slowly drains water from the pipe and then refills the pipe to the original level. Figure A.2-1 is a noding diagram of the TRACE model.

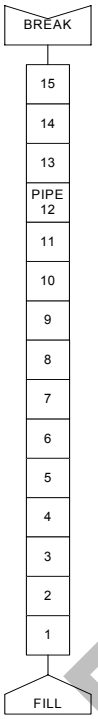

Figure A.2-1. Noding Diagram of 1D Drain and Fill Test

The PIPE component is made up of 15 cells each 1.0 m long and having a flow area of 0.14593 m^2. The PIPE component is initially full of 10 m of water at a temperature of 298.3 K.

The flow rate of the FILL component is a function of time as shown in Figure A.2-2. Negative flow means that the FILL component drains water from the pipe, while positive flow means that the pipe is refilling.

A.2.3. Cases Simulated with TRACE

This test problem was run for 200 seconds using TRACE V5.0. The following four cases were calculated and examined.

Case (1): The 1D level tracking model switched on globally through setting the NAMELIST variable NOLT1D equal to -1.

Case (2): The 1D level tracking model switched on locally in the PIPE component through setting the NAMELIST variable NOLT1D equal to 0 and specifying the ILEV input variable in PIPE 700 equal to 1. We expect that the results for this case should give the same results as Case 1 above.

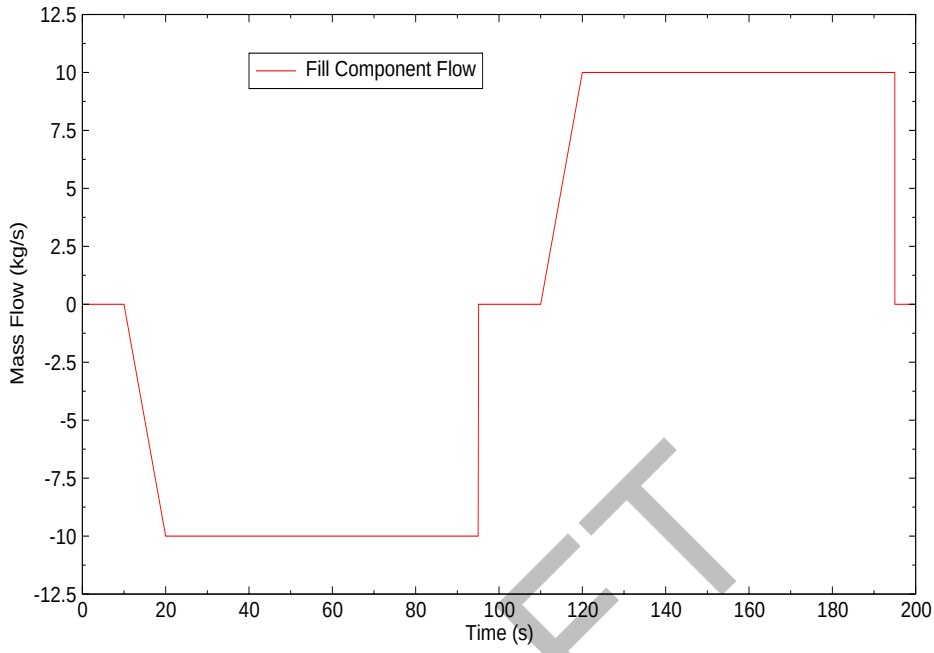

Figure A.2-2. Mass Flow Rate of Fill Component

Case (3): The 1D level tracking model switched off globally through setting the NAMELIST variable NOLT1D equal to 1.

Case (4): The 1D level tracking model switched off locally in the PIPE component by setting the NAMELIST variable NOLT1D equal to 0 and specifying the ILEV input variable in PIPE 700 equal to -1. We expect that the results for this case should give the same results as Case 3 above.

In addition, the exact analytical solutions were calculated and compared to the TRACE results. Table A.2.1 summarizes the test cases exercised in this study.

Table A.2.1. 1D Fill and Drain Model Test Cases Exercised

Case No.	Input File Name	1D Level Tracking Model Exercised	Level Tracking Variables Defined	
			NAMELIST	PIPE 700
1	fill_drain_1.inp	Global LT on	NOLT1D = -1	n/a
2	fill_drain_2.inp	Local LT on	NOLT1D = 0	ILEV = 1
3	fill_drain_3.inp	Global LT off	NOLT1D = 1	n/a
4	fill_drain_4.inp	Local LT off	NOLT1D = 0	ILEV = -1

A.2.4. Assessment Results Summary

The calculational results for all four cases modeled are presented in this section. All figures have been plotted using a plot frequency (for the predicted quantities) of 10 Hz.

A.2.4.1. Results for Cases 1 and 2 (Level Tracking On)

The TRACE calculations of void fraction, mass flow and pressure in the first (bottom) cell of the pipe obtained with the 1D level tracking model switched on globally (Case 1) were compared against the analytical solutions for this test problem. The results predicted by TRACE compare very well to the analytical solutions except for some pressure spikes calculated at the very beginning and end of the draining phase of the simulation. In addition, there is some insignificant disagreement in the mass flow rates when the water level crosses a cell boundary during the draining period.

Figure A.2-3 shows the comparison of cell void fractions. The TRACE results obtained with the 1D level tracking model switched on globally are almost indistinguishable from the analytical solution..

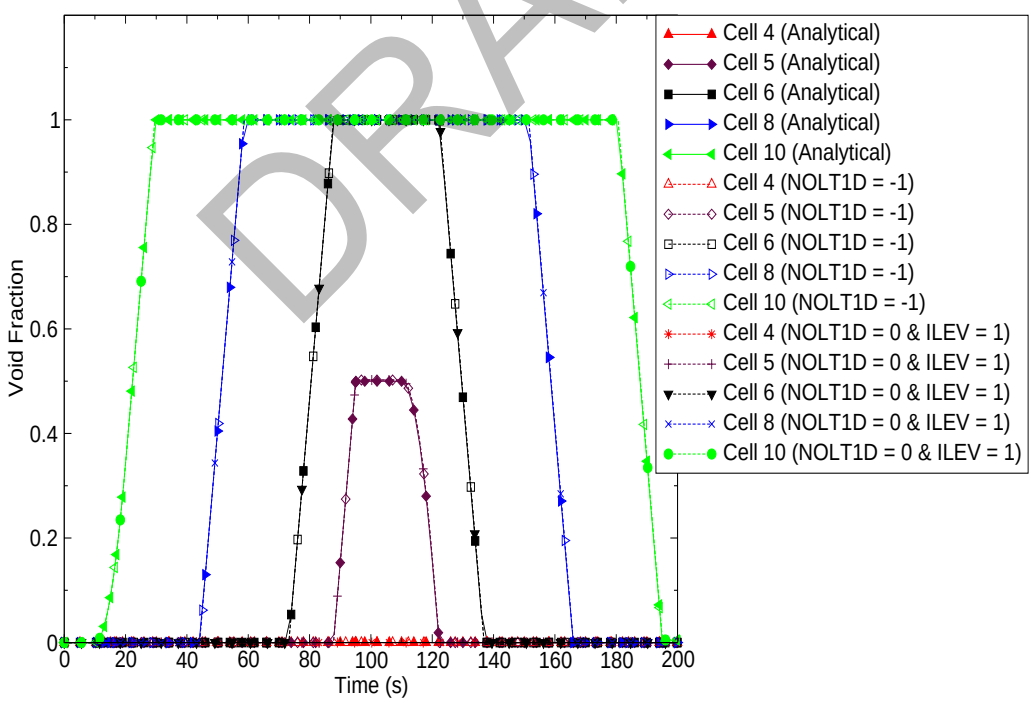

Figure A.2-3. Void Fraction vs. Time

Figure A.2-4 shows TRACE calculated mass flow rates with the 1D level tracking model switched on globally and their comparison with the analytical solution. Overall, the TRACE prediction is in very good agreement with the analytical solution except when the water level crosses a cell boundary during draining. The mass flow rate of a cell should be undergoing a step change when the water crosses the cell boundary, but TRACE predicted the mass flow rates had an asymptotic change.

A comparison of the TRACE calculated pressure in cell 1 of PIPE 700 with the 1D level tracking model switched on globally against the analytical solution is shown in Figure A.2-5. The difference between the TRACE and analytical solutions cannot be distinguished on the plots except for the two spikes at around 10 s and 95 s into the simulation when the draining begins and stops respectively. This problem is probably due to a numerical problem associated with the level tracking. This phenomenon, being localized in time, does not appear to affect the overall solution

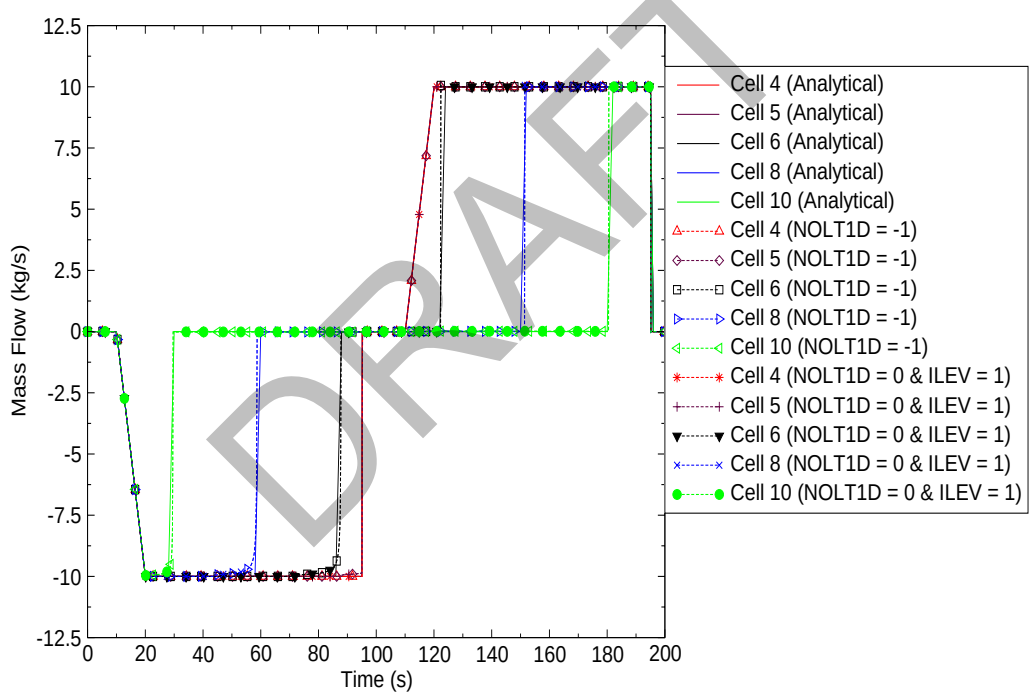

Figure A.2-4. Mass Flow Rate vs. Time

As Figure A.2-3, Figure A.2-4, and Figure A.2-5 demonstrate, the TRACE predictions obtained with the 1D level tracking model switched on locally (by specifying NOLT1D=0 and ILEV=1 for PIPE 700) are essentially identical to the solutions obtained with the level tracking model turned on globally with NOLT1D set equal to -1.

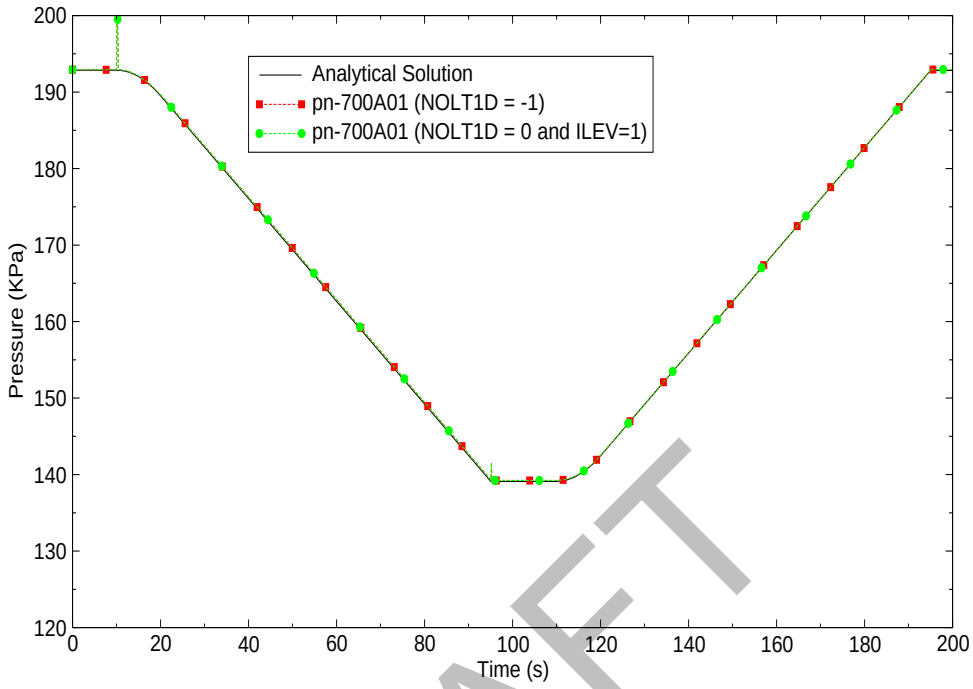

Figure A.2-5. Pressure vs. Time

A.2.4.2. Results for Cases 3 and 4 (Level Tracking Off)

Figure A.2-6 shows the pressure calculated by TRACE in cell 1 of PIPE 700. For comparison, the analytical solution is also shown in the same figure.

The red line in Figure A.2-6 represents the pressure in cell 1 computed with the 1D level tracking model turned off globally (NOLT1D=1). The green line illustrates the prediction with the 1D level tracking model turned off locally in PIPE 700. The black solid line in the same figure shows the exact analytical solution for the pressure in this cell. While both cases exhibit the same behavior, as we should expect, as the figure indicates, with the level tracking turned off, the solution exhibits an unrealistic nonlinear behavior during the draining phase of the transient. Such behavior is observed for all liquid-filled cells during this phase of the transient. In addition, unphysical pressure oscillations of a small amplitude are observed in the liquid-filled cells during the stagnation phase that follows the tube draining. The amplitude of these high-frequency oscillations is approximately 750 Pa with a period of about 0.5 s.

For a vertically-oriented computational cell with a height of 1 m that accommodates the interface between the liquid and gas phases under fully stratified conditions, a variation of 1% in the cell

void fraction translates into a change of the liquid column equal to 0.01 m. The corresponding change of the gravitational head can be assessed as follows:

$$\Delta P = (0.01\ \text{m}) \cdot (997.4\ \text{kg/m}^3) \cdot (9.81\ \text{m/s}^2) = 97.8\ \text{Pa} \tag{2-1}$$

The pressure oscillations observed during the period of stagnation, if coupled with corresponding oscillations in the void fraction of cell 5 that accommodates the liquid interface, would result in a void fraction amplitude calculated as follows:

$$\Delta\alpha = (750\ \text{Pa})/(97.8\ \text{Pa}) \times 1.0\ \% = 7.7\ \% \tag{2-2}$$

It is important to note that no oscillations in the void fraction of cell 5 were observed during the period of stagnation as Figure A.2-7 reveals.

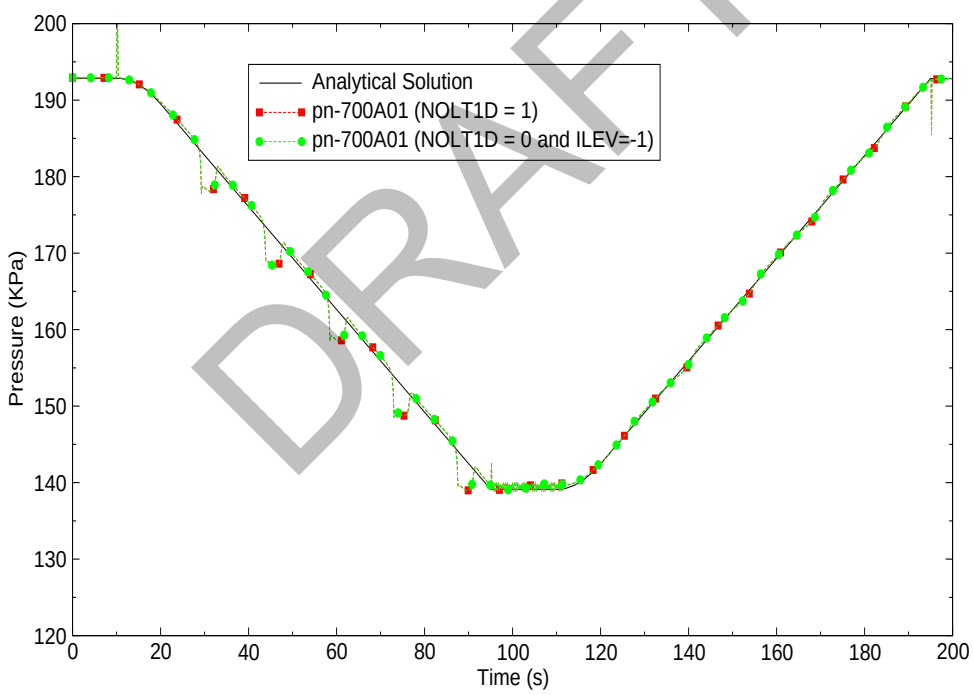

Figure A.2-6. Pressure vs. Time

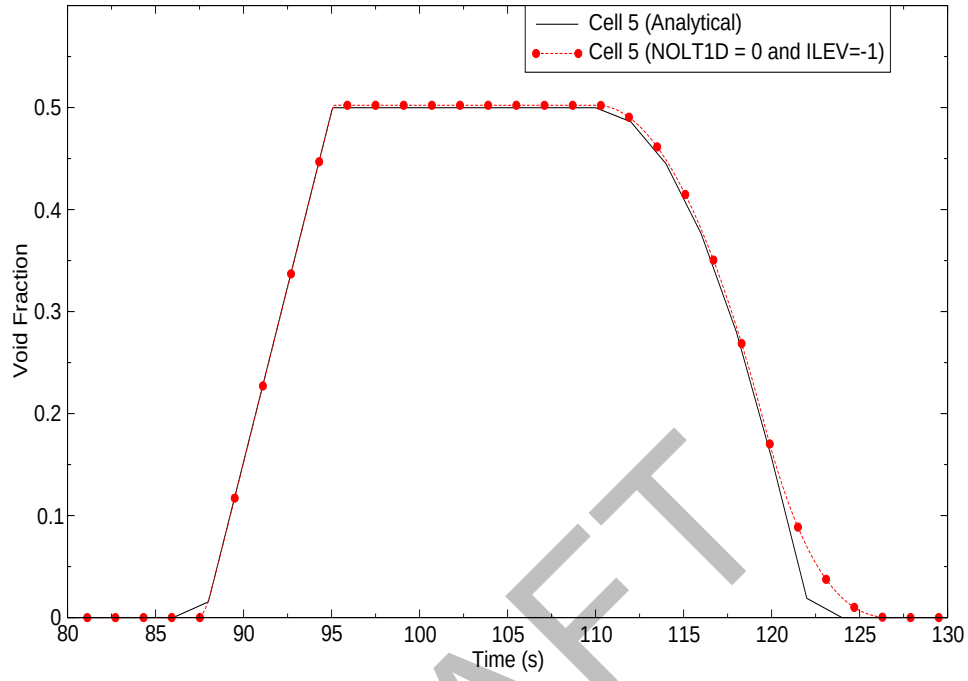

Figure A.2-7. Void Fraction of Cell 5 vs. Time

A.2.5. Summary and Conclusions

The results from the test cases analyzed in this study are summarized in Table A.2.2 below. It is seen that the code closely predicts the initial cell 1 pressure before the drain starts and the final cell 1 pressure at the end of the fill transient. As the pipe component is initially full of 10 m of water, the cell-center pressure of cell 1 should correspond to the gravitational head of a water column of 9.5 m height plus the pressure defined by the BREAK component:

$$P_{max} = 1.0\times10^5 \text{ Pa} + (9.5 \text{ m}) \cdot (997.4 \text{ kg/m}^3) \cdot (9.81 \text{ m/s}^2) = 1.929\times10^5 \text{ Pa} \tag{2-3}$$

The code also captures closely the minimum pressure in cell 1 that corresponds to the minimum level of 4 m of water above the center of cell 1 (void fraction of 50% in cell 5):

$$P_{min} = 1.0\times10^5 \text{ Pa} + (4.0 \text{ m}) \cdot (997.4 \text{ kg/m}^3) \cdot (9.81 \text{ m/s}^2) = 1.391\times10^5 \text{ Pa} \tag{2-4}$$

Table A.2.2. 1D Fill and Drain Model Test Cases Exercised

Case No	1D LT Model	Steady Pressure in Cell 1 (kPa)			Minimum Void in Cell 5 (%)	Void in Cell 10 at End (%)
		0 s to 10 s	95 s to 110 s	195 s to 200 s		
1	Global LT on	192.9[a]	139.2[b]	192.9	50.2	0.50
2	Local LT on	192.9[a]	139.2[b]	192.9	50.2	0.50
3[c]	Global LT off	192.9[a]	139.5[d]	192.8[e]	50.2	1.24
4[c]	Local LT off	192.9[a]	139.5[d]	192.8[e]	50.2	1.24

a. A pressure spike up to 202.4 kPa was observed at about 10.1 s

b. A pressure spike up to 141.6 kPa observed briefly at 95.2 s

c. Unphysical nonlinear pressure behavior in the liquid-filled cells during draining

d. A pressure spike up to 142.6 kPa observed briefly at 95.2 s. Value then oscillates (unphysically) between 139.1 and 139.8 kPA until about 112 s

e. A pressure dip down to 185.4 kPa observed at about 195.2 s

The examination of selected computational results revealed that the TRACE predictions obtained with the 1D level tracking model switched on locally (through specifying NOLT1D=0 and ILEV=1 for PIPE 700) appear identical to the solutions obtained with the level tracking model turned on globally (with NOLT1D set equal to -1). The code accurately calculates the gravity head as the cells slowly drain and refill except for very short time intervals occurring at the very beginning and at the end of the draining phase of the simulation when unphysical pressure deviations are observed. No corresponding short-lasting unphysical deviations in the void fraction of the cells accommodating the liquid interface were observed.

The TRACE predictions obtained with the 1D level tracking model switched off, either globally or locally, differ somewhat from the analytic solution and the solutions obtained with the level tracking model turned on. In particular, the solution with the 1D level tracking model turned off exhibits an unrealistic nonlinear behavior during the draining phase of the transient. Such behavior is observed for all liquid-filled cells during this phase of the transient. In addition, unphysical pressure oscillations of a considerable amplitude are observed in the liquid-filled cells during the stagnation phase that follows the tube draining. The amplitude of these high-frequency oscillations is about 0.75 kPa with a period of about 0.5 s. No corresponding unphysical oscillations in the void fractions were observed.

A.2.6. References

1 R. G. Steinke, "A Description of the Test Problems in the TRAC-P Standard Test Matrix", Los Alamos National Laboratory Report, LA-UR-96-1475, May 1996.

2 B. Aktas, "Level Tracking in Thermal-Hydraulic Simulations of Nuclear Reactors", Ph.D. Thesis, Penn State University, May 2003.

A.3. Oscillating Manometer

Author(s): Dan Prelewicz

Affiliation: Information Systems Laboratories, Inc.

Code Version: TRACE V5.0

Platform and Operating System: Intel x86, Windows XP

A.3.1. Introduction

The capability of TRACE to predict motion of the interface between liquid and gas is assessed by the oscillating manometer case. Of particular interest is the ability to track liquid level across node boundaries. An analytical solution for liquid motion in a frictionless U-tube manometer can be obtained from the governing equation of motion for the liquid interface motion derived by Moody (Ref. 1).

In this section TRACE predictions made with two slightly different models are compared to the analytical solution of the governing equation presented by Moody. One of the models has the vertical legs of the manometer represented by concentric cylinders using a VESSEL component. The other has the vertical legs represented by PIPE components. Since these cases are mathematically equivalent , the same results should be obtained for both cases. Comparisons are presented for predicted liquid level, fluid velocity and pressure.

The U-tube manometer case was included in the TRAC-P test matrix (Ref. 2) and was also a sample case used by Aktas in his thesis (Ref. 3) documenting development of the level tracking model.

A.3.2. Analytical Solution Description

The oscillating manometer is shown schematically in Figure A.3-1. It consists of a U-tube shaped frictionless pipe of constant cross-sectional area containing a water column of length L. The water column is set in motion by applying a small initial displacement and an initial velocity to the fluid. An exact analytical solution is obtained by Moody for the resulting oscillatory motion, shown in the schematic as X(t). The fluid is assumed to be incompressible so the velocity of the fluid in the entire tube is equal to the time derivative of X(t).

From Reference 1, the displacement X(t) satisfies the following equation.

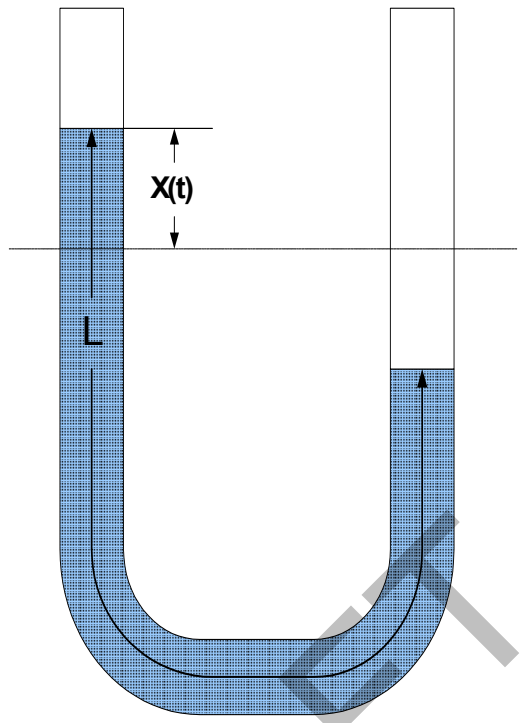

Figure A.3-1. Schematic of the Oscillating Manometer

$$\frac{d^2}{dt^2}X(t) + 2\frac{g}{L}X(t) = 0.0 \tag{3-1}$$

where g is the acceleration of gravity.

In the assessment case, the total length of the water column is taken as 10 meters, with one meter in the horizontal section of the U-tube. At equilibrium conditions there will then be 4.5 meters of liquid in each leg, so the equilibrium level is 4.5 meters. The flow area of the tube is taken as 0.01 m^2. No form or friction losses are included.

Initial conditions are an initial water level of 4.502 m (avoids starting with the liquid interface at a node boundary) and an initial velocity of 2.1 m/s. With these initial conditions, the solution of equation (3-1) is:

$$X(t) = \left(4.5 + \frac{2.1}{\sqrt{2\frac{g}{L}}}\sin\left(\sqrt{2\frac{g}{L}}t\right) + 0.002\cos\left(\sqrt{2\frac{g}{L}}t\right)\right) \tag{3-2}$$

The U-tube models both have a constant flow area of one square meter over their entire length. Hence the liquid velocity is equal to the derivative of the level. That is,

$$V(t)=\dot{X}(t)=\left(2.1\cos\left(\sqrt{2\frac{g}{L}}t\right)-(0.002)\sqrt{2\frac{g}{L}}\sin\left(\sqrt{2\frac{g}{L}}t\right)\right) \tag{3-3}$$

Moody also gives the equations from which the pressure can be determined at the ends of the horizontal section at the bottom of the manometer. From Moody's momentum equation for the right manometer leg, the pressure at the bottom of this leg, designated P_2, is:

$$P_2(t)=P_\infty+\rho X(t)\left(g-\frac{d^2}{dt^2}X(t)\right) \tag{3-4}$$

where ρ is the density of liquid and P_∞ is the atmospheric pressure imposed at the top of each leg of the manometer U-tube. These analytical solutions are included in the TRACE models using control systems for purposes of comparison with the solutions obtained from the TRACE hydrodynamics models.

A.3.3. TRACE Model Description

The solution for the oscillating manometer should be independent of the choice of components. Two equivalent nodalizations were used in this assessment, one with the U-tube modeled using a VESSEL component and the other using a PIPE component. In each case BREAK components were used to specifiy the pressure at the ends of the manometer. A nodalization diagram of the TRACE model that uses a VESSEL component is shown in Figure A.3-2. Figure A.3-3 is a noding diagram of the TRACE model that uses PIPE components. In both cases the gas above the oscillating liquid is steam, which is treated as a noncondensable gas (IEOS = 1).

Since the BREAK components cannot connect to the VESSEL, PIPE components are placed between the VESSEL and the BREAKS. The same PIPE components are used with the TRACE model that uses PIPE components to model the legs of the manometer. The VESSEL and PIPES that model the legs of the manometer have eight axial levels, each one meter high. Pipe 11 has a one meter horizontal run with a one meter vertical rise at each end.

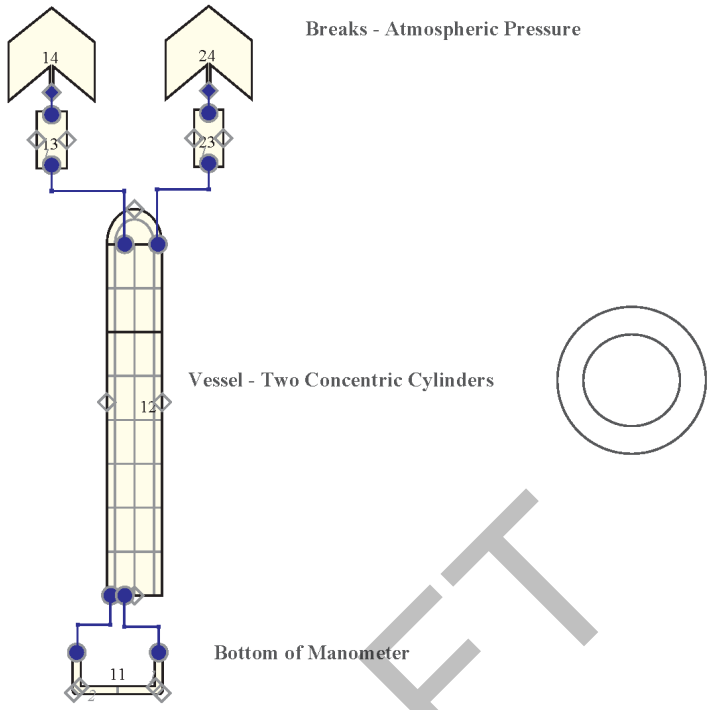

Figure A.3-2. TRACE Nodalization of the Manometer.

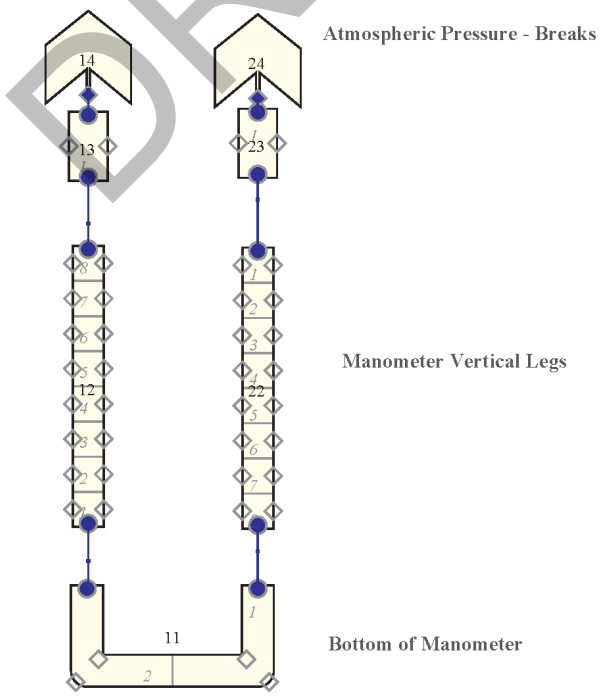

Figure A.3-3. Noding Diagram for Manometer with PIPE Components

A.3.4. Cases Simulated with TRACE

A single case with the initial conditions described in **Section A.3.2.** was run for 50 seconds, approximately 11 cycles of the oscillation, with both the VESSEL and the PIPE models. The analytical solutions were calculated using control variables and compared to the comparable variables of the TRACE solution of the hydrodynamics equations. Figure A.3-4 shows the level response for the VESSEL model. The TRACE results are indistinguishable from the analytical solution. Figure A.3-5 shows the TRACE calculated level response compared to the analytical solution for the PIPE model. Again, the TRACE response is indistinguishable from the analytical solution.

A comparison of TRACE calculated fluid velocity for the VESSEL model with the analytical solution is shown in Figure A.3-6. Figure A.3-7 shows the same comparison for the PIPE model. In each case, the difference between the TRACE and analytical solutions cannot be distinguished on the plots.

TRACE calculated pressure responses for the VESSEL and PIPE models are compared to the analytical solution in Figure A.3-8 and Figure A.3-9. In both cases the comparison is very good except for non physical pressure spikes that ocassionally appear in the TRACE solutions. The VESSEL model shows considerably more of these non-physical spikes. The water packing option was turned on for these simulations. However, the spikes appear at the same times with essentially the same magnitude whether the water packing option is turned on or off. They do not affect the overall comparison of the TRACE calculated pressure responses. On the plots there is no discernable difference between the analytical solution and the TRACE calculations, except for the pressure spikes.

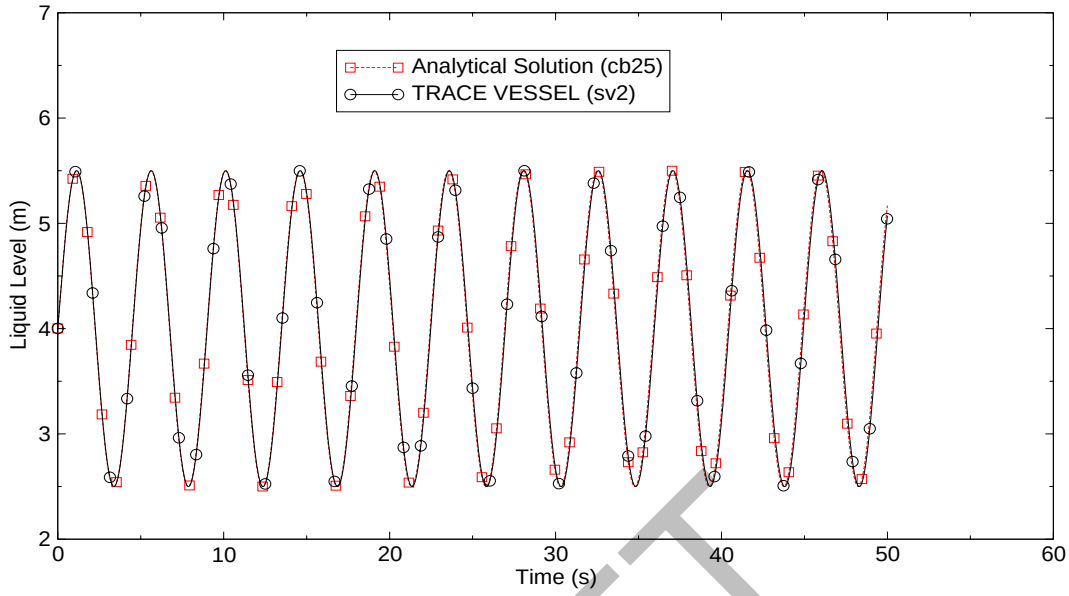

Figure A.3-4. Liquid Level vs Time for VESSEL Manometer Model

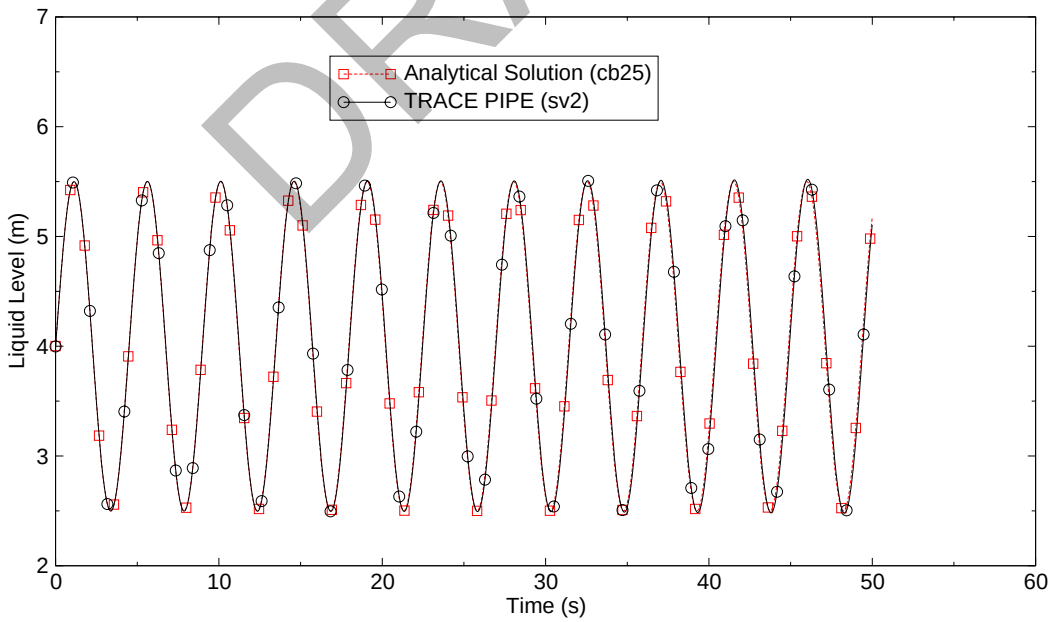

Figure A.3-5. Liquid Level vs Time for PIPE Manometer Model

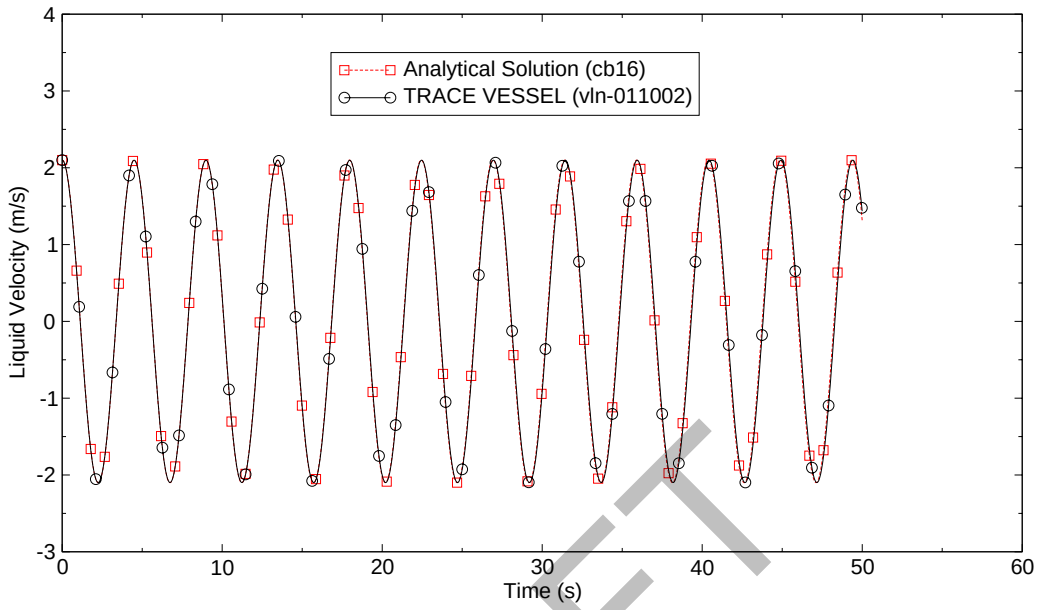

Figure A.3-6. Fluid Velocity vs Time for VESSEL Model

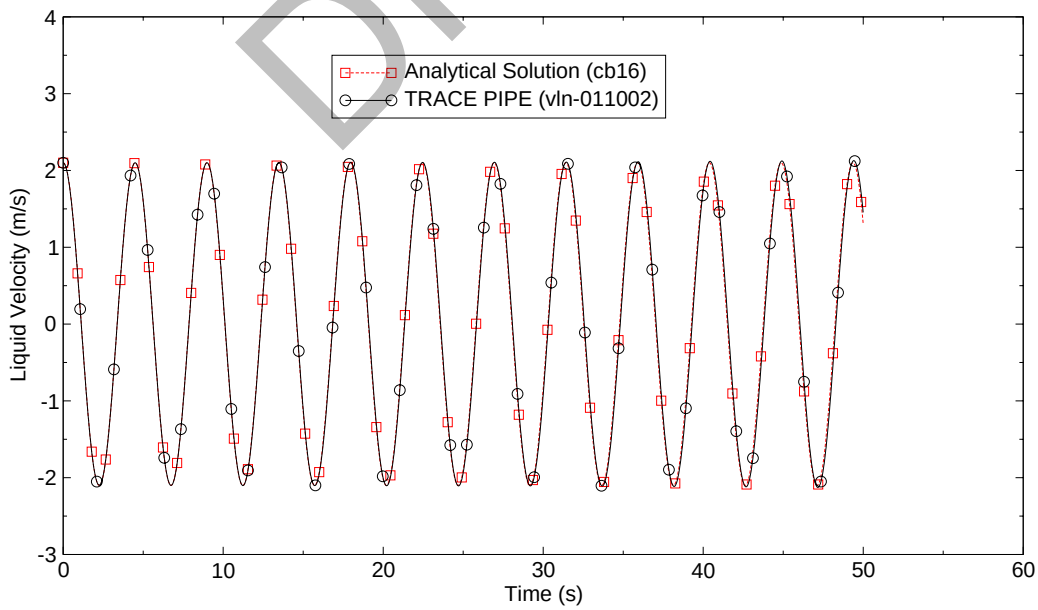

Figure A.3-7. Liquid Velocity vs Time for PIPE Manometer Model

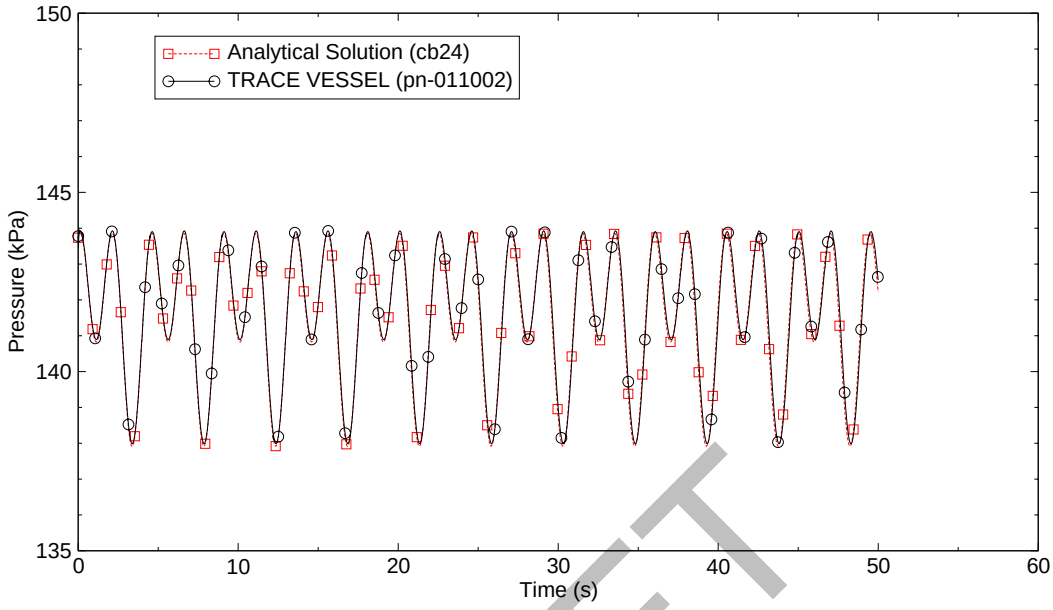

Figure A.3-8. Pressure vs Time for VESSEL Manometer Model

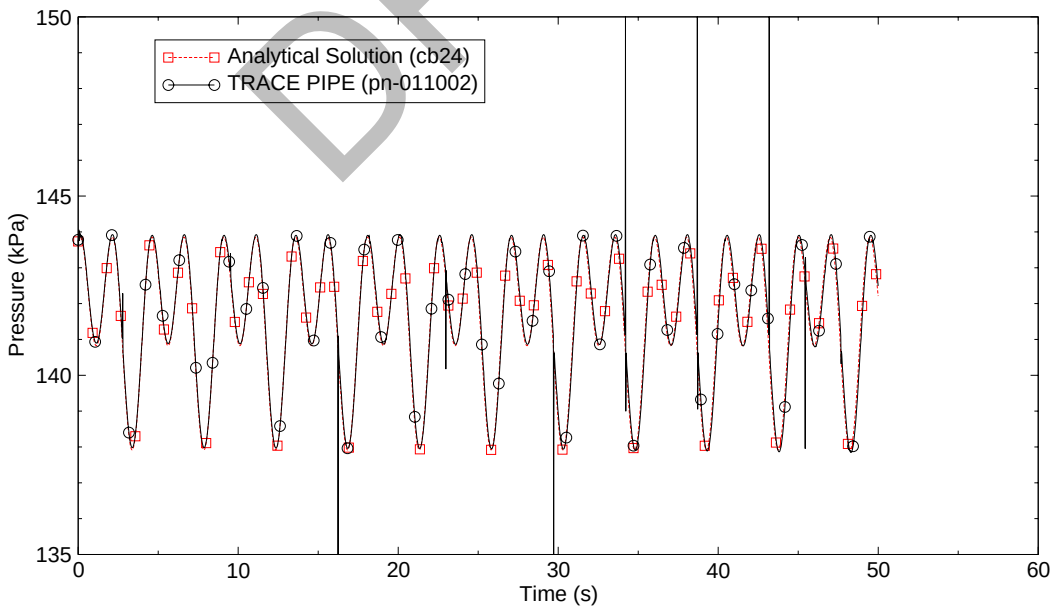

Figure A.3-9. Pressure vs Time for PIPE Manometer Model

A.3.5. Assessment Results Summary

TRACE calculations of water level, fluid velocity and pressure at the bottom of the U-tube were compared to an analytical solution for oscillations in a U-tube manometer. The response calculated by TRACE using either one-dimensional VESSEL or PIPE components is equivalent to the analytical solution, except for the presence of a few non-physical pressure spikes in the calculated pressure. The spikes do not affect the overall solution, i.e. there is no discernable difference between the TRACE calculations and analytical solutions at times when the spikes do not occur. The spikes occur whether or not water packing is turned on or off, and appear to coincide with the water level crossing node boundaries or center of node (momentum cell) boundaries.

The ACAP program was used to calculate Figures of Merit (FOM) based on the Mean Square Error (MSE) weighted at 1.0. Table A.3.1.ACAP-generated Figure of Merit Values shows these FOMs that compare TRACE results to the base analytical solution, also calculated by TRACE using control varaibles. It is apparent that the differences between the TRACE results and the analytical solutions for the level, velocity and pressure are insignificant.

Table A.3.1. ACAP-generated Figure of Merit Values

FOM based on MSE	VESSEL Model	PIPE Model
Level	0.999544	0.999678
Velocity	0.999789	0.999761
Pressure	0.999154	0.999132

A.3.6. References

1 F. J. Moody, "Introduction to Unsteady Thermofluid Mechanics", page 589, Eq. 10.6, John Wiley & Sons, New York, 1990.

2 R. G. Steinke, "A Description of the Test Problems in the TRAC-P Standard Test Matrix", Los Alamos National Laboratory Report, LA-UR-96-1475, May 1996.

3 B. Aktas, "Level Tracking in Thermal-Hydraulic Simulations of Nuclear Reactors", Ph.D. Thesis, Penn State University, May 2003.

A.4. ANL Vertical Two-Phase Flow Tests

Author: Vesselin V. Palazov (ISL)

Affiliation: Information Systems Laboratories (ISL), Inc.

Code Version: TRACE V5.0

Platform and Operating System: Intel x86, Windows XP

A.4.1. Introduction

The thermal-hydraulic response of both a pressurized water reactor (PWR) and a boiling water reactor (BWR) during loss-of-coolant accidents (LOCAs) involves the occurrence of vertical two-phase flow in components of the reactor coolant system such as core fuel bundles or steam generator heat transfer tubes. The adequate modeling of the two-phase flow behavior is decisive for the realistic prediction of the coolant inventory distribution in the primary reactor system hence the cooling conditions in the core region.

The objective of this test problem was to examine TRACE base capabilities for predicting the behavior of adiabatic two-phase up-flow in a simple vertical pipe geometry by comparing code predictions against experimental data. The experimental database used in this study consisted of two-phase flow data obtained from experiments carried out with non-circulating and slowly circulating air-water mixtures at the Argonne National Laboratory (ANL) loop facility. The experiments of interest were performed on adiabatic vertical up-flow in a natural circulation loop at an atmospheric pressure. The inner diameter of the test section pipe was equal to 7.0 cm (2.75 in). The tests were performed with the liquid superficial velocities varying from 0.0 to 0.305 cm/s (1.0 ft/s) while the gas superficial velocities ranged from 0.03 m/s (0.1 ft/s) to 11.0 m/s (36.1 ft/s).

A.4.2. ANL Natural Circulation Loop Description

The test loop consisted of two vertical channels: a riser and a downcomer. At the top, the channels were connected to a vented separator tank while a horizontal pipe made the connection at the bottom. The air and the liquid were mixed at a special mixer sleeve at the bottom of the riser. After passing through the test section, the gas was separated from the liquid in the separator tank and the liquid was recirculated through the downcomer to the mixing sleeve. The gas-liquid mixer was constructed from a pipe tee with the air entering from the bottom and the liquid entering from the side. For providing uniform gas distribution and bubble size at the entrance of the test section, the air was passed through a mesh screen.

The riser was a 0.07-m (2.75-in) Lucite pipe made from two equal sections glued together. The lower 5-ft long section of the riser was used as a stabilizing zone for neutralizing the entrance effects. The upper 5-ft long section of the riser constituted the actual test section. To prevent the occurrence of pressure pulses in the test section as a result from the liquid motion in the separator tank, the test section was extended 9.5 in into the separator tank. The liquid level in the tank was kept one inch above the top of the pipe. The total length of the test section was equal to 3.188 m (125.5 in).

The test section was instrumented with four pressure taps and a fifth tap was arranged at the wall of the separator tank at the elevation of the test section exit. Differential manometers were used to measure the pressure differences between the taps. The test section was also equipped with a γ-densitometer. The centerline of the source pellet and the scintillation detector was 2.5 in below the centerline of tap No. 2. The void fraction was determined from pressure-drop measurements or by means of γ-traversing equipment. The void fraction data for the air-water tests considered here were derived from pressure drop measurements and corresponded to the axial location of test point No. 2 (pressure tap No. 2), which was located 1.041 m (41.0 in) below the test section outlet.

During the test procedures, the following quantities were recorded: liquid flow rate, gas flow rate, the average temperature of the two-phase mixture, the barometric pressure, and the pressure differences between the taps on the test section. The flow rates were measured by means of orifice flow meters and thermocouples were installed at the top and the bottom of the riser to determine the average fluid temperature in the test section. The liquid circulation rate was controlled by means of a bypass control line in the downcomer. The gas flow rate was controlled by means of a pressure regulator and a bypass control line installed on the gas line upstream of the mixing tee.

The experimental work was carried out on three different two-phase flow mixtures: air-water, nitrogen-mercury and nitrogen-freon-13. As mentioned, only the air-water test data were used in this study to assess the TRACE code performance.

A description of the ANL test loop can be found in a series of reports prepared by Smissaert (Refs. 1 and 2). The air-water measurements by Smissaert were used by Wallis (Ref. 3) to correlate two-phase flow data using the drift-flux theory.

A.4.3. TRACE ANL Loop Model Description

The TRACE ANL loop model represented the entire test section and the mixing tee at the inlet to the test section. The model allowed for imposing well-defined boundary conditions at the inlet end of the test section model in terms of mass flow rates for each fluid phase.

The test section of the model was represented by a vertical PIPE-component with ten cells. All cells of the PIPE-component, except for both end cells, have the same length of 0.3048 m (12 in). The first cell at the pipe inlet (cell one) had a length of 0.4699 m (18.5 in) and the last cell at the

pipe exit (cell ten) had a length of 0.2794 m (11.0 in). This nodalization scheme was chosen so that the axial position of test point No. 2 coincided with the center-point position of cell seven. The void fraction values predicted for this cell were used to compare the code-predicted void fractions against the experimentally derived values. The total length of the PIPE-component was 3.188 m (125.5 in) and the hydraulic diameter for all cells was equal to 0.07 m (2.75-in).

The gas-liquid mixer was modeled by a TEE-component with its main side oriented vertically. The top end of the main TEE-branch was connected to the test section inlet. The main branch consisted of three cells with its mid-cell connected to the horizontal side branch, which consisted on two cells. All cells of the TEE-component had the same length of 3 in.

The boundary conditions were specified in terms of mass flow rates for the liquid and gas phase using two FILL-components. The FILL-component connected to the bottom end of the TEE main branch was used to specify the gas-phase mass flow rate. The second FILL-component was connected to the side branch of the TEE and defined the liquid-phase mass flow rate. One BREAK component was connected to the top end of the test section PIPE component to define outlet boundary conditions in terms of absolute pressure.

Figure A.4-1 shows the TRACE nodalization scheme of the ANL loop model.

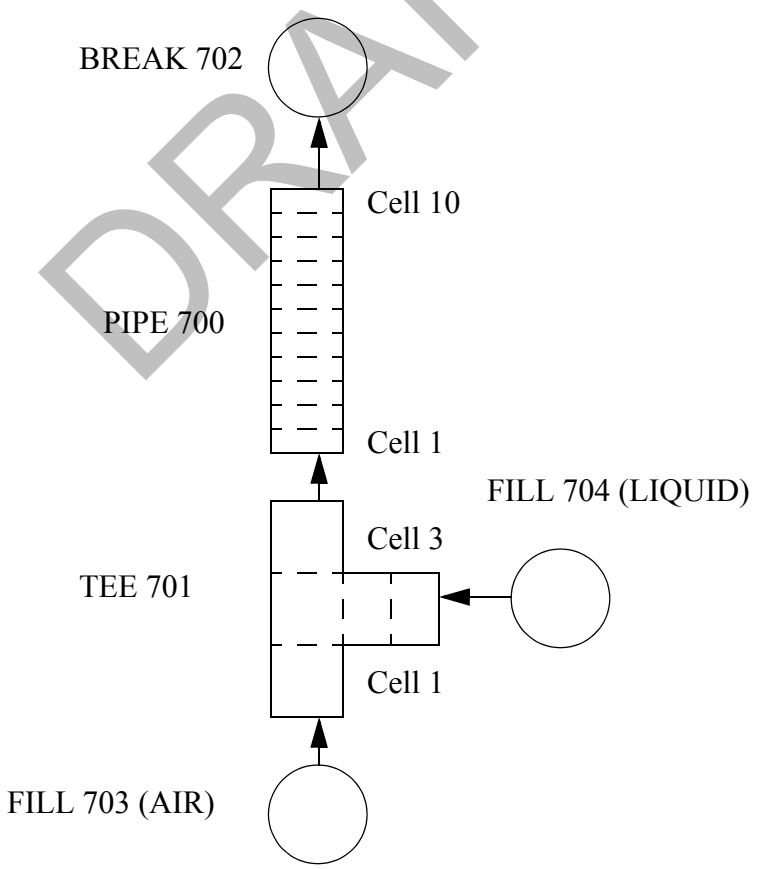

Figure A.4-1. Noding Diagram of the ANL Loop TRACE Model

A.4.4. TRACE Assessment Against ANL Air-water Void Faction Test Data

This section presents the assessment of the TRACE performance for the ANL loop air-water test runs. As mentioned, all air-water test runs were carried out at atmospheric pressure.

A.4.4.1. Description of the ANL Loop Test Runs Applied for TRACE Assessment

The ANL loop test runs, performed with air-water mixture, consisted of seven test series (series A through H) that comprise 161 tests in total. A description of the test data can be found in References 1 and 2. In each test series, the liquid superficial velocity was kept constant while the gas superficial velocity was varied substantially. The values of the liquid superficial velocities exercised in the test series A through H amounted to 0.0, 0.1, 0.2, 0.3, 0.4, 0.6, 0.8 and 1.0 ft/s, respectively. Reference 1 contains tabulated test data and for a subset of 71 test runs it lists explicitly the liquid superficial velocity, J_L, the gas superficial velocities, J_G, and the void fraction, α, measured at test point No. 2. For the remainder of the test runs, the report does not document explicitly the gas superficial velocity. This subset of 71 test runs encompasses the whole range of test conditions studied in the air-water tests and it was used for TRACE assessment purposes in this study. Table A.4.1 summarizes the ANL loop test runs against which the TRACE capabilities in predicting the void fraction in a vertical channel geometry was examined.

As seen from the table below, the gas superficial velocities vary between 0.03 m/s (0.1 ft/s) and 11.0 m/s (36.1 ft/s) and the void fractions observed cover a range from from 6.7 to 84.7%. The slip ratio for the tests performed under co-current flow conditions varied between 3.3 and 49.3. It is mentioned that according to the two-phase flow regime map proposed by Taitel et. al (Ref. 4), the test conditions corresponded to bubbly flow regime for Runs B-14 and B-16 and slug/churn flow regime for all remaining test runs.

Table A.4.1. Summary of ANL Air-water Tests Applied for TRACE Assessment

Test Series	Runs Performed	Runs Studied	J_L (m/s)	J_G (m/s)	α (-)
A	21	21	0.0	0.210 – 7.248	0.339 – 0.847
B	22	10	0.031	0.032 – 3.664	0.067 – 0.763
C	16	8	0.061	0.287 – 7.431	0.377 – 0.809
D	14	7	0.091	0.482 – 7.254	0.450 – 0.794
E	28	7	0.122	0.283 – 10.970	0.338 – 0.813
F	30	7	0.183	0.296 – 10.994	0.313 – 0.794
G	25	6	0.224	0.677 – 7.001	0.425 – 0.747
H	5	5	0.305	1.759 – 3.417	0.609 – 0.659

A.4.4.2. TRACE Assessment Analysis

The TRACE code was run in a transient mode for 100 s of transient time for each individual test run. The code-predicted void fraction for cell seven of the test section PIPE component was used to assess the code performance through comparison against the experimental void fractions. Figure A.4-2 exhibits the time history of the computed test section void fraction as predicted by TRACE.

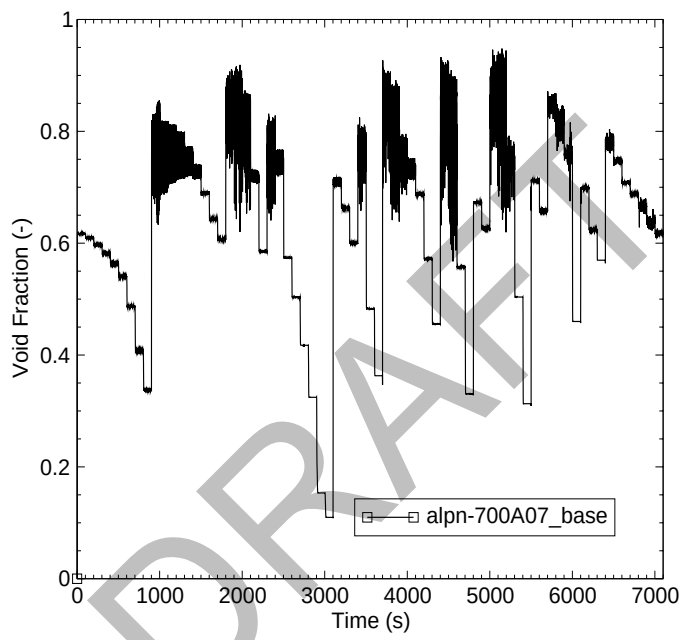

Figure A.4-2. TRACE Void Fraction Prediction for ANL Air-water Tests

It is seen from Figure A.4-2 that the TRACE code yielded stable and well-defined void fraction predictions for computed channel voids of up to ~70%. For higher test section void fractions, the code predictions were highly transitory in nature exhibiting high-frequency oscillations of significant amplitude.

Table A.4.2 compares test data and computational results for 47 test runs for which the code yielded a steady-state void fraction predictions or such with low-amplitude (<2.5%) oscillations in the void fraction response. The table documents the liquid and gas superficial velocities, J_L and $_G$, the flow quality, X, the experimentally observed void fraction, α_{EXP}, the TRACE-predicted void fractions, α_{TRACE}, as well as the difference between the experimental and the predicted void fraction values, Δ.

Table A.4.2. Comparison of ANL Loop Test Data and TRACE Void Fraction Predictions

No.	Run	J_L (ft/s)	J_G (ft/s)	J_L (m/s)	J_G (m/s)	X (-)	α_{EXP} (-)	α_{TRACE} (-)	Δ (%)
1	A-1	0.00	2.870	0.000	0.875	0.000	0.597	0.617	-2.0
2	A-2	0.00	2.740	0.000	0.835	0.000	0.600	0.610	-1.0
3	A-3	0.00	2.530	0.000	0.771	0.000	0.584	0.597	-1.3
4	A-4	0.00	2.310	0.000	0.704	0.000	0.553	0.564	-1.1
5	A-5	0.00	2.090	0.000	0.637	0.000	0.553	0.581	-2.8
6	A-6	0.00	1.840	0.000	0.561	0.000	0.514	0.540	-2.6
7	A-7	0.00	1.410	0.000	0.430	0.000	0.481	0.488	-0.7
8	A-8	0.00	0.970	0.000	0.296	0.000	0.419	0.407	1.2
9	A-9	0.00	0.690	0.000	0.210	0.000	0.339	0.339	0.0
10	A-15[a]	0.00	6.650	0.000	2.027	0.000	0.733	0.720	13
11	A-16	0.00	4.680	0.000	1.426	0.000	0.689	0.688	0.1
12	A-17	0.00	3.320	0.000	1.012	0.000	0.619	0.645	-2.6
13	A-18	0.00	2.630	0.000	0.802	0.000	0.577	0.607	-3.0
14	B-1[a]	0.10	6.780	0.030	2.067	0.076	0.703	0.709	-0.6
15	B-5	0.10	2.610	0.030	0.796	0.031	0.559	0.585	-2.6
16	B-10	0.10	2.450	0.030	0.747	0.029	0.566	0.574	-0.8
17	B-11	0.10	1.690	0.030	0.515	0.021	0.475	0.503	-2.8
18	B-12	0.10	1.120	0.030	0.341	0.014	0.419	0.417	0.2
19	B-13	0.10	0.711	0.030	0.217	0.009	0.303	0.324	-2.1
20	B-14	0.10	0.156	0.030	0.048	0.002	0.108	0.153	-4.5
21	B-16	0.10	0.105	0.030	0.032	0.001	0.067	0.109	-4.2
22	C-1[a]	0.20	6.790	0.061	2.070	0.039	0.694	0.706	-1.2
23	C-2	0.20	4.650	0.061	1.417	0.028	0.644	0.662	-1.8
24	C-3	0.20	3.100	0.061	0.945	0.019	0.578	0.599	-2.1
25	C-9	0.20	1.670	0.061	0.509	0.010	0.475	0.483	-0.8
26	C-10	0.20	0.940	0.061	0.287	0.006	0.377	0.356	2.1
27	D-3[a]	0.30	6.090	0.091	1.856	0.024	0.678	0.689	-1.1
28	D-4	0.30	2.850	0.091	0.869	0.012	0.541	0.572	-3.1
29	D-11	0.30	1.580	0.091	0.482	0.007	0.450	0.455	-0.5
30	E-1	0.40	2.830	0.122	0.863	0.009	0.530	0.557	-2.7
31	E-7	0.40	0.930	0.122	0.283	0.003	0.338	0.330	0.8
32	E-13[a]	0.40	5.830	0.122	1.777	0.017	0.659	0.673	-1.4
33	E-14	0.40	4.220	0.122	1.286	0.013	0.614	0.623	-0.9

Table A.4.2. Comparison of ANL Loop Test Data and TRACE Void Fraction Predictions

34	F-3	0.60	2.450	0.183	0.747	0.005	0.480	0.504	-2.4
35	F-7	0.60	0.970	0.183	0.296	0.002	0.313	0.311	0.2
36	F-11[a]	0.60	9.270	0.183	2.825	0.018	0.683	0.711	-2.8
37	F-13[a]	0.60	5.970	0.183	1.820	0.012	0.617	0.658	-4.1
38	G-4	0.80	2.220	0.244	0.677	0.003	0.425	0.460	-3.5
39	G-8[a]	0.80	9.210	0.244	2.807	0.014	0.659	0.700	-4.1
40	G-10	0.80	5.340	0.244	1.628	0.008	0.589	0.623	-3.4
41	G-11	0.80	3.880	0.244	1.183	0.006	0.534	0.568	-3.4
42	G-17	0.80	15.340	0.244	4.676	0.023	0.709	0.747	-3.8
43	H-1	1.00	11.210	0.305	3.417	0.014	0.659	0.706	-4.7
44	H-2	1.00	9.430	0.305	2.874	0.011	0.652	0.688	-3.6
45	H-3[a]	1.00	7.960	0.305	2.426	0.010	0.647	0.666	-1.9
46	H-4[a]	1.00	6.600	0.305	2.012	0.008	0.613	0.639	-2.6
47	H-5	1.00	5.770	0.305	1.759	0.007	0.609	0.617	-0.8

a. Low-amplitude (<2.5%), high-frequency void fraction oscillations observed.

For the majority of the test runs included in the table, the computed void fraction in cell seven of the test section component was constant in time for all 100 s of transient time computed for each test run. For a small fraction of test runs listed in Table A.4.2, the computed void fraction response exhibited some low-amplitude high-frequency oscillations. Such test runs are marked with the star symbol in the second column of the table. For all such cases however, the amplitude of high-frequency void fraction oscillations observed was less than 2.5%. When such an oscillating void fraction response was predicted for a specific test run, the average value around which the void fraction oscillated was stable and constant in time. The predicted void fraction values shown in Table A.4.2 vary between 11% and 71.3% whereas the experimentally observed void fraction values for the same test runs documented in Table A.4.2 range from 6.7% up to 73.3%. As the results from Table A.4.2 show, no low-amplitude (<2.5%), high-frequency oscillations were observed for void fractions that were predicted to be less than ~65%. The results obtained also indicate that the absolute value of the deviations between the void fraction values experimentally observed and the values predicted do not exceed 5% for all test runs listed in Table A.4.2 Such a degree of scatter is perceived as being of the same order of magnitude as the experimental repeatability of the test data itself and constitute an excellent outcome .

Figure A.4-3 compares the TRACE predictions for the test section void fractions in cell seven against the experimentally measured values for all runs documented in Table A.4.2 Different symbols are used to distinguish between test runs performed at different liquid superficial velocities ranging from 0.0 to 1.0 ft/s.

Further analysis indicates that the remaining 24 runs for which the code predicted highly transitory and oscillatory in nature void fraction responses involved highly voided two-phase flow

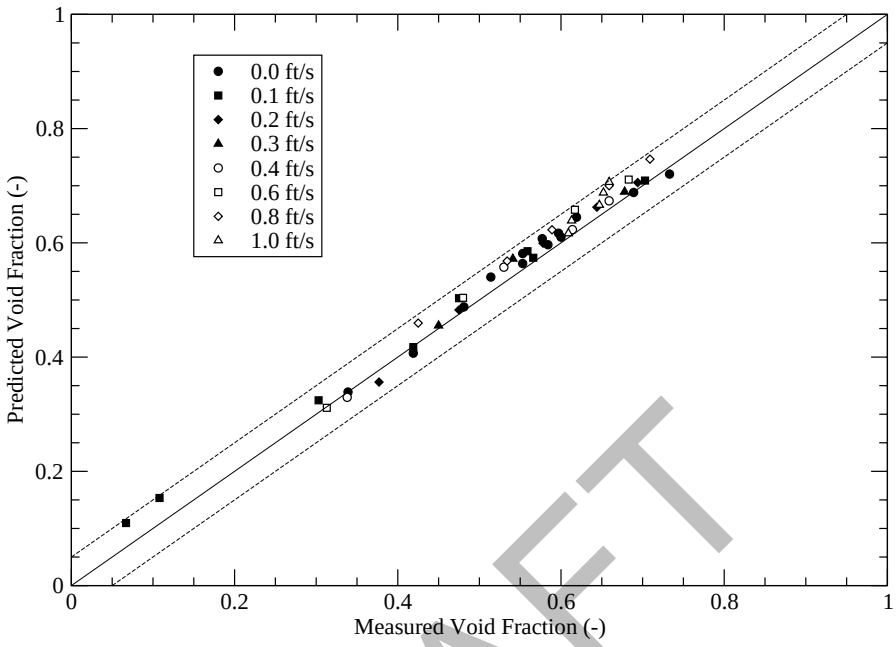

Figure A.4-3. Comparison of Measured and Predicted Void Fractions for ANL Test Runs

conditions. In particular, for all such test runs, the experimentally observed void fraction was higher than 73.1%. Table A.4.3 presents the test data for the ANL loop test runs for which TRACE predicted a highly oscillatory void fraction behavior. The maximum observed void fraction for the test runs in Table A.4.3 is equal to 84.7%.

A.4.4.3. Test Data Analysis Using the Drift-flux Approach

The drift-flux approach allows distinguishing between the test cases listed in Table A.4.3 that yielded transitory void fraction code predictions and the test runs for which stable void fraction predictions were obtained as documented in Table A.4.2 Thus, Figure A.4-4 shows the gas phase drift-flux, J_{GL}, plotted as a function of the experimentally observed void fraction, α, for each test run examined in this study. The drift-flux values shown were computed using the following relationship:

$$J_{GL} = (1 - C_o\,\alpha)\,J_G - C_o\,\alpha J_L \tag{4-1}$$

The concentration parameter, C_o, in the above written formula was set equal to 1.2, which is the value appropriate for bubbly and slug flow according to Zuber and Findlay (Ref. 5). It is

Table A.4.3. ANL Loop Test Data with Highly-voided Two-phase Flow Conditions[a]

No.	Run	J_L (ft/s)	J_G (ft/s)	J_L (m/s)	J_G (m/s)	X (-)	α_{EXP} (-)
1	A-10	0.00	11.800	0.000	3.597	0.000	0.778
2	A-11	0.00	11.300	0.000	3.444	0.000	0.784
3	A-12	0.00	10.600	0.000	3.231	0.000	0.783
4	A-13	0.00	9.450	0.000	2.880	0.000	0.766
5	A-14	0.00	8.190	0.000	2.496	0.000	0.752
6	A-19	0.00	23.780	0.000	7.248	0.000	0.847
7	A-20	0.00	18.900	0.000	5.761	0.000	0.823
8	A-21	0.00	13.290	0.000	4.051	0.000	0.803
9	B-6	0.10	12.020	0.030	3.664	0.126	0.763
10	B-7	0.10	8.800	0.030	2.682	0.096	0.744
11	C-4	0.20	11.930	0.061	3.636	0.067	0.753
12	C-14	0.20	24.380	0.061	7.431	0.127	0.809
13	C-16	0.20	15.350	0.061	4.679	0.084	0.772
14	D-1	0.30	11.890	0.091	3.624	0.046	0.750
15	D-2	0.30	9.230	0.091	2.813	0.036	0.731
16	D-12	0.30	23.800	0.091	7.254	0.087	0.794
17	D-14	0.30	16.190	0.091	4.935	0.061	0.763
18	E-16	0.40	35.990	0.122	10.970	0.097	0.813
19	E-17	0.40	27.420	0.122	8.358	0.076	0.805
20	E-20	0.40	13.650	0.122	4.161	0.040	0.758
21	F-16	0.60	36.070	0.183	10.994	0.067	0.794
22	F-18	0.60	27.230	0.183	8.300	0.052	0.772
23	F-20	0.60	16.180	0.183	4.932	0.032	0.734
24	G-15	0.80	22.970	0.244	7.001	0.033	0.747

a. Highly oscillatory void fraction code predictions observed.

mentioned that the value of the concentration parameter applied yielded positive drift-flux values for all test runs examined except for Run A-19 (for this run the drift-flux predicted was -0.12 m/s). Thus, the figure below shows all data points examined except for this single run.

As seen from Figure A.4-4, all data points from Table A.4.2 for which stable void fraction predictions were obtained scatter around a straight line with the degree of scattering sharply increasing as the value of the void fraction approaches ~70%. This value also appears in the drift-flux plot as the void fraction boundary that separates the highly voided test runs for which TRACE exhibited significant oscillations in the void fraction response from the remaining test runs. As Figure A.4-4 indicates, all test runs in the high void fraction domain listed in Table A.4.3

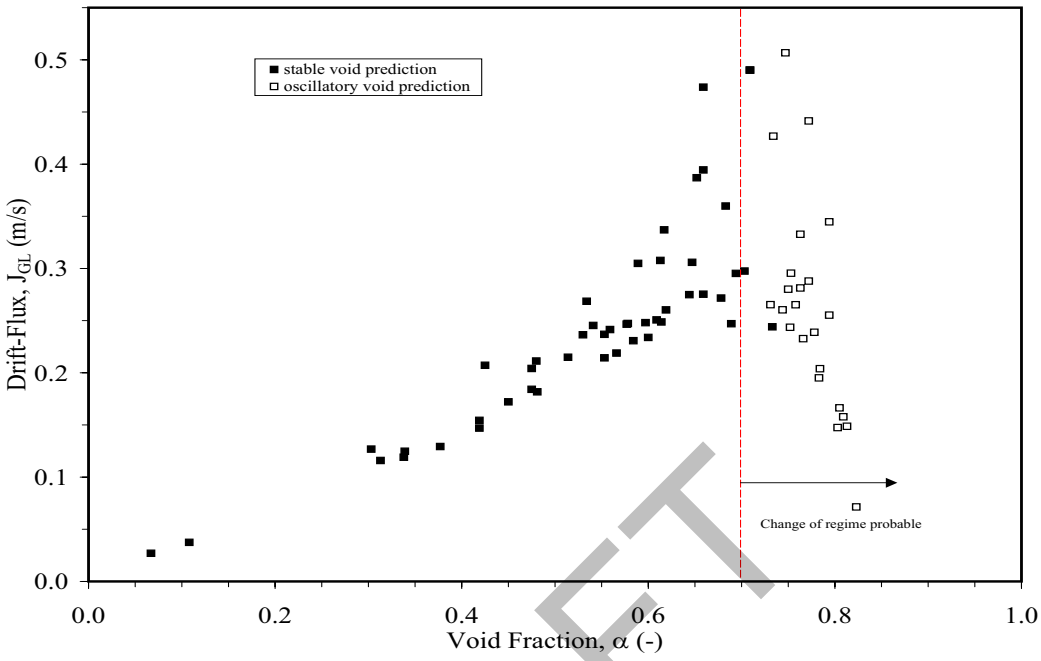

Figure A.4-4. Drift-flux Plot of ANL Air-water Test Data

(α greater than ~70%) sharply deviate from the straight line around which the test runs from Table A.4.2 scatter. This behavior of the experimental data in the drift-flux plane suggests a change in a change in the coupling pattern between the gas and liquid phases as the void fraction approaches ~80% in the tests performed. It appears that the change in the type of code response, observed for the high void fraction tests, as indicated by the appearance of significant oscillations in the void fraction predictions, is associated with a probable transition in the experimentally observed two-phase flow pattern itself. An analysis performed by Wallis (Ref. 3) also indicated such a change in the flow regime as the value of α approaches 80%.

A.4.5. Summary and Major Observations

The ANL loop air-water test data have been used in this study to assess the TRACE capabilities to model the steady-state behavior of adiabatic two-phase up-flow in simple vertical pipe geometry at atmospheric pressure.

The ANL test data examined here covered two-phase flow conditions with liquid superficial velocities ranging between 0 and 0.305 m/s, gas superficial velocities varying between 0.032 and 10.1 m/s and flow void fractions spanning from 6.7 to 84.7%. The slip ratio for the tests performed varied between 3.3 and 49.3.

The main observation from the results obtained is that TRACE yielded a steady-state void fraction prediction or such with low-amplitude (<2.5%) oscillations in the void fraction response for the test data in the void fraction domain below ~70%. For such test runs, the magnitude of the deviation between the experimental and predicted void fraction values did not exceed 5%. This is an excellent outcome, as such a degree of scatter is of the same order of magnitude as the experimental repeatability of the test data itself.

The results also revealed that the code predicted highly transitory and oscillatory void fraction responses for the test runs involving highly voided two-phase flow conditions with α greater than ~70%. In particular, for all such test runs the experimentally observed void fraction was higher than 73.1%. Table A.4.3 presents the test data for the ANL loop test runs for which TRACE predicted a highly oscillatory void fraction behavior. The maximum observed void fraction for the test runs in Table A.4.3 is equal to 84.7%.

The analysis of the drift-flux behavior of the experimental data in the drift-flux versus void fraction plane indicates a change in the coupling pattern between the gas and liquid phases as the void fraction approaches ~80%. It appears that the change in the type of code response, observed for the high void fraction tests as indicated by the appearance of significant oscillations in the void fraction predictions, is associated with a probable transition in the experimentally encountered two-phase flow pattern itself.

A.4.6. References

1 G. Smissaert: "Two-Component Two-Phase Flow Parameters for Low Circulation Rates," Argonne National Laboratory Report ANL-6755, July 1963.

2 G. Smissaert: "Two-phase Flow Data for Non-circulating and Slowly Circulating Mixtures," Nuclear Structural Engineering, Vol. 2, pp. 36-39, 1965.

3 G. B. Wallis: “One-dimensional Two-phase Flow,” McGraw Hill, Inc., 1969.

4 Y. Taitel, D. Bornea, A. E. Duckler: "Modelling Flwo Pattern Transitions for Steady Upward Gas-liquid Flow in Vertical Tubes," AIChE Journal, Vo. 26, No. 3, pp. 345-54, 1980.

5 N. Zuber, J. A. Findlay: “Average Volumetric Concentration in Two-phase Flow Systems,” J. Heat Transfer, Trans. ASME, Vol. 87, pp. 453-468, 1965.

A.5. TPTF Horizontal Flow Tests

Authors: Vesselin Palazov (ISL)

Affiliation: Information Systems Laboratories (ISL), Inc.

Code Version: TRACE V5.0

Platform and Operating System: Intel x86, Windows XP

A.5.1. Introduction

The thermal-hydraulic response of a pressurized water reactor (PWR) during a small-break (SB) loss-of-coolant accident (LOCA) involves the development of a stratified flow pattern in the horizontal reactor legs of the primary coolant system. The adequate modeling of the two-phase flow behavior and its stratification in horizontal channels is important for the realistic prediction of the coolant inventory distribution in the primary reactor coolant system during SB LOCA transients.

The objective of this test problem is to examine TRACE capabilities for predicting the behavior of horizontal two-phase flow in a relatively large-diameter pipe via comparing code void fraction predictions against experimental data obtained at the two-phase flow test facility (TPTF). The TPTF separate-effect test data used in this study describe horizontal co-current steam-water flow at high pressures (3.0 MPa to 8.0 MPa) in a horizontal test section of a 0.18 m (7.09 in) internal diameter.

A.5.2. TPTF Facility Description

The TPTF facility consisted of a horizontal test section discharging into a large vertical boiler vessel with an internal diameter of 1.30 m (4.27 ft). The test section was a 10.0 m (32.81 ft) long stainless steel pipe with an internal diameter of 0.18 m (7.09 in) corresponding to a length-to-diameter (L/D) ratio of 55.56. The demineralized water in the boiler was heated electrically to the saturated condition at the desired system pressure. Saturated steam was then pumped from the top of the boiler vessel into a T-shaped mixer located at the test section inlet, whereas saturated liquid was drawn from the bottom of the boiler and also pumped into the same fluid mixing device. The facility, including the test section and both steam and liquid lines, was well insulated to minimize heat losses and to prevent steam condensation and liquid subcooling.

The tests used in this study were produced with two different test facility configurations that involved the same test section with two different T-shaped mixer designs: (1) a bubbly-flow type mixer and (2) a separated-flow type mixer. The bubbly-flow mixer provided well-mixed inlet

conditions and contained a bundle of tubes with perforated walls oriented along the axis of the test section. The steam was introduced into the tubes and then dispersed in the liquid volume through the holes across the tube walls. The liquid was injected from the bottom of the mixer into the volume outside of the tube bundle where the steam and the liquid mixed with each other. The separated-flow mixer contained a horizontal dividing plate that allowed introducing the steam horizontally above the dividing plate. The liquid was injected again from the bottom section of the mixer beneath the separating plate. Thus, this mixer provided for completely separated introduction of the fluid phases into the test section.

The effects of the test section exit conditions on the two-phase flow behavior in the test section were also investigated. For this purpose, the water level in the test vessel was adjusted either above or below the test section outlet in order to account for possible variations in the prototypical flow conditions. Both types of boundary conditions are relevant when considering possible PWR hot/cold leg exit flow conditions.

The experiments were conducted in a steady-state mode by providing a co-current flow of saturated steam and liquid through the test section. The flow rate of each phase was adjusted and stabilized before recording the test data.

The horizontal test section was equipped with various instruments to measure phase and momentum distributions across pipe cross-sections at selected axial locations. Two γ-densitometers were used to measure the two-phase flow area-averaged void fraction at two different axial locations along the channel. Both densitometers included a single vertically shot γ-ray beam that was traversed horizontally to scan the whole cross-sectional area of the test section. The first (upstream) location was chosen near the test section inlet at L/D=17 and the second (downstream) location was located near the test section outlet at L/D=48. A third γ-densitometer with a single horizontally shot γ-ray beam traversed vertically was installed at an axial location of L/D=21. A fourth γ-densitometer with three fixed γ-ray beams was installed at an axial location of L/D=40. A vertical water-purged Pitot tube for momentum flux measurement was located at L/D=25 and five conductivity probes along the vertical centerline were mounted at L/D=36. The measurements were sampled at a rate of 5 Hz for 400 s in each test run. The uncertainty in the void fraction measurement was estimated to be less than 2%. The flow rates were measured by orifice flow meters with a measurement uncertainty of less than ~1.5%.

A description of the test facility can be found in Kawaji et al. (Ref. 1) and Nakamura (Ref. 2). It is mentioned that TPTF test data were used in the past by Asaka et al. (Ref. 3) for assessing the TRAC-PF1 code. Kukita et al. (Ref. 4) also used TPTF data for assessing the RELAP5/MOD2 code in a separate study.

A.5.3. TRACE TPTF Model Description

The TRACE TPTF model represents both the test section pipe and the test vessel into which the two-phase flow discharges. The portion of the test section pipe located between the first (upstream) γ-densitometer station at L/D=17 and the inlet mixer was excluded from the modeling

domain. This was done for two reasons: (1) the flow in this section is most strongly influenced by the inlet flow conditions that reflect both the mixer configuration and the test conditions and (2) no void fraction measurements were taken within the excluded portion of the channel. This modeling decision also allowed for imposing well-defined boundary conditions at the inlet end of the test section model that included the void fractions measured at that location.

The test section part of the model is represented by a horizontal PIPE-component with eleven cells. The first ten cells represent the portion of the modeled portion of the test section with a total length of 6.94 m (22.77 ft). The eleventh cell in this component represents the nozzle that connects the test section to the test vessel (~0.5 m long with 0.268 m internal diameter). The first six cells have a length of 0.792 m (31.18 in) each that corresponds to a length-to-diameter ratio of 4.4. Cells seven through nine have a length of 0.552 m (21.73 in) each yielding a length-to-diameter ratio of 3.07. The length of cell ten is set equal to 0.532 m (20.94 in) with a slightly modified length-to-diameter ratio of 2.96 to accommodate for the total length of the portion of the test section modeled (6.94 m or 22.77 ft). With this nodalization scheme, the axial position of the γ-densitometer at L/D=48 coincides with the center-point position of cell eight.

The test vessel was modeled by a second PIPE component that was oriented vertically. This component contains five cells of an equal length of 0.50 m (1.64 ft) and an internal diameter of 1.30 m (4.27 ft). The exit end of the PIPE component modeling the test section was connected to the middle cell of the test vessel PIPE component using a side junction.

The boundary conditions were specified in terms of phase velocities, phase temperatures and void faction at the inlet end of the test section PIPE using a FILL component. Two BREAK components connected to both ends of the test vessel component were used to define outlet boundary conditions in terms of pressure.

Figure A.5-1 shows the TRACE nodalization scheme of the TPTF model.

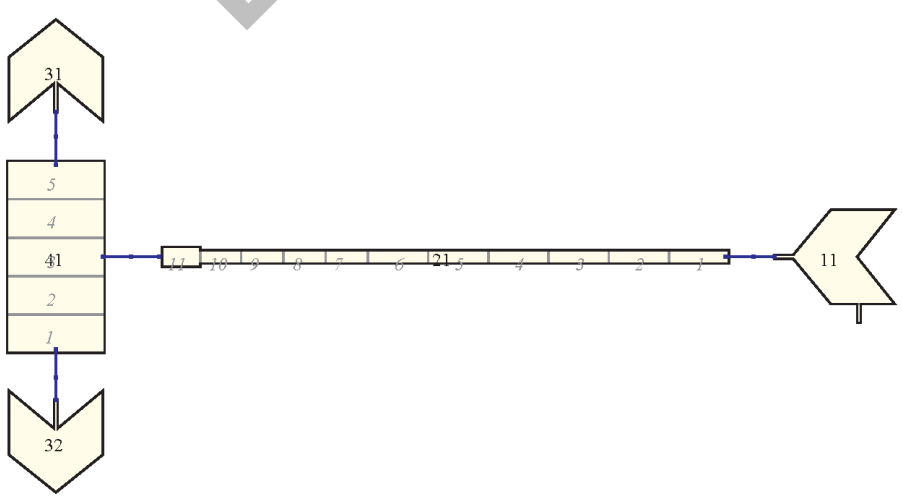

Figure A.5-1. Noding Diagram of the TPTF Model

A.5.4. TRACE Assessment

Two different sets of test runs were used in this study to assess TRACE capabilities of modeling two-phase flow behavior in a horizontal channel. The first set of test runs consisted of runs performed with a test facility configuration that used the bubbly-flow type mixer while the second set of runs involved tests performed with the separated-flow type mixer. All experiments were performed at a specified constant pressure under steady-state conditions at the saturation point. Results from the TRACE TPTF predictions are discussed in the following sections.

A.5.4.1. TPTF Tests with Bubbly-Flow Inlet Conditions

The tests in this category comprise 46 runs that were performed at system pressures ranging between 7.3 MPa and 8.0 MPa. The tests were carried out with the bubbly-flow mixer and the tests results were published in Reference 1.

The runs involved both types of test section exit conditions with different water levels in the test boiler vessel. Thus, 28 of the cases, considered in this group, were performed under high exit water level conditions in the boiler vessel when the water level in the vessel was kept at an elevation located approximately 0.4 m above the centerline of the test section exit. In the remaining 18 runs in this group, the water level in the boiler was adjusted at an elevation, which was located below the exit opening of the test section. All tests in this group exhibited separated flow conditions (stratified or wavy-stratified). According to Reference 1, this was the only flow pattern observed using the bubbly-flow mixer. For the runs in this group, the paper documented the void fraction measurements taken at both axial locations of L/D=17 and L/D=48. The void fractions measured at L/D=17 were used to specify the inlet boundary conditions in the TRACE test section model. The void fractions measured at L/D=48 were used to assess the TRACE performance via comparing the predicted void fraction values against the measured ones.

A.5.4.1.1. Tests with High Exit Water Level

Table A.5.1 lists the test conditions for the runs with the high exit water level in the test vessel. Such conditions can be relevant to the flow behavior in the reactor cold/hot legs depending on the coolant level in the reactor downcomer and the presence of coolant in the steam generator inlet plenum during a small-break LOCA.

It shows the test pressure, P, the liquid and vapor superficial velocities, J_L and J_V, and the measured void fractions at both axial locations of L/D=17 and L/D=48.

Figure A.5-2 compares the TRACE predictions for the test section void fractions at L/D=48 against the experimentally measured values for the TPTF runs with well-mixed (bubbly) inlet flow conditionsl. The circular symbols in this plot represent the test runs with the high exit water level. The figure shows the TRACE predictions for the void fraction in the cell of the test section

PIPE component whose center point axial location corresponds to the location of the γ-densitometer at L/D=48. The last two columns in Table A.5.1 show the TRACE predictions for the void fraction and the flow regime number. The last quantity can vary within the range from 5.0 (pre-CHF flow configuration) to 6.0 (stratified flow configuration) and it is used as an weighting factor when the code interpolates between closure relations appropriate for each of the configurations.

The results obtained show that the deviations between the predicted values and the experimental data fall within an error band of ±10% for all of the test runs considered. For the runs in this group, TRACE overpredicted the measured void fraction in 15 cases and underpredicted the experimental data for the remaining 13 cases.

Table A.5.1. TPTF Test Data and TRACE Predictions for High Exit Water Level Tests with Bubbly-Flow Mixer

Run	P (MPa)	J_L (m/s)	J_V (m/s)	$\alpha_{L/D=17}$ (-)	$\alpha_{L/D=48}$ (-)	α_{TRACE}	Regime No.
779	7.3	1.380	0.085	0.060	0.090	0.050	5.3
781	7.3	1.370	0.130	0.090	0.130	0.072	5.4
775	7.3	1.370	0.260	0.130	0.150	0.133	5.6
773	7.3	1.240	2.580	0.570	0.500	0.519	5.7
730	7.3	0.440	2.060	0.660	0.640	0.626	6.0
783	7.3	0.510	1.110	0.430	0.470	0.449	6.0
785	7.3	0.540	0.410	0.260	0.270	0.258	5.9
728	7.3	0.055	1.570	0.910	0.690	0.634	6.0
708	7.3	0.100	0.760	0.650	0.530	0.440	6.0
710	7.3	0.083	1.020	0.760	0.610	0.511	6.0
720	7.3	0.017	0.720	0.630	0.480	0.446	6.0
722	7.3	0.022	0.610	0.570	0.440	0.411	6.0
712	7.3	0.033	0.410	0.480	0.380	0.337	6.0
714	7.3	0.044	0.210	0.310	0.240	0.240	5.9
751	7.4	1.350	0.510	0.190	0.150	0.203	5.6
749	7.4	1.310	1.280	0.380	0.290	0.358	5.7
747	7.4	1.270	2.020	0.480	0.410	0.458	5.7
743	7.4	1.100	5.100	0.730	0.690	0.705	5.3
732	7.4	0.033	4.100	0.840	0.810	0.820	5.6
755	7.4	0.550	0.210	0.130	0.130	0.170	5.9
757	7.4	0.520	0.100	0.160	0.120	0.106	5.8
759	7.4	0.520	0.050	0.080	0.060	0.064	5.8
761	7.4	0.520	0.031	0.060	0.040	0.044	5.7

Table A.5.1. TPTF Test Data and TRACE Predictions for High Exit Water Level Tests with Bubbly-Flow Mixer

Run	P (MPa)	J_L (m/s)	J_V (m/s)	$\alpha_{L/D=17}$ (-)	$\alpha_{L/D=48}$ (-)	α_{TRACE}	Regime No.
726	7.4	0.028	2.060	0.970	0.830	0.730	6.0
1545	7.4	0.120	0.440	0.320	0.310	0.334	6.0
1547	7.4	0.130	0.260	0.200	0.200	0.253	5.9
1549	7.4	0.140	0.130	0.120	0.110	0.174	5.9
763	7.4	0.140	0.027	0.050	0.040	0.070	5.9

A.5.4.1.2. Tests with Low Exit Water Level

Table A.5.2 shows the test conditions for the runs with the low exit water level in the test boiler vessel. As in the case of a high exit water level, the runs performed with a low exit water level can be relevant to the flow behavior in the reactor cold/hot leg depending on the coolant level in the reactor downcomer and the absence of coolant in the steam generator inlet plenum.

As in the case of Table A.5.1, it shows the test pressure, P, the liquid and vapor superficial velocities, J_L and J_V, and the measured void fractions at both axial locations of L/D=17 and L/D=48.

Table A.5.2. TPTF Test Data and TRACE Predictions for Low Exit Water Level Tests with Bubbly-Flow Mixer

Run	P (MPa)	J_L (m/s)	J_V (m/s)	$\alpha_{L/D=17}$ (-)	$\alpha_{L/D=48}$ (-)	α_{TRACE}	Regime No.
857	7.4	1.120	5.150	0.670	0.640	0.704	5.3
855	7.4	1.260	2.690	0.510	0.470	0.526	5.6
853	7.4	1.330	1.550	0.350	0.330	0.394	5.7
851	7.4	1.370	0.520	0.170	0.170	0.213	5.7
849	7.4	1.380	0.280	0.080	0.100	0.153	6.7
845	7.4	0.380	4.170	0.760	0.770	0.791	5.6
843	7.4	0.540	1.370	0.420	0.420	0.511	6.0
847	7.4	0.570	0.230	0.160	0.220	0.449	6.0
838	7.4	0.056	1.790	0.830	0.870	0.900	6.0
836	7.5	0.030	2.330	0.890	0.910	0.947	6.0
834	7.5	0.025	0.620	0.820	0.880	0.933	6.0
1561	7.6	0.140	0.450	0.670	0.680	0.788	6.0
1563	7.6	0.140	0.270	0.650	0.660	0.787	6.0
1565	7.6	0.150	0.150	0.640	0.650	0.776	6.0

Table A.5.2. TPTF Test Data and TRACE Predictions for Low Exit Water Level Tests with Bubbly-Flow Mixer

Run	P (MPa)	J_L (m/s)	J_V (m/s)	$\alpha_{L/D=17}$ (-)	$\alpha_{L/D=48}$ (-)	α_{TRACE}	Regime No.
1567	7.7	0.160	0.110	0.640	0.670	0.765	6.0
1559	7.7	0.053	0.130	0.790	0.820	0.889	6.0
1557	7.8	0.049	0.230	0.830	0.790	0.895	6.0
1555	8.0	0.041	0.420	0.870	0.830	0.907	6.0

The results indicate that the code overpredicted the void fraction values measured at L/D=48 for all 18 cases in this category. In five runs, the discrepancies between the predicted values and the experimental data exceeded the error band of +10% with the biggest deviation of +22.9% being observed for Run 847. For the remaining runs, the deviation between the measured and predicted values was less than +10%. The last two columns in Table A.5.2 show the TRACE predictions for the void fraction and the flow regime number.

Figure A.5-2 compares the TRACE predictions for the test section void fractions at L/D=48 against the experimentally measured values for all TPTF runs with well-mixed (bubbly) inlet flow conditions considered in this study. The square symbols in this plot represent the test runs with the low exit water level and, as mentioned, the circular symbols indicate the test runs with the high exit water level. For all data points shown, the figure plots the TRACE predictions for the void fraction in the cell of the test section PIPE component whose center point axial location corresponds to the location of the γ-densitometer located at L/D=48.

A.5.4.2. TPTF Tests with Separated-Flow Inlet Conditions

The tests in this category were carried out using the separated-flow mixing device and the test data were documented in Reference 2. The tests considered in this study included 64 runs that were performed at system pressures ranging between 3.0 MPa and 8.6 MPa. All tests were carried out with the water level in the boiler vessel kept at an elevation approximately 0.5 m above the centerline of the test section exit.

When the separated-flow mixer was used to introduce the steam and liquid phases in a stratified way with a certain relative velocity (slip), a transition to intermittent flow was observed in the test section for some test runs. At the same time, the test conditions for the runs that exhibited stratified flow were such that the flow in the test section was supercritical for all runs with the only exception being Run 473. Thus, for the runs that exhibited stratified flow the liquid level decreased only slightly toward the downstream end of the test section.

A comparison by Nakamura of the void fractions at L/D=17 and L/D=48 for test runs that exhibited stratified-wavy (SW), wavy-dispersed (WD) and stratified-wavy-to-slug (SW-SL) flow patterns at 3.0 MPa revealed a discrepancy that was less than ±3%. For the purpose of the present study, the void fraction values obtained at L/D=28 and documented for each individual test run

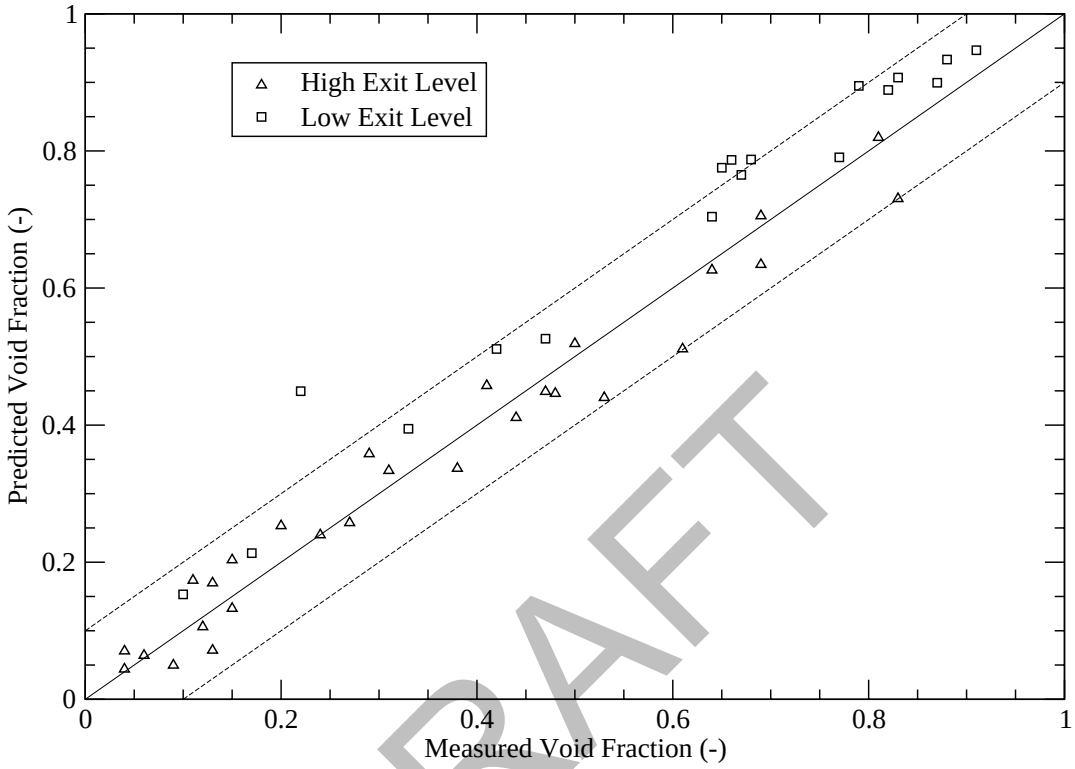

Figure A.5-2. Comparison of Measured and Predicted Void Fractions for the TPTF Test Runs with Bubbly-Flow Inlet Conditions (Axial Location L/D=48)

were considered representative for both void fraction measurement axial locations at L/D=17 and L/D=48. Thus, these experimental void fractions were used to specify the inlet boundary conditions in the TRACE test section model for the each test run. In addition, the same experimental values were applied to assess the TRACE performance via comparing the test data against the predicted void fractions at L/D=48.

Table A.5.3 lists the test conditions for the runs with the separated-flow mixer that were performed at system pressures of 3.0 MPa and Table A.5.4 documents the remaining test runs in this group that were performed at system pressures of 5.0 MPa, 7.3 MPa and 8.6 MPa, respectively. The tables show the test pressure, P, the liquid superficial velocity J_L, and the vapor superficial velocity, J_V. In addition, the measured void fraction is listed for each run along with the flow pattern observed in the test section. The last two columns in Table A.5.3 and in Table A.5.4 show the TRACE predictions for the void fraction and the flow regime number.

Figure A.5-3 compares the TRACE predictions for the test section void fractions at L/D=48 against the experimentally measured values for all TPTF runs with separated-flow inlet conditions considered in this study. Differently shaped symbols in this plot distinguish between cases run at different system pressures.

As seen from Figure A.5-3, the code predicted closely the experimental void fractions for all test cases analyzed. Thus, the predicted values differed from the experimental void fractions by a margin of less than $\pm$10% for all 64 of the test runs. For the runs in this group, TRACE overpredicted the measured void fraction in ten tests with the maximum deviation being +5% for Test 547 and underpredicted the experimental data for the remaining 54 test runs with the largest deviation being -9.6% for Test 493.

Table A.5.3. TPTF Test Data and TRACE Predictions for High Exit Water Level Tests with Separated-Flow Mixer at 3.0 MPa

Run	P (MPa)	J_L (m/s)	J_V (m/s)	Pattern	$\alpha_{L/D=17}$ (-)	α_{TRACE}	Regime No.
486	3.0	0.414	4.080	SW	0.730	0.697	5.9
478	3.0	0.414	1.710	SW	0.606	0.548	6.0
482	3.0	0.414	2.570	SW	0.683	0.625	6.0
473	3.0	0.414	0.411	SW	0.223	0.224	6.0
474	3.0	0.413	1.010	SW	0.429	0.347	6.0
477	3.0	0.616	1.010	SW-SL	0.448	0.359	5.5
481	3.0	0.559	1.700	SW-SL	0.565	0.491	6.0
485	3.0	0.539	2.560	SW-SL	0.608	0.563	5.6
495	3.0	0.592	1.350	SW-SL	0.452	0.407	6.0
2473	3.0	0.601	1.010	SW-SL	0.398	0.350	6.0
2474	3.0	0.590	1.820	SW-SL	0.519	0.472	6.0
2475	3.0	0.571	2.780	SW-SL	0.628	0.579	6.0
487	3.0	1.010	4.090	WD	0.649	0.591	6.0
488	3.0	0.583	4.090	WD	0.704	0.658	6.0
489	3.0	0.473	4.090	WD	0.717	0.680	6.0
490	3.0	0.415	7.760	WD	0.840	0.831	6.0
491	3.0	1.010	7.740	WD	0.779	0.735	6.0
2476	3.0	0.547	4.090	WD	0.709	0.666	6.0
2477	3.0	0.496	6.740	WD	0.811	0.781	6.0
475	3.0	1.010	1.010	SL	0.402	0.315	6.0
476	3.0	0.724	1.010	SL	0.429	0.347	6.0
479	3.0	1.010	1.740	SL	0.538	0.456	6.0
480	3.0	0.672	1.700	SL	0.579	0.498	6.0

Table A.5.3. TPTF Test Data and TRACE Predictions for High Exit Water Level Tests with Separated-Flow Mixer at 3.0 MPa

Run	P (MPa)	J_L (m/s)	J_V (m/s)	Pattern	$\alpha_{L/D=17}$ (-)	α_{TRACE}	Regime No.
483	3.0	1.010	2.580	SL	0.547	0.484	6.0
484	3.0	0.646	2.580	SL	0.604	0.549	6.0
493	3.0	0.607	2.390	SL	0.606	0.510	5.9
494	3.0	0.631	1.580	SL	0.511	0.447	5.9
492	3.0	0.679	3.440	SL-WD	0.659	0.606	5.4

Table A.5.4. TPTF Test Data and TRACE Predictions for High Exit Water Level Tests with Separated-Flow Mixer at 5.0 MPa, 7.3 MPa and 8.6 MPa

Run	P (MPa)	J_L (m/s)	J_V (m/s)	Pattern	$\alpha_{L/D=17}$ (-)	α_{TRACE}	Regime No.
515	5.0	0.412	1.667	SW	0.555	0.535	6.0
519	5.0	0.412	2.548	SW	0.669	0.641	6.0
523	5.0	0.413	4.054	SW	0.753	0.736	5.8
513	5.0	0.624	1.000	SW-SL	0.386	0.379	5.3
518	5.0	0.602	1.666	SW-SL	0.516	0.486	5.5
2480	5.0	0.623	0.992	SW-SL	0.391	0.378	5.8
2481	5.0	0.620	1.694	SW-SL	0.507	0.484	5.7
522	5.0	0.600	2.562	SW-WD	0.611	0.580	5.9
527	5.0	0.578	4.037	SW-WD	0.708	0.694	5.9
2482	5.0	0.579	2.457	SW-WD	0.609	0.577	5.9
2483	5.0	0.527	3.976	SW-WD	0.719	0.701	6.0
2484	5.0	0.463	5.954	SW-WD	0.814	0.810	5.9
524	5.0	1.011	4.049	WD	0.644	0.625	5.9
525	5.0	1.011	7.702	WD	0.794	0.777	5.6
526	5.0	0.414	7.674	WD	0.864	0.893	5.2
542	7.3	0.414	2.530	SW	0.690	0.669	6.0
546	7.3	0.412	4.030	SW	0.778	0.773	5.6
2527	7.3	0.488	2.300	SW	0.642	0.619	5.1
2528	7.3	0.493	2.290	SW	0.640	0.617	6.0
541	7.3	1.010	2.560	WD	0.549	0.543	6.0
543	7.3	1.860	2.550	WD	0.468	0.453	5.5
544	7.3	1.860	4.040	WD	0.581	0.564	5.7
545	7.3	1.010	4.040	WD	0.656	0.659	5.6

Table A.5.4. TPTF Test Data and TRACE Predictions for High Exit Water Level Tests with Separated-Flow Mixer at 5.0 MPa, 7.3 MPa and 8.6 MPa

Run	P (MPa)	J_L (m/s)	J_V (m/s)	Pattern	$\alpha_{L/D=17}$ (-)	α_{TRACE}	Regime No.
547	7.3	0.415	7.670	WD	0.895	0.945	5.4
2487	8.6	0.668	0.827	SW	0.370	0.373	5.6
2489	8.6	0.635	1.310	SW	0.466	0.470	5.5
2490	8.6	0.580	2.100	SW	0.606	0.588	5.9
2458	8.6	1.864	1.000	WD	0.268	0.272	5.9
2459	8.6	1.009	1.010	WD	0.358	0.356	5.9
2462	8.6	1.011	1.670	WD	0.441	0.458	5.8
2463	8.6	1.862	1.670	WD	0.349	0.370	5.7
2464	8.6	1.860	2.580	WD	0.479	0.467	5.7
2465	8.6	1.01	2.56	WD	0.557	0.560	5.4
2467	8.6	0.412	4.06	WD	0.798	0.796	5.5
2468	8.6	1.01	4.08	WD	0.676	0.676	5.6
2492	8.6	0.44	4.14	WD	0.8	0.792	5.6

A.5.4.3. Summary and Major Observations

Altogether, 110 TPTF test runs have been analyzed in this study in order to assess the TRACE capabilities to model the behavior of two-phase flow in a relatively large-diameter (0.18 m) horizontal pipe through comparing void fraction predictions against experimentally measured data. The tests examined were performed with water steam and water liquid under saturated conditions at system pressures ranging from 3.0 MPa up to 8.6 MPa. The test facility was well insulated to minimize heat losses and prevent steam condensation and liquid subcooling in the test section. The test facility configurations used to produce the test data included two different T-shaped mixing devices installed at the test section inlet for introduction of the steam and liquid phases. The bubbly-flow mixer provided well-mixed inlet flow conditions whereas the separated-flow mixer was used to introduce steam and liquid in a stratified flow configuration. All tests performed with the bubbly-flow mixer exhibited separated flow conditions (stratified or wavy-stratified). For some of the tests carried out with the separated-flow mixer, transition to intermittent (slug) flow was observed in the test section.

The effects of the test section exit conditions on the two-phase flow behavior in the test section were investigated. For this purpose, the water level in the test vessel was adjusted either above or below the test section outlet in order to account for possible variations in the prototypical flow conditions. The experiments were conducted in a steady-state mode by providing a co-current flow of saturated steam and liquid trough the test section. The flow rate of each phase was adjusted and stabilized before recording the test data.

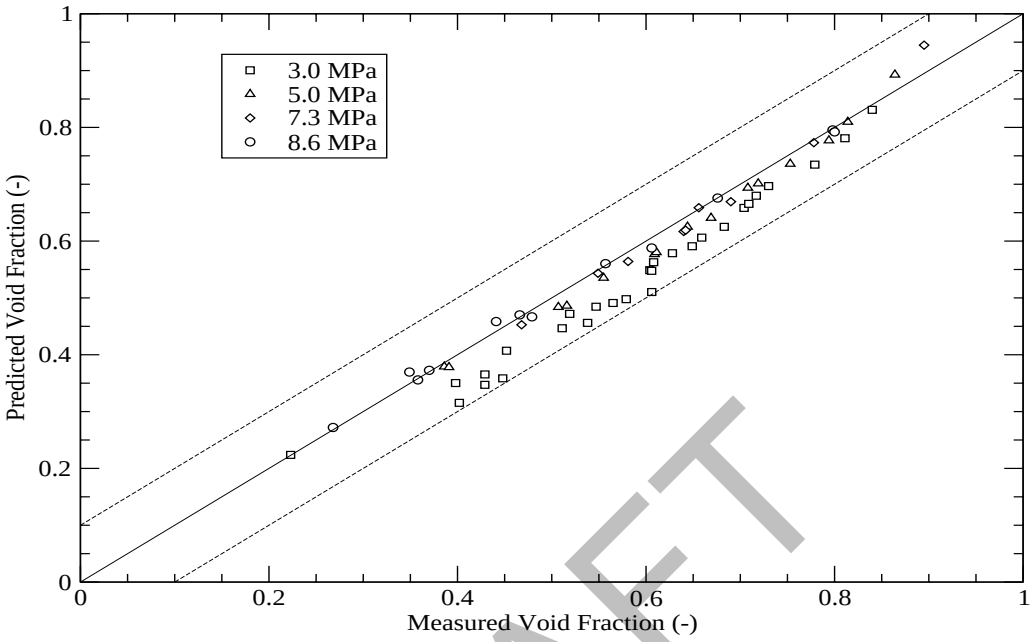

Figure A.5-3. Comparison of Measured and Predicted Void Fractions for the TPTF Test Runs with Separated-Flow Inlet Conditions (Axial Location L/D=48)

For the vast majority of test runs analyzed, TRACE predicted the void fraction near the test section exit (at L/D=48) with a discrepancy of less than ±10% between the computed void fractions and the experimental test data. Such code performance was observed for 105 of the test runs considered. The remaining five test cases that exhibited a larger deviation between the predicted and experimental void fractions were performed with the bubbly-flow mixer under low exit water level conditions with the largest discrepancy observed amounting to +22.9%. For the runs performed under high exit water level conditions and with a separated-flow mixer, the code exhibited a tendency of underpredicting the experimental data. Only for the test runs performed with the bubbly-flow mixer under low exit water level conditions, the code systematically overpredicted the exit void fraction data for all 18 test runs analyzed.

A.5.5. References

1 M. Kawaji, A. Anoda, H. Nakamura, T. Tasaka: "Phase and Velocity Distributions and Holdup in High-Pressure Steam/Water Stratified Flow in a Large Diameter Horizontal Pipe," Int. J. Multiphase Flow, Vol. 13, No. 2, pp. 145-159, 1987.

2 H. Nakamura: "Slug Flow Transitions in Horizontal Gas/Liquid Two-Phase Flows (Dependence on Channel Height and System Pressure for Air/Water and Steam/Water Two-Phase Flows)," Japan Atomic Energy Research Institute, Report JAERI-Research 96-022, May 1996.

3 H. Asaka, Y. Kukita, Y. Anoda, H. Nakamura, K. Tasaka: "Improvement of TRAC-PF1 Interfacial Drag Model for Analysis of High-Pressure Horizontally-Stratified Two-Phase Flow," Journal of Nuclear Science and Technology, Vol. 28, No. 1, pp. 33-44, December, 1991.

4 Y. Kukita, Y. Anoda, H. Nakamura, and K. Tasaka, "Assessment and Improvement of RELAP5/MOD2 Code's Interphase Drag Models," 24th ASME/AIChE National Heat Transfer Conference, Pittsburgh, PA, August 9-12, 1987.

A.6. Single and Two-Phase Wall Friction

Author(s): Mark Bolander

Affiliation: Information Systems Laboratories, Inc.

Code Version: TRACE V5.0

Platform and Operating System: Intel x86, Windows XP

A.6.1. Introduction

The ability of TRACE to correctly predict the pressure drop due to wall friction in single and two-phase flow situations has been assessed. Pressure drop is a function of fluid density, flow velocity, and hydraulic diameter. Analytical values calculated using the Churchill correlation (Ref. 1) for wall friction factor were compared against TRACE predictions for single and two-phase flow. Reynolds number (Re number) versus dimensionless film thickness data from several free falling film experiments (Ref. 2) were also used to assess the wall friction model in TRACE. Additionally, data from two-phase flow experiments by Ferrell and McGee (Ref. 3) and Ferrell and Bylund (Ref. 4) were also used to assess the TRACE wall friction model.

A.6.2. Two-Phase Experimental Facilities

Two-phase flow experiments were conducted at North Carolina State University in 1966. One set of experiments examined two-phase flow through abrupt expansions and contractions (Ref. 3). The other set of experiments examined low pressure steam-water flow in a heated vertical channel (TPF series experiments) (Ref. 4). Data from these experiments are useful in verifying the wall friction model under two phase conditions.

The experimental apparatus used to conduct the two-phase flow through abrupt expansions and contractions experiments consisted of a vertically oriented lower section (40.5 inches long) and a vertically oriented upper section (49.5 inches) that were connected together by mating flanges. There were three lower section tubes and three upper section tubes having inside diameters of 0.34, 0.46, and 0.59-inches. The design made it possible to study three expansions, three contractions, or three uniform channels. The experiments were conducted under steady-state conditions with inlet mass flow rates, pressures and void fractions along the test section, and inlet quality values recorded. A sketch of the test section showing instrument locations is provided in Figure A.6-1

The experimental apparatus used to conduct the low pressure steam-water flow experiments consisted of a vertically-oriented uniform diameter tube. The test section was about 94.5 inches

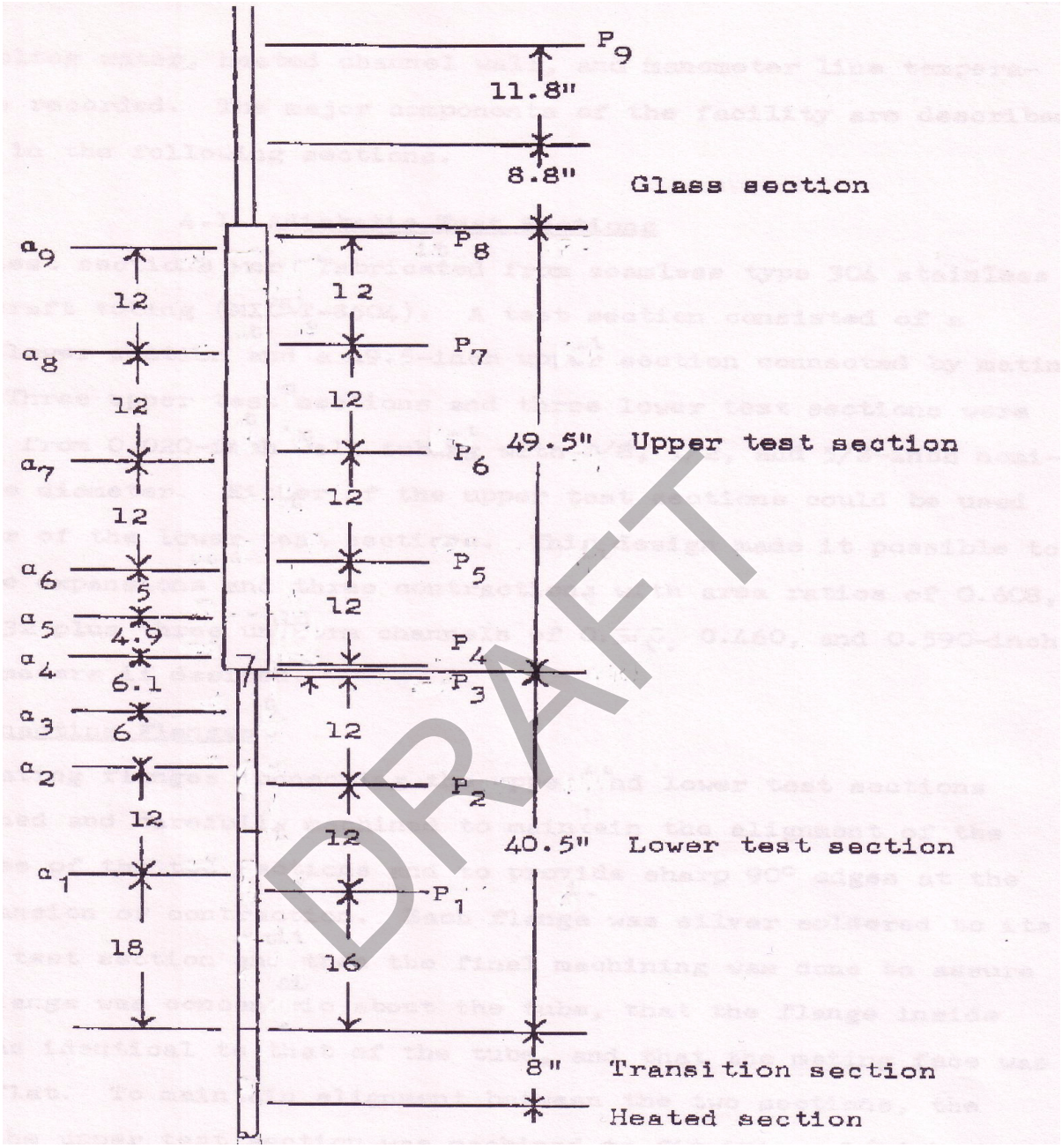

Figure A.6-1. Test Section and Instrumentation Locations for the Two-Phase Flow with Abrupt Expansion or Contraction Experiments.

long. The test section walls were heated during the experiments. Figure A.6-2 shows a diagram of the test section along with instrumentation locations for pressure and void fraction measurements. The experiments were conducted under steady-state conditions with inlet mass flow rates, pressures and void fractions along the test section, and inlet quality values recorded.

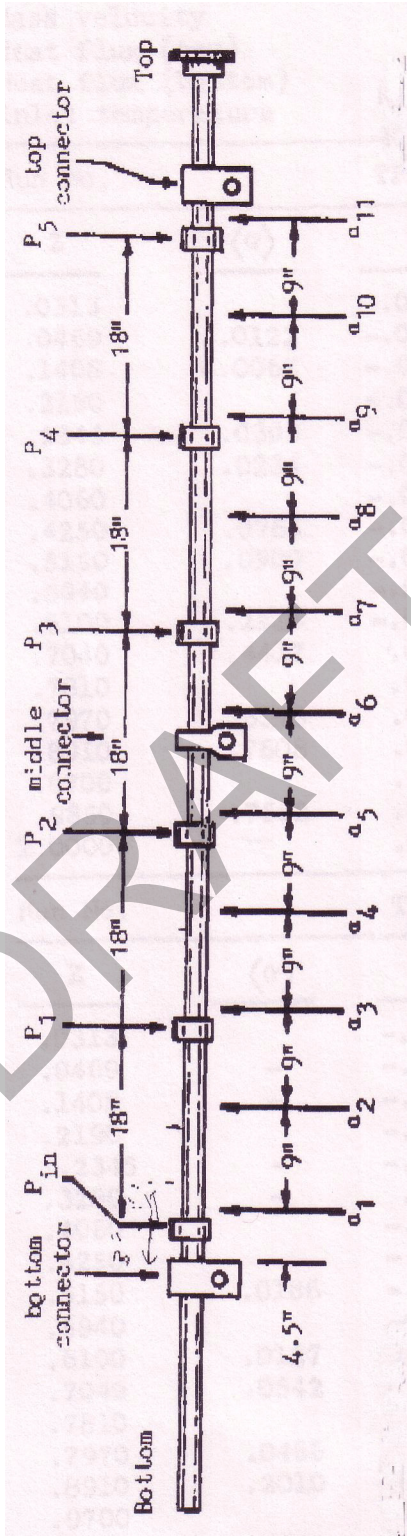

Figure A.6-2. Diagram of the Test Section and Instrumentation Locations for the Low Pressure Steam-Water Flow Experiments.

A.6.3. TRACE Model Description

Five TRACE input files were used in the wall friction assessment study. Two of the input files were set up to check code results against analytical solutions for single-phase liquid and single-phase vapor. Another input file was set up to simulate a falling liquid film in a vertically oriented pipe. The other two input files were used to simulate two-phase experiments using the test apparatus described in **Section A.6.2.**.

The input models used for the single-phase fluid calculations consisted of a PIPE, FILL and BREAK component. The PIPE component represented a 0.0508 m (2 inch) diameter pipe and consisted of three 10 m (32.8 ft) horizontal cells. The FILL component was connected to the PIPE inlet and set liquid/vapor velocities with step increases. The BREAK component represented a constant pressure sink and was connected to the PIPE outlet. Figure A.6-3 shows the nodalization scheme for the TRACE input. The initial condition assumed for the single-phase liquid case was 70 K subcooled liquid at 1.023 MPa. The initial condition assumed for the single-phase vapor case was 30 K super-heated steam at 1.023 MPa. The TRACE control system was used to calculate Re numbers and wall friction factors. Figure A.6-4 shows the signal variables and control blocks used in the control system scheme. A more detailed description and listing of the input models is given in References 5 and 6 .

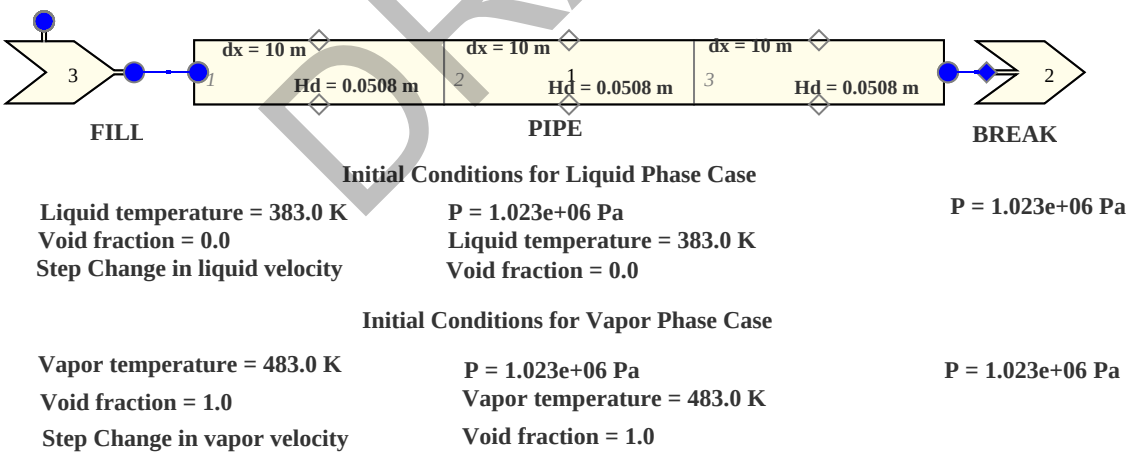

Figure A.6-3. Nodalization for the Single-Phase Fluid Simulations.

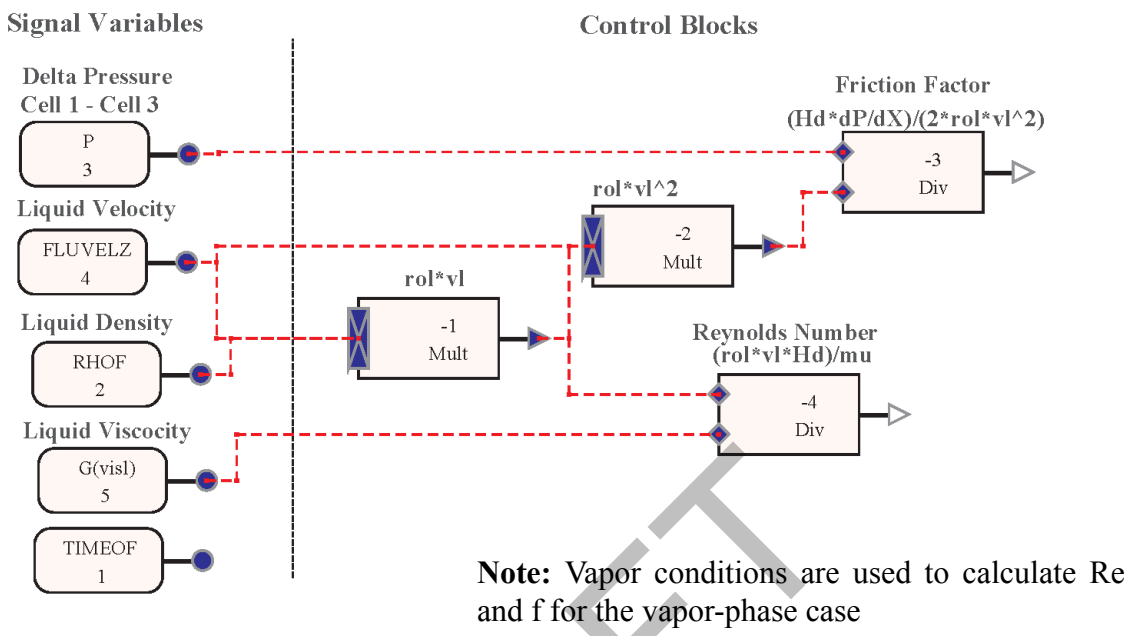

Figure A.6-4. Signal Variables and Control Blocks used to Calculate Reynolds Number and Wall Friction Factors for the Single-Phase Fluid Calculations.

The input model used for the falling film calculation is shown in Figure A.6-5. The input model consisted of a PIPE, FILL and two BREAK components. The PIPE component was vertically oriented downward and contained 20 cells of 0.1 m length. A PIPE diameter of 0.1 m was used. This pipe diameter was selected to assure the liquid injected into the pipe from the FILL remained in annular film flow. The FILL component was attached to PIPE cell 2 and set the liquid inlet velocities with step increases to simulate various film thicknesses with various Re numbers. The BREAK components supply the vapor and pressure conditions in the PIPE component. The falling film data (Ref. 2) used for the comparison are in terms of dimensionless film thickness and Re number. Therefore, the TRACE control system was used to calculate the dimensionless film thickness and Re number for the falling film calculation. Figure A.6-6 shows the signal variables and control blocks used in the control system scheme. A more detailed description and listing of the input models is given in Reference 7.

The TRACE input for the two two-phase flow tests simulated are similar. Both models contain a PIPE, FILL and BREAK component. The PIPE is oriented vertically upward. The FILL is attached to the PIPE inlet and provides the constant two-phase flow conditions into the PIPE. The BREAK is connected to the PIPE outlet and sets a constant pressure. The TPF series experiments applied a constant heat flux to the test section wall. Thus HTSTR components were added to the TRACE input model that simulated these experiments.

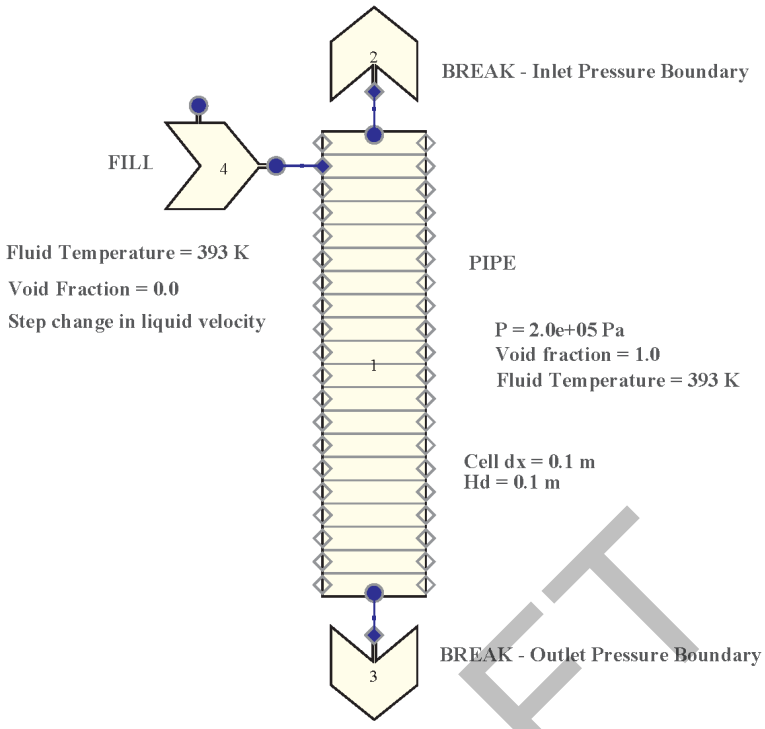

Figure A.6-5. TRACE Nodalization of the Falling Film Input Model.

Figure A.6-7 shows the TRACE noding scheme for the non-heated test section experiments. The PIPE component was divided into 8 axial cells. The centers of cells 1 through 7 correspond to the pressure tap locations for P1, P2, P3, P4, P5, P6, and P7. The BREAK component provides the pressure boundary condition at pressure tap P8 (cell 8). The inlet flow conditions are simulated with the FILL component. A more detailed description and listing of the input models is given in Reference 8.

Figure A.6-8 shows the TRACE noding scheme for the heated test section experiment (Test TPF-46). The PIPE component was divided into 16 axial cells. The centers of cells 1, 4, 7, 10 and 13 correspond to the pressure tap locations for Pin, P1, P2, P3, and P4. The BREAK component provides the pressure boundary condition at pressure tap P5 (cell 16). The inlet flow conditions are simulated with the FILL component. A more detailed description and listing of the input models is given in Reference 9.

A.6.4. Single-Phase Wall Friction Factor Verification

Single-phase flow is a limiting condition of two-phase flow. From the Darcy pressure drop equation (for a horizontal pipe):

$$\frac{dP}{dx} = \frac{1}{2D} f \rho V^2 \tag{6-1}$$

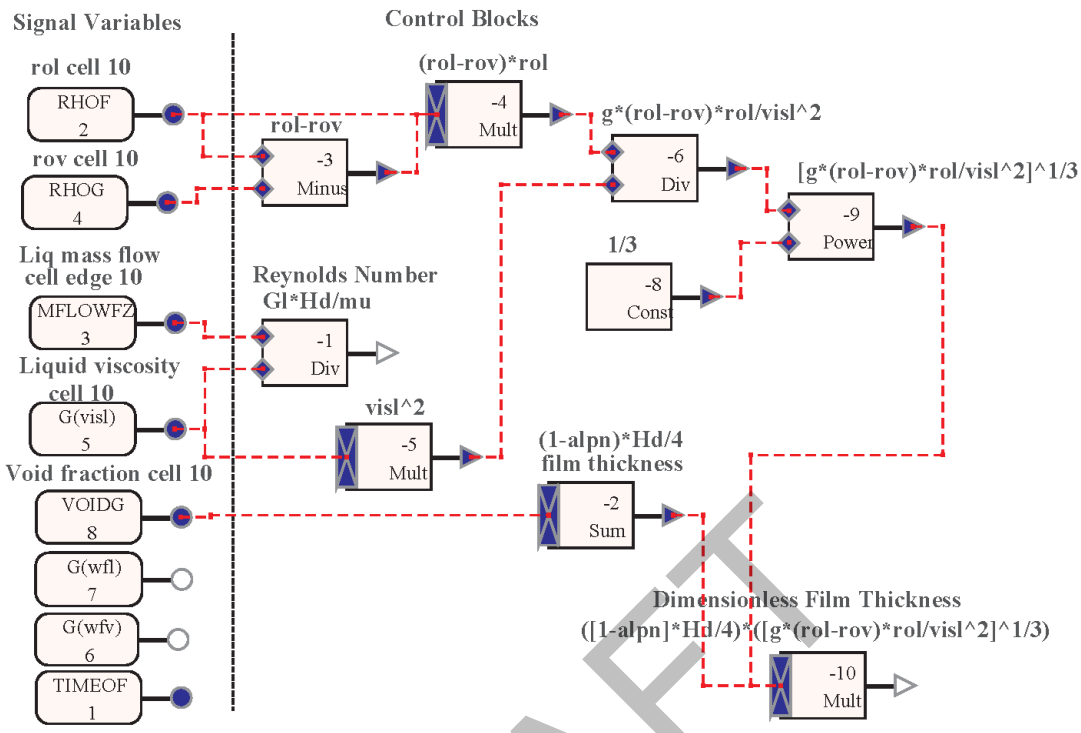

Figure A.6-6. Control System used to Calculate Reynolds Number and Dimensionless Film Thickness for the Falling Film Calculation.

the wall friction factor for a given fluid density, velocity and pressure drop can be calculated. For step increases in flow rates, a profile of wall friction factors versus Re numbers can be obtained. This profile can be compared against a profile generated from wall friction factors calculated using the Churchill friction factor correlation. The Churchill friction factor correlation is used in TRACE. The Churchill correlation is,

$$f = 2\left[\left(\frac{8}{Re}\right)^{12} + \frac{1}{(A+B)^{3/2}}\right]^{1/12} \tag{6-2}$$

where:

$$A = \left[2.457 \ln\left(\frac{1}{\left(\frac{7}{Re}\right)^{0.9} + 0.27\left(\frac{e}{D}\right)}\right)\right]^{16}$$

$$B = \left[\frac{37530}{Re}\right]^{16}$$

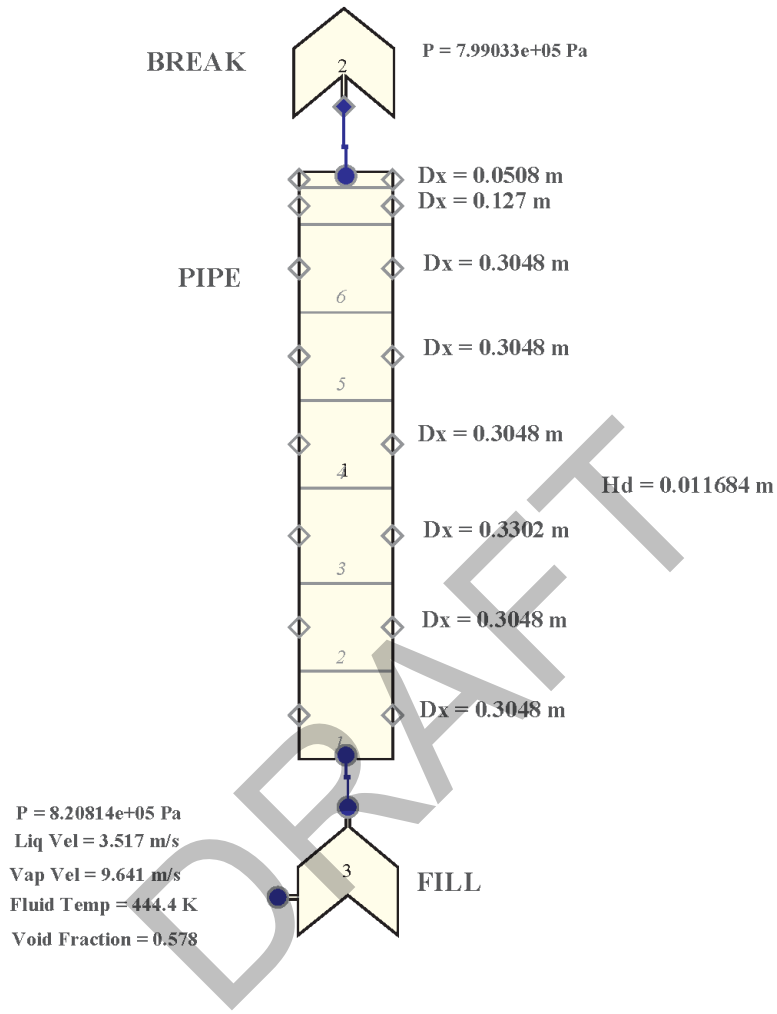

Figure A.6-7. TRACE Nodalization for the Two-Phase Non-Heated Test Series.

where

Re is the Reynold's Number, *e* is the surface roughness, and *D* is the pipe diameter

Wall friction factors calculated for given Re numbers using the Churchill correlation are given in column 3 of Table A.6.1.

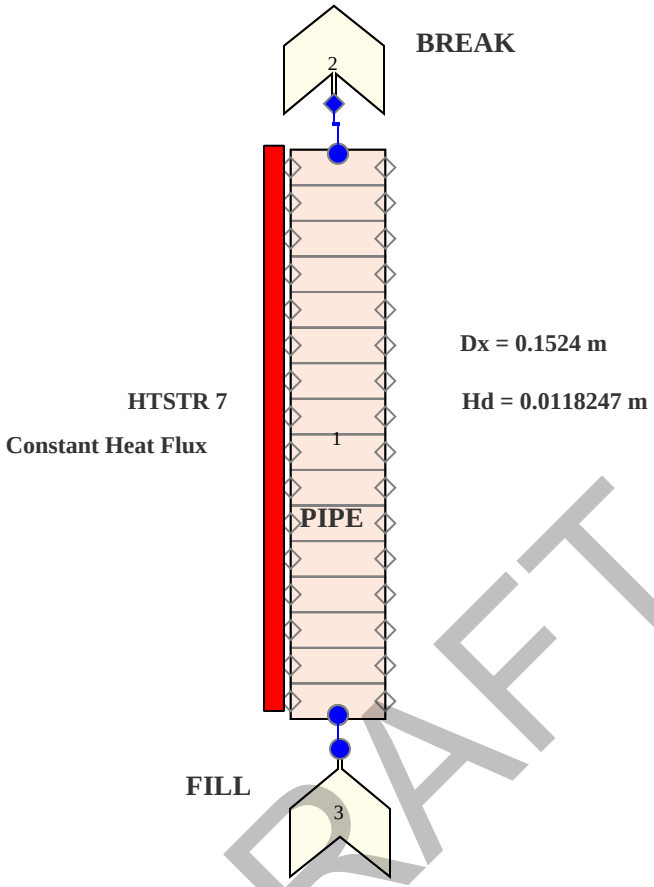

Figure A.6-8. TRACE Nodalization of the TPF Series Pipe Apparatus.

A.6.4.1. Single-Phase Liquid Wall Friction Factor

Liquid velocities for the Re numbers are given in Table A.6.1 and the initial conditions provided in Figure A.6-3 are obtained using the dimensionless relationship:

$$Re = \rho V D / \mu \tag{6-3}$$

where

$\rho =$ 951.4877 kg/m^3

$\mu =$ 2.63612e-04 kg/m-s

and

$D =$ 0.0508 m

The calculated liquid velocities were input into the velocity table in the FILL component (see Figure A.6-3). Reynolds numbers and wall friction factors (based on equation (6-1)) are output values from the TRACE calculation. Table A.6.1 compares the TRACE calculated friction factor based on pressure differential against the Churchill wall friction factor for the given Re number. Exact agreement is shown for Re numbers 500 and greater. For Re numbers less than 500 TRACE under-predicts the Churchill wall friction factor. An investigation showed the liquid velocity is limited to values of 0.001 and greater in the code. At the conditions given for the PIPE component, a velocity of 0.001 yields a Re number of 183.32. The Churchill wall friction factor based on Re number of 183.32 is 0.08728 which is exactly equal to the code-calculated value. The comparison not only shows the friction factor is being calculated correctly, but also assures that the total pressure drop, velocity and density calculated by the code satisfies the fundamental pressure drop equation (6-1).

Table A.6.1. Single-Phase Liquid Wall Friction Factors Based on Pressure Differential Compared to Churchill Calculated Wall Friction Factors.

Reynolds Number	Corresponding Liquid Velocity (m/s)	Churchill Calculated Friction Factor	TRACE Predicted Wall Friction Factor
10	5.4538e-05	1.6	0.08728
100	5.4538e-04	0.16	0.08728
500	2.7269e-03	0.032	0.032
1,000	5.4538e-03	0.016	0.016
5,000	2.7269e-02	9.481e-03	9.482e-03
10,000	5.4538e-02	7.764e-03	7.764e-03
50,000	2.7269e-01	5.224e-03	5.225e-03
100,000	5.4538e-01	4.514e-03	4.514e-03

A.6.4.2. Single-Phase Vapor Wall Friction Factor

Verification of the wall friction factor under single-phase vapor conditions has also been performed using the same process used in the single-phase liquid case. The same input model for the single-phase liquid case is used except all vapor conditions were input. Vapor velocities corresponding to the Re numbers used in the single-phase liquid calculation are given in Table A.6.2.

Table A.6.2 compares the TRACE calculated friction factor based on the differential pressure against the Churchill wall friction factor for the given Re number. The code calculated value for the friction factor matches exactly the value derived from the Churchill correlation except for Re numbers of 50,000 and 100,000. Although the friction factors predicted by the code for these Re

numbers are slightly higher the difference is deemed insignificant and is most likely caused by round off error introduced during the conversion of Reynold's numbers to velocities.

Table A.6.2. Single-Phase Vapor Wall Friction Factors Based on Pressure Differential Compared to Churchill Calculated Wall Friction Factors.

Reynolds Number	Corresponding Vapor Velocity (m/s)	Churchill Calculated Friction Factor	TRACE Predicted Wall Friction Factor
10	7.07755e-04	1.6	1.6
100	7.07755e-03	0.16	0.16
500	3.53878e-02	0.032	0.032
1,000	7.07755e-02	0.016	0.016
5,000	3.53878e-01	9.481e-03	9.481e-03
10,000	7.07755e-01	7.764e-03	7.764e-03
50,000	3.53878e+00	5.224e-03	5.225e-03
100,000	7.07755e+00	4.513e-03	4.516e-03

A.6.5. Wall Friction Factor Verification using Falling Film Data.

Falling Film data (Ref. 2) can be used to verify code calculated wall friction factors in annular flow situations. The falling film input model described in **Section A.6.3.** (refer to Figure A.6-5) injects liquid into the top of the vertical pipe. The liquid flows down the pipe, forming a liquid film. The liquid film thickness is affected by the wall friction factor. The liquid film will reach a constant velocity after a certain distance down the pipe. Values of dimensionless film thickness and film Re numbers are calculated for various liquid injection rates. The calculated dimensionless film thickness and Re numbers are compared to the falling film data.

The dimensionless film thickness is defined as:

$$\delta^* = \delta\left[\frac{g(\rho_f - \rho_g)\rho_f}{\mu^2}\right]^{1/3} \tag{6-4}$$

where:

$$\delta = \frac{(1-\alpha)Hd}{4} \text{ is the dimensional liquid film thickness} \tag{6-5}$$

The film Re number is defined as:

$$\frac{G_l D}{\mu_l} \tag{6-6}$$

where:

G_l is the liquid mass flux, D is the pipe diameter, and μ_l is the liquid viscosity.

Figure A.6-9 shows the TRACE predictions compared to data. The code predicted values show excellent agreement with the falling film data.

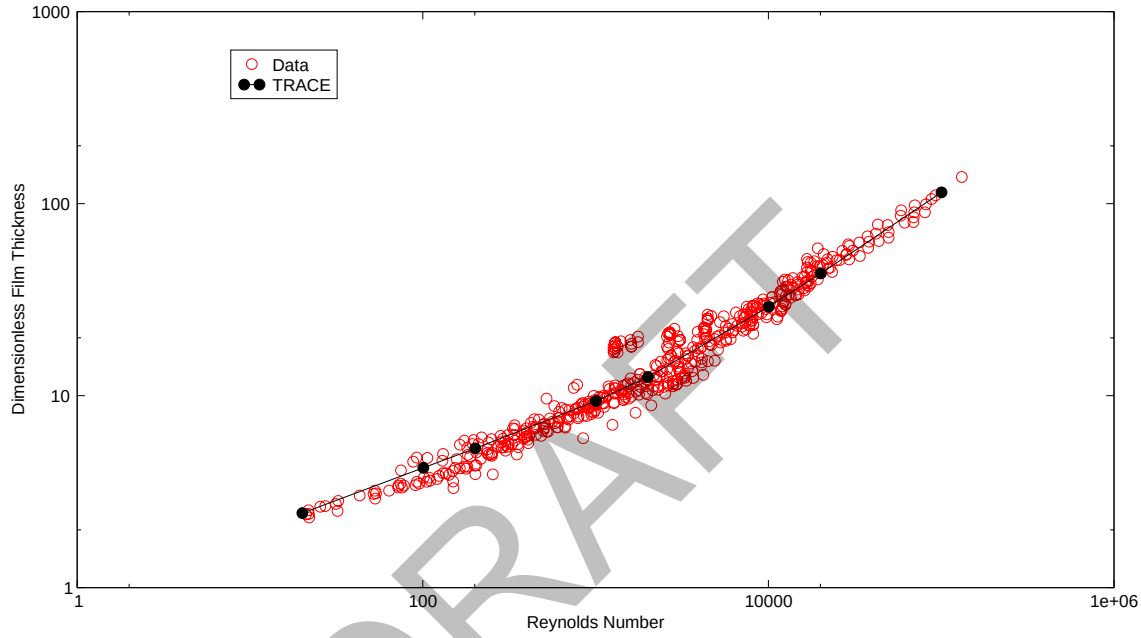

Figure A.6-9. Falling Film Thickness Comparison.

A.6.6. Two-Phase Flow (TPF) Tests

Several two-phase tests performed by Ferrell and McGee (Ref. 3) and Ferrell and Bylund (Ref. 4) are used to assess the TRACE wall friction model.

There were a total of 8 tests simulated from the abrupt expansion and contraction test series (Ferrell and McGee). Because the lower and upper test sections could be arranged to give an abrupt area expansion or contraction, or a straight-through test section (see **Section A.6.2.**), several test section combinations could be made. The assessment study only considered those tests that were conducted in a straight through test section. Thus eliminating the effects of abrupt area expansion or contraction on the two-phase flow. The test sections were adiabatic, i.e. no heat was added to the test section tube walls. Two-phase flow was injected into the test pipe inlet (lower pipe section). Inlet mass flow rate and quality and pressures and void fractions along the

test section were recorded. Table A.6.3 lists the test numbers and thermal-hydraulic conditions of the tests simulated.

Table A.6.3. Test ID and Boundary Conditions for the Two-Phase Test Series without Heated Tube Walls that were Simulated with TRACE.

Test ID	Test Section Diameter (lower and upper) (m)	Pressure (kPa)	Inlet Flow Rate (kg/s)	Inlet Void Fraction
1A-2	0.01168	821.1	0.0581	0.825
1A-6	0.01168	824.6	0.0580	0.981
1A-8	0.01168	818.4	0.0582	0.536
1B-2	0.01168	821.6	0.1157	0.655
1C-3	0.01168	820.8	0.1448	0.578
1D-4	0.01168	406.2	0.0580	0.858
1E-6	0.01168	1647.2	0.0581	0.806
4A-6	0.00864	822.5	0.0582	0.517

The TPF test series was performed under low pressure steam-water flow conditions (Ref. 4). There were 11 tests from this test series simulated with TRACE. The test procedure was similar to the abrupt expansion and contraction test series except the tube wall of the test section was heated. Subcooled liquid was injected into the pipe inlet (at the pipe bottom). Inlet flow and quality, heat flux applied to the tube wall, and pressure and void fraction along the test section were recorded. Table A.6.4 lists the test numbers and thermal-hydraulic conditions of the tests simulated.

Table A.6.4. Test ID and Boundary Conditions for the Two-Phase Heated Tube Test Series Simulated with TRACE.

Test ID	Outlet Pressure (kPa)	Flow Rate (kg/s)	Inlet Temperature (K)[a]	Lower Test Section Heat Flux (W/m^2)[b]	Upper Test Section Heat Flux (W/m^2)
TPF 5	802.4	0.0576	395.0	3.52543e+05	3.40144e+05
TPF 12	806.7	0.0597	426.57	2.71601e+05	2.67858e+05
TPF 20	795.9	0.1163	370.03	5.12789e+05	4.95946e+05
TPF 26	812.3	0.1163	369.05	3.42016e+05	3.30085e+05
TPF 27	808.2	0.1120	365.15	3.49268e+05	3.32190e+05
TPF 37	805.9	0.1164	374.09	2.71834e+05	2.71367e+05
TPF 46	798.6	0.1412	401.45	3.34997e+05	3.25874e+05
TPF 49	812.1	0.1431	383.64	3.44121e+05	3.31488e+05
TPF 50	802.9	0.1946	408.84	3.39208e+05	3.30085e+05
TPF 60	394.6	0.0597	345.28	2.71367e+05	2.69261e+05
TPF 76	1644.4	0.0593	362.98	2.73940e+05	2.67390e+05

a. An inlet enthalpy was calculated based on the pressure and inlet quality. The inlet temperature was then determined from the inlet enthalpy.

b. The heat flux reported was based on the tube inside diameter. The heat flux used in the TRACE simulations was adjusted to the tube outside diameter.

A.6.6.1. TRACE Results from the Simulation of the Adiabatic Tube Test Series.

The two-phase flow pressure drop and void fraction profile along a one-dimensional component predicted by TRACE depends on all of the source terms in the two-phase flow momentum equation working in concert. Wall friction is only one of several momentum source terms. Comparing TRACE predictions to two-phase flow data will give an overall picture of how well the wall friction model is working. The simulated results of Test 1C-3 will be presented in detail. The effects of different inlet flow rates in the simulations are examined using data from Tests 1A-8, 1B-2, and 1C-3. System pressure effects on the simulations are examined using data from Tests 1D-4, 1A-2, and 1E-6. The effects of using different inlet void fractions in the simulations are examined with data from Tests 1A-8 and 1A-6. Finally, simulated effects for different inlet mass fluxes (similar inlet mass flow, but different tube diameters) are examined using data from Tests 1A-8 and 4A-6.

Calculation results for Cell 3, Cell 4 and Junction 4 of PIPE 1 (see Figure A.6-7) of the simulation of Test 1C-3 are used to verify the TRACE momentum equation. The calculation had reached steady-state conditions by 100 seconds.

The first verification is to compare the code calculated wall friction factor with the wall friction factor using the Churchill correlation. The code calculated wall friction factor is obtained through the relationship:

$$wlf = \frac{2f(wfmfl)}{(1-\alpha_{edge})} \tag{6-7}$$

Where *wlf* is a function of the code calculated wall friction factor and a user-supplied wall friction multiplier (*wfmfl*). The variable α_{edge} is the volume-averaged void fraction at a junction. Using a signal variable to define *wlf* and control blocks to calculate α_{edge} at junction 4, the code calculated wall friction factor is 3.982132e-03. The corresponding Re number at junction 4 (calculated by control blocks) is 2.682205e+05. The wall friction factor calculated using the Churchill correlation and the Re number at junction 4 is 3.984681e-03 which compares well with the code calculated value.

A second verification is to compare the frictional pressure drop from the momentum equation with the friction pressure drop using equation (6-1). The frictional pressure drop from the momentum equation is obtained by using steady-state phasic momentum equations for the liquid and vapor. Summing the two phasic momentum equations cancels the interfacial friction terms. After rearranging the terms in the resultant equation, the frictional pressure drop is defined as the total pressure drop minus the acceleration and gravity terms:

$$\nabla P|_f = \nabla P|_{total} - [\alpha\rho_g g + (1-\alpha)\rho_l g + \alpha\rho_g V_g \nabla V_g + (1-\alpha)\rho_l V_l \nabla V_l] \quad (6\text{-}8)$$

The frictional pressure drop was calculated using signal variables and control blocks between Cells 3 and 4. The TRACE-calculated frictional pressure drop is 1.055725e+04 Pa.

The frictional pressure drop using equation (6-1) yields a value of:

$$\nabla P|_f = \frac{2f\rho_l V_l^2}{D_h} = 2 * 3.982132\text{e-}03 * 896.2441 * (4.148)^2 / 0.01168 = 1.051493\text{e+}04 \text{ Pa}$$

The frictional pressure drop from the momentum equation compares well with the frictional pressure drop using equation (6-1).

The calculated void fraction and pressure profiles are compared to data from Test 1C3. Figure A.6-10 compares the void fraction profile from the data with the results from TRACE. The predicted void fraction profile shows good agreement with the data. Figure A.6-11 compares the pressure profile in the test section for Test 1C3. The pressure predicted by TRACE agrees fairly well with the data, although the prediction is obviously better higher up the test section.

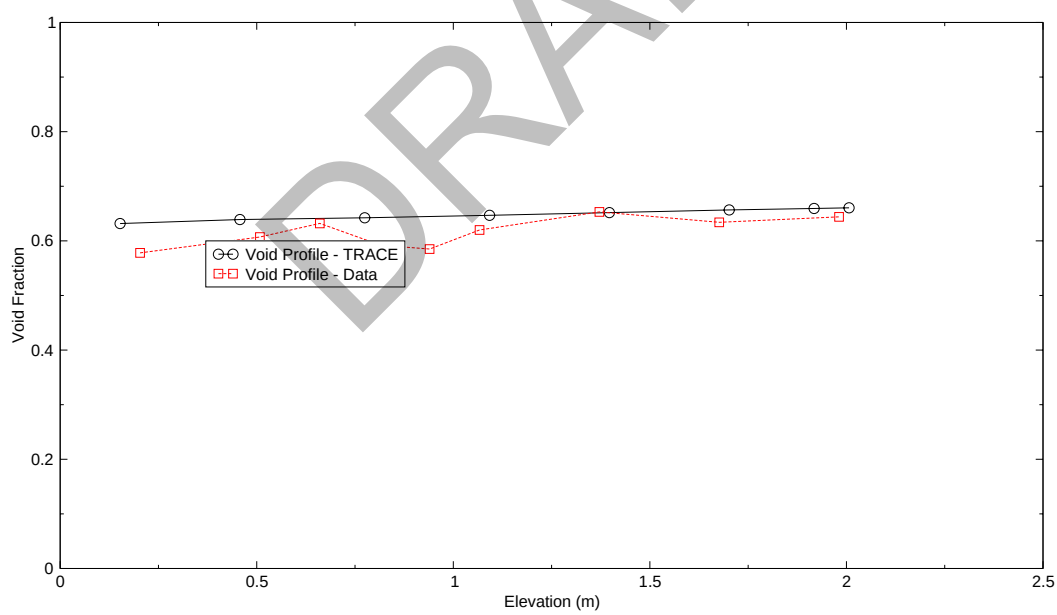

Figure A.6-10. Void Fraction Profile Comparison for Two-Phase Test 1C3.

TRACE simulations of Tests 1A-8, 1B-2, and 1C-3 were made to see how well the code performs in predicting the pressure drop under different two-phase inlet flow rates. Phasic velocities are a

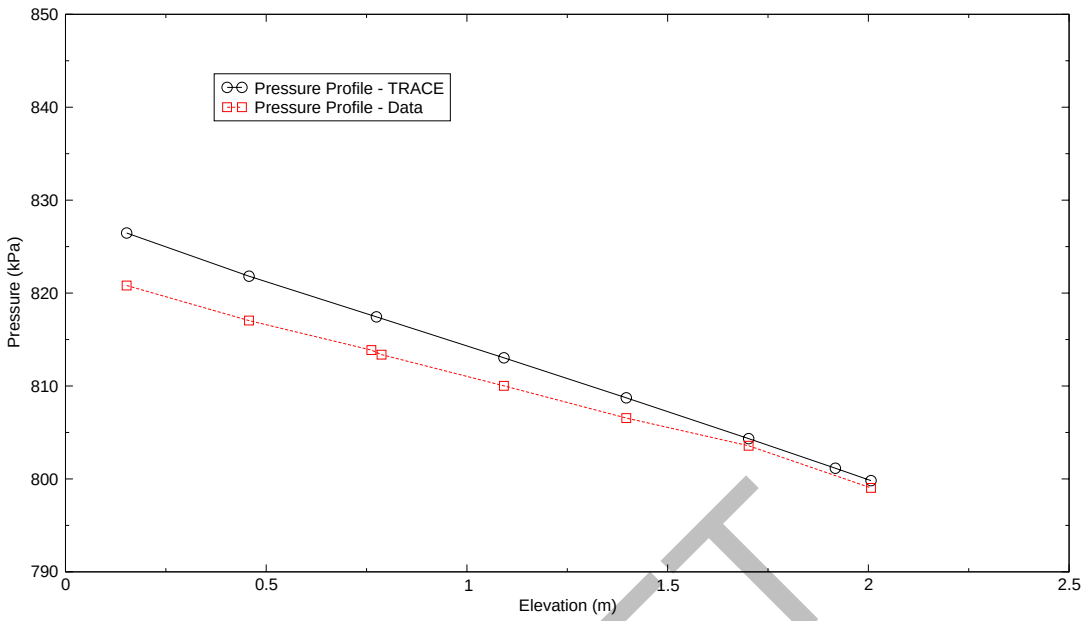

Figure A.6-11. Pressure Profile Comparison along the Test Section for Test 1C3.

function of the inlet flow quality[1] (χ), inlet void fraction (α), fluid density (ρ_l, ρ_v) and the two-phase mass flow rate ($G = (massflow)/(area)$).

The vapor velocity is defined as:

$$V_l = \frac{\chi G}{\alpha \rho_v} \tag{6-9}$$

The liquid velocity is defined as:

$$V_l = \frac{(1-\chi)G}{(1-\alpha)\rho_l} \tag{6-10}$$

There is more slip between the phases at the higher two-phase inlet mass flow rates (3.5 to 9.3 m/s) versus the low mass flow rate (1.3 to 2.6 m/s). Figure A.6-12 shows the comparison of the

1. The qualities reported for the experiments are equilibrium qualities and were calculated from a heat balance assuming that the two phases were in equilibrium. A TRACE calculation was made assuming the phasic velocities were the same. The pressure drop was under-calculated, therefore it was concluded that there was some slip between the phases. There was not enough information given in the data report to calculate the flow quality therefore the equilibrium quality was used to estimate the phasic velocities.

predicted and measured pressure along the tube length for each of the three mass flow rates. The low flow rate case shows excellent agreement with the data. At the higher mass flow rates the predicted pressure at the bottom of the test section is higher than the measured values.

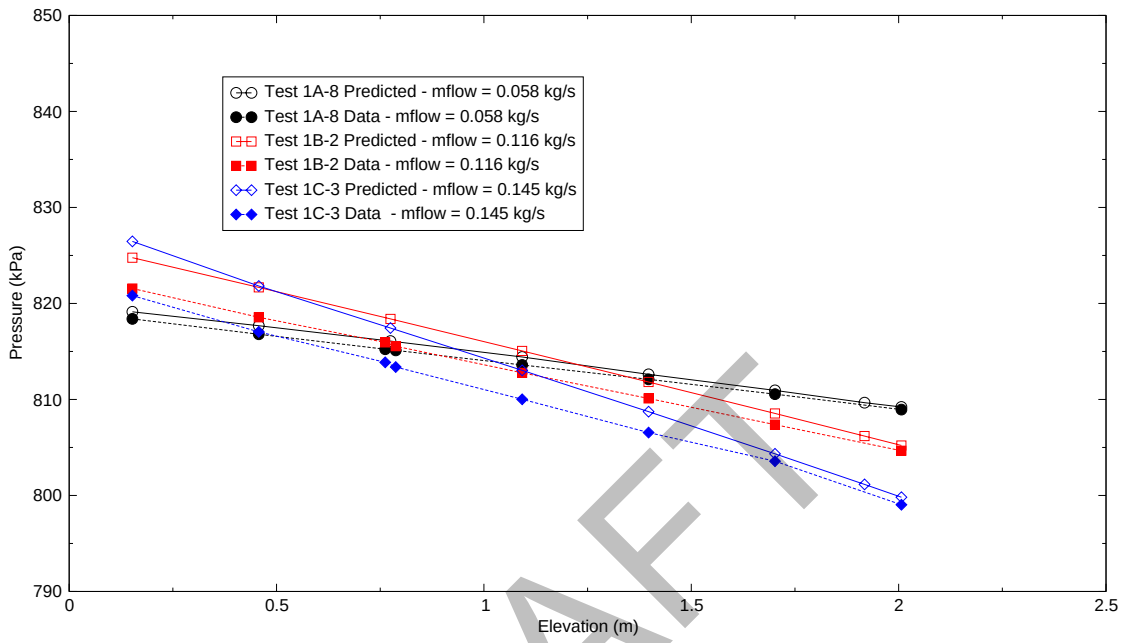

Figure A.6-12. Predicted Versus Measured Pressure Response Along the Tube Length for Different Inlet Mass Flow Rates - Non-Heated Tube.

TRACE simulations of Tests 1D-4, 1A-2, and 1E-6 were made to see how well the code does in predicting the pressure drop under different system pressures. Figure A.6-13 through Figure A.6-15 show the predicted versus measured pressure along the tube length for Test 1D-4 (P = 410 kPa), Test 1A-2 (P = 820 kPa), and Test 1E-6 (P = 1647 kPa), respectively. The predicted pressure along the tube length at the higher system pressure shows excellent agreement with the data. At the lower system pressure the pressure drop is over-predicted. The vapor density at the lower system pressure is smaller than the vapor density at the higher system pressure (about 4 times smaller). As a result the vapor velocity at the lower system pressure is much higher than the vapor velocity at the higher system pressure.

Tests 1A-6 and 1A-8 had similar boundary conditions except for the inlet void fraction. The reported inlet void fraction for Test 1A-8 was 0.536 while the reported inlet void fraction for Test 1A-6 was 0.981. These two tests were simulated to see the effects of inlet void fraction on the pressure drop. Figure A.6-16 shows the predicted and calculated pressure drop along the tube length for Tests 1A-8 and 1A-6. TRACE shows excellent agreement with the data for Test 1A-8 (void = 0.536), however at the higher void fraction TRACE over-predicted the pressure drop. At high void fraction TRACE assumes annular flow, thus a higher pressure drop is expected.

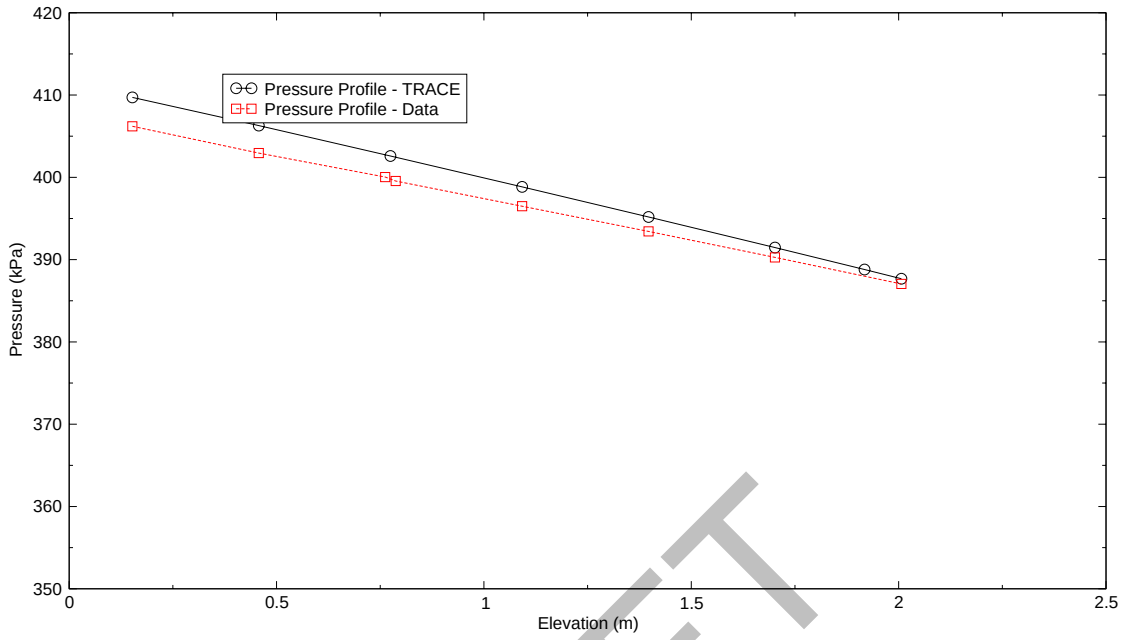

Figure A.6-13. Predicted and Measured Pressure Response Along the Tube Length for a System Pressure of 410 kPa (Test 1D-4) - Non-Heated Tube.

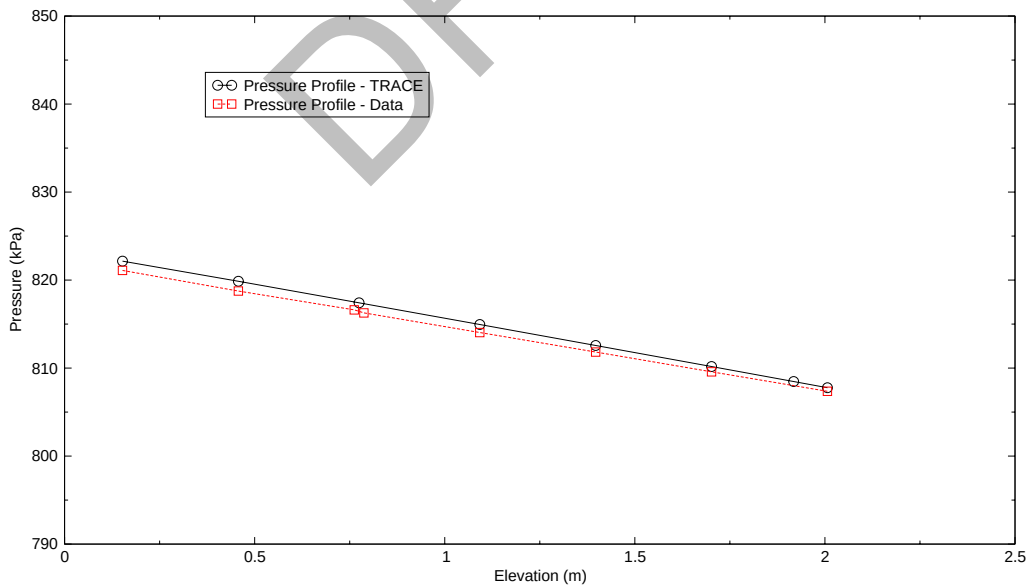

Figure A.6-14. Predicted and Measured Pressure Response Along the Tube Length for a System Pressure of 820 kPa (Test 1A-2) - Non-Heated Tube.

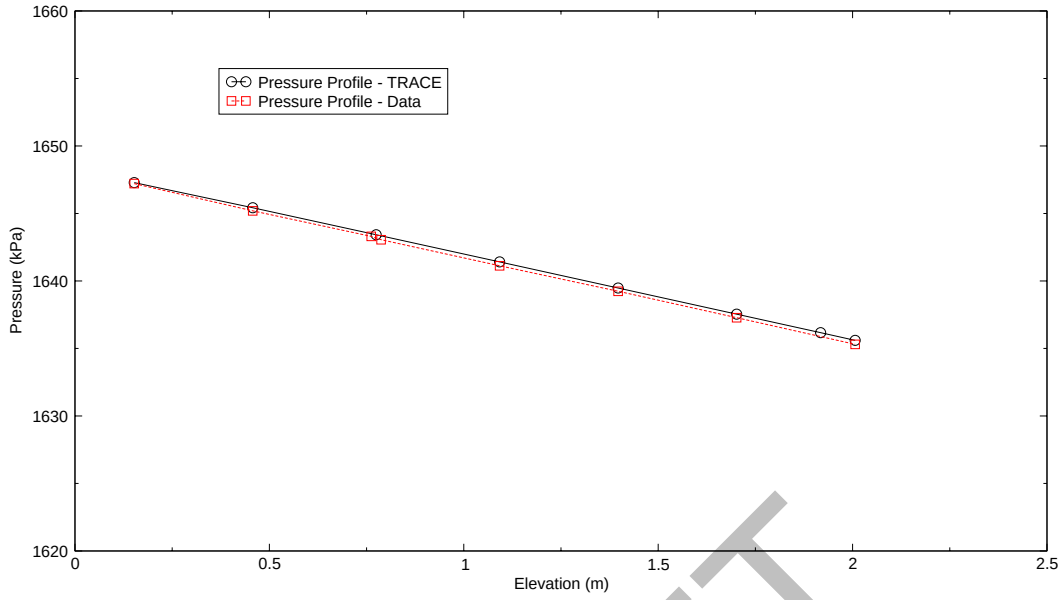

Figure A.6-15. Predicted and Measured Pressure Response Along the Tube Length for a System Pressure of 1647 kPa (Test 1E-6) - Non-Heated Tube.

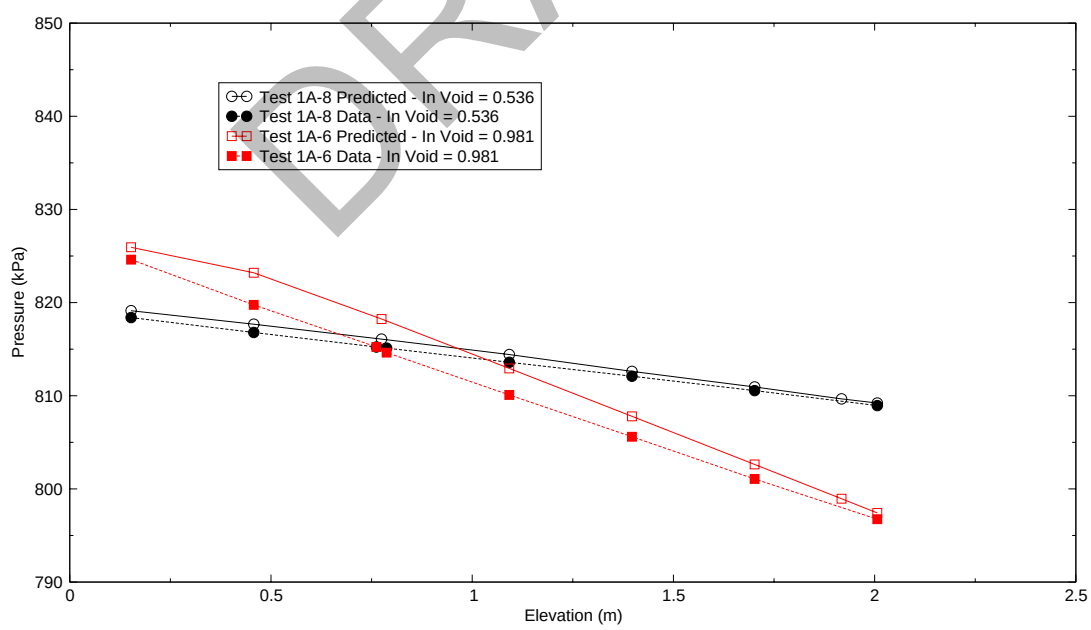

Figure A.6-16. Predicted Versus Measured Pressure Response Along the Tube Length for Different Inlet Void Fractions - Non-Heated Tube.

Tests 1A-8 and 4A-6 were simulated with TRACE to examine the effect of phasic velocities. The boundary conditions were nearly identical for the two tests except Test 1A-8 used a tube diameter of 0.01168 m, whereas Test 4A-6 used a tube diameter of 0.00864 m. Since Test 1A-8 has a larger tube diameter, the phasic velocities are smaller (1.3 [liquid] and 2.6 [vapor] m/s versus 2.3 [liquid] and 5.4 [vapor] m/s). Figure A.6-17 shows the predicted and measured pressure drop along the tube length for these two tests. The mass flux (G) for the smaller diameter tube is larger, thus higher phasic velocities. At higher velocities, the wall friction is higher and consequently a larger pressure drop. This is clearly seen in both the measured data and the calculation in Figure A.6-17. TRACE slightly over-predicted the pressure drop for the case with the smaller diameter tube.

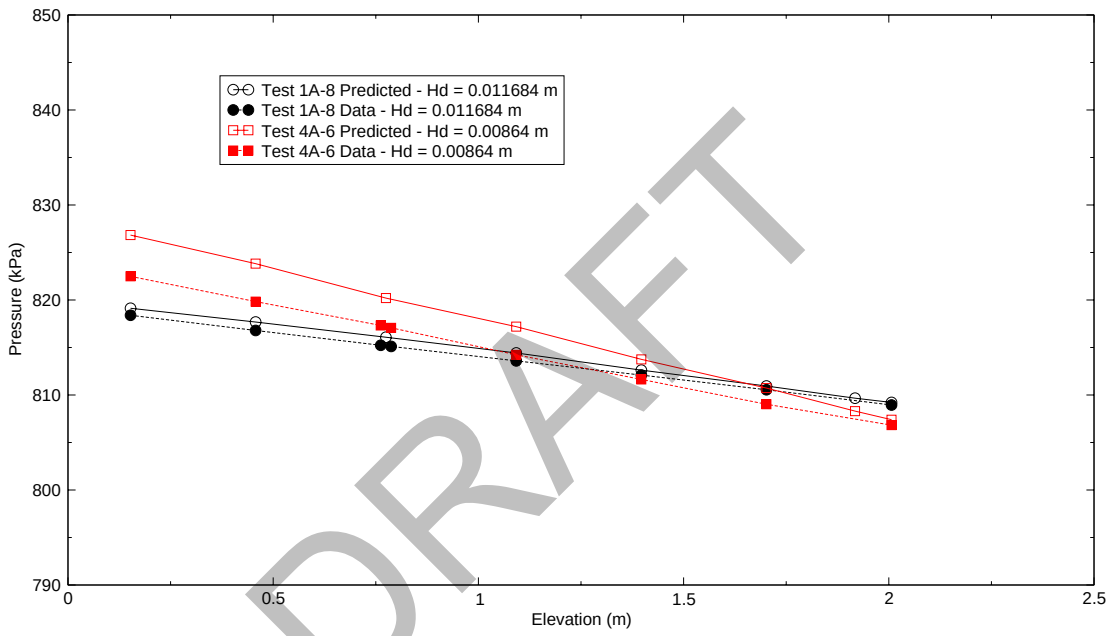

Figure A.6-17. Predicted Versus Measured Pressure Response Along the Tube Length for Different Tube Diameters - Non-Heated Tube.

A figure of merit showing how well the code performs in calculating the wall friction under two-phase flow conditions for the adiabatic test series is a comparison of the measured versus calculated pressure at pressure tap 4 (modeled Cell 4). Figure A.6-18 through Figure A.6-20 shows the measure versus calculated pressure at Cell 4 for the low pressure case (~410 kPa), medium pressure cases (~820 kPa), and high pressure case (~1647 kPa), respectively. As shown, the code shows excellent agreement with the data.

A.6.6.2. TRACE Results from the Simulation of the Heated Tube Test Series.

The method used to verify the momentum equation in **Section A.6.6.1.** is used for the simulation of Test TPF-46. The process is applied to Cells 10 and 11 and Junction 11 (see Figure A.6-8). The

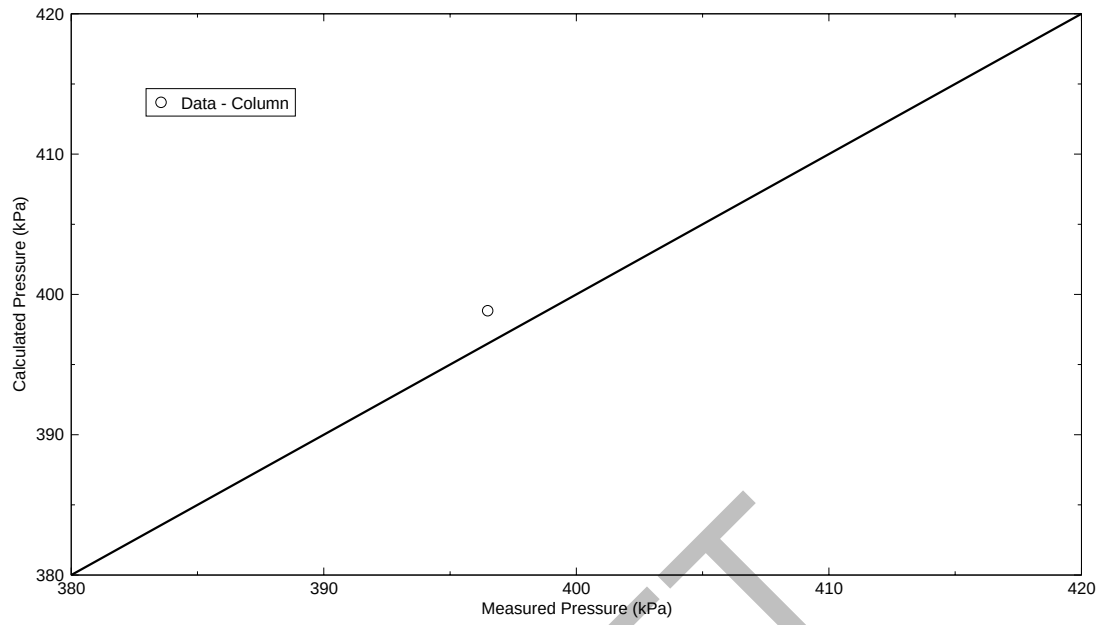

Figure A.6-18. Measured Versus Predicted Pressure at Pressure Tap 4 (Cell 4) for the Non-Heated Tube Test Series Simulated with TRACE - Low Pressure Case.

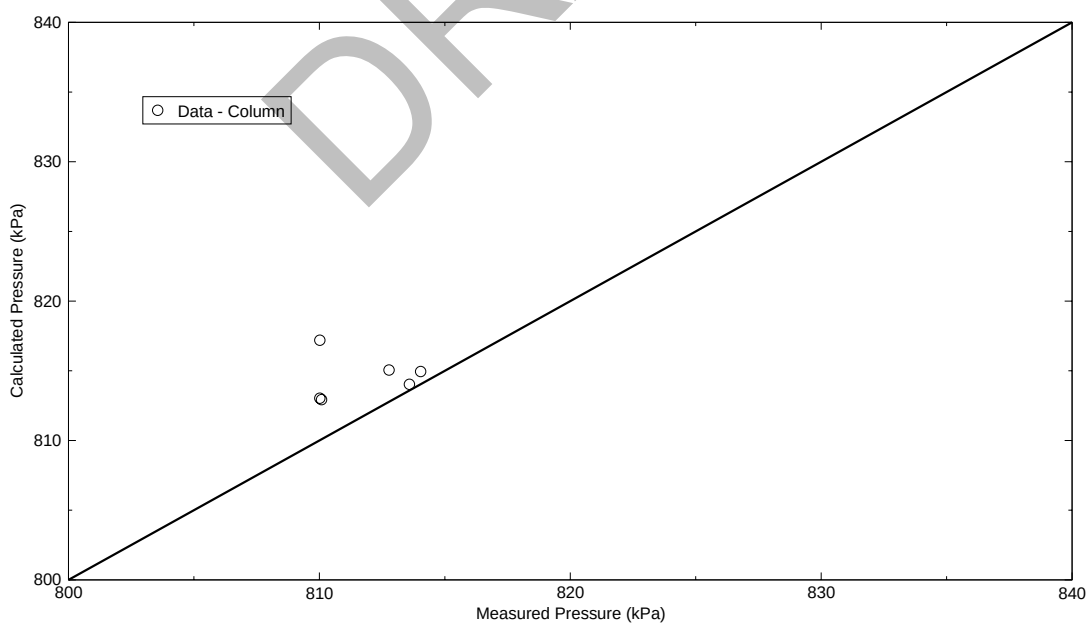

Figure A.6-19. Measured Versus Predicted Pressure at Pressure Tap 4 (Cell 4) for the Non-Heated Tube Test Series Simulated with TRACE - Medium Pressure Case.

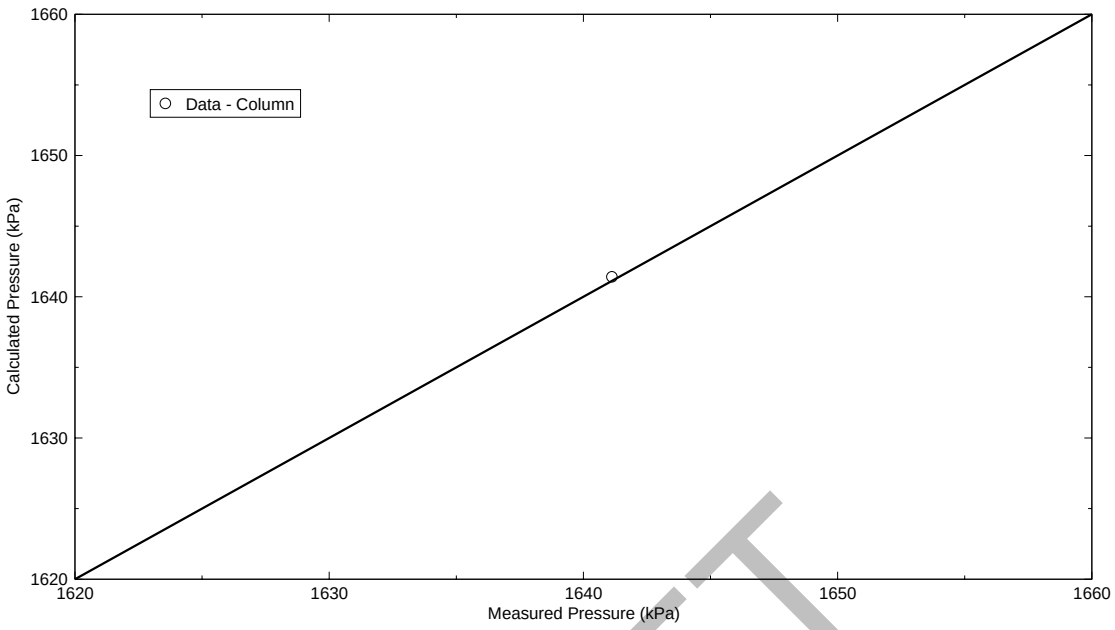

Figure A.6-20. Measured Versus Predicted Pressure at Pressure Tap 4 (Cell 4) for the Non-Heated Tube Test Series Simulated with TRACE - High Pressure Case.

TRACE simulations of Tests TPF-5, TPF-27, TPF-49, and TPF-50 were used to see how variations in the inlet flow rate affect the predicted pressure profile along the heated tube length. Tests TPF-60, TPF-12 and TPF-76 were simulated to examine the effect of different system pressures. TRACE simulations of Tests TPF-37, TPF-26 and TPF-20 were used to examine the effects of tube wall heat flux variations.

Similar differences in the calculated frictional pressure drop observed in **Section A.6.6.1.** are also observed with the simulation of Test TPF-46. With TRACE, the calculated frictional pressure drop using the momentum equation is 6.09429e+03 Pa. The frictional pressure drop using equation (6-1) is 6.40561e+03 Pa.

The calculated void fraction and pressure profiles are compared to data from Test TPF-46. Figure A.6-21 compares the void fraction profile from the data with the results from the prediction. The prediction shows excellent agreement with the data.

Figure A.6-22 compares the pressure profile in the test section for test TPF-46. Although the predicted pressure near the top of the test section is nearly the same for both the base code and the modified code, the pressure predicted by the modified code near the bottom of the test section agrees much better with the data.

Figure A.6-23 shows the comparison of calculated and measured pressure along the tube length for the tests simulated with different inlet mass flow rates (Test TPF-5, TPF-27, TPF-49, and TPF-50). Similar results observed in the tests simulated with different inlet flow rates for the non-

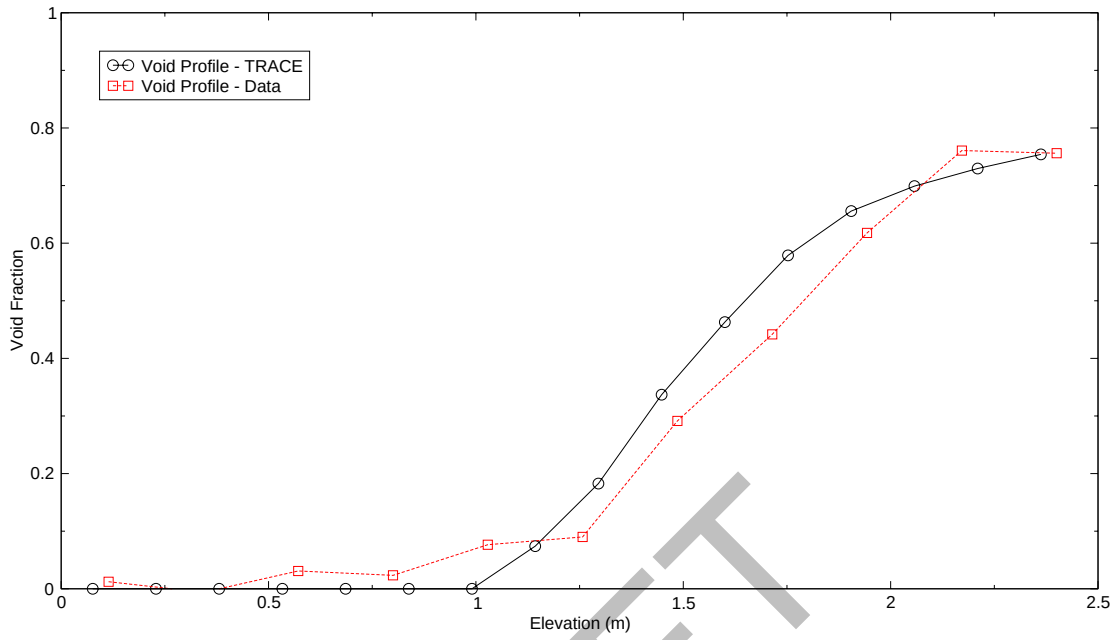

Figure A.6-21. Void Fraction Profile Comparison for Two-Phase Test TPF-46.

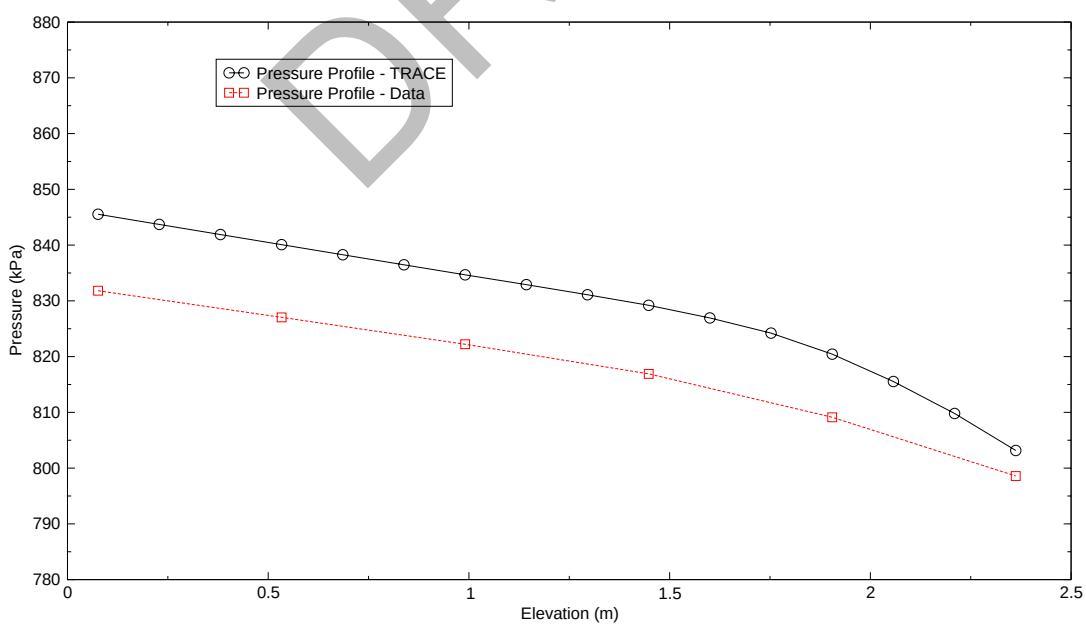

Figure A.6-22. Pressure Profile Comparison along the Test Section for Test TPF-46

heated tube are also noted in these simulations, i.e. the lower the inlet flow rate the better the predicted pressure compares to data.

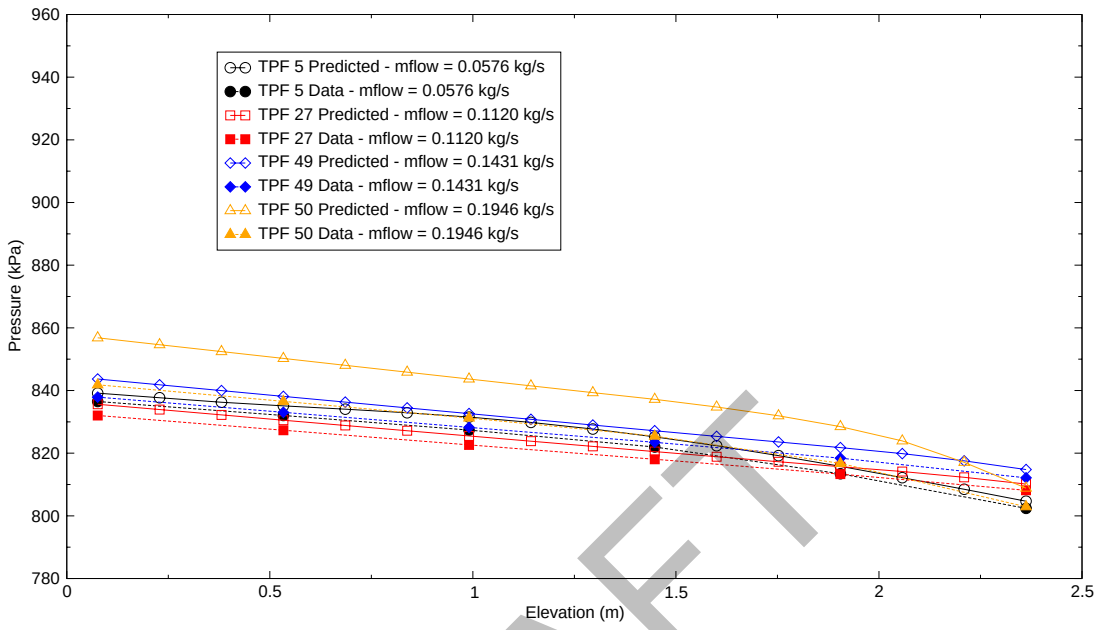

Figure A.6-23. Predicted Versus Measured Pressure Response Along the Tube Length for Different Inlet Mass Flow Rates - Heated Tube.

The calculated pressure response along the tube length compared to data for variations in system pressure is shown in Figure A.6-24 through Figure A.6-26. The system pressures for Tests TPF-60, TPF-12, and TPF-76 are 420, 830 and 1665 kPa, respectively. As in the non-heated tube test series, the higher system pressures resulted in better pressure drop predictions. The predicted pressure drop for the simulations of Tests TPF-12 and TPF-76 show excellent agreement.

Tests TPF-37, TPF-26, and TPF-20 applied different constant heat fluxes to the tube wall. The constant heat flux applied to the tube wall was 366.18 kW/m^2, 453.07 kW/m^2, and 680.00 kW/m^2 for Tests TPF-37, TPF-26, and TPF-20, respectively. The calculated pressure response along the tube length compared to data for different constant heat fluxes applied to the tube wall are shown in Figure A.6-27. The higher heat flux produces more steam and a larger difference between the phasic velocities, thus a higher pressure drop through the tube length. The predicted pressure drop at the higher heat flux was a little higher than observed in the data.

A figure of merit showing how well the code performs in calculating the wall friction under two-phase flow conditions for the heated tube series is a comparison of the measured versus calculated pressure at pressure tap 3 (model Cell 10). Figure A.6-28 through Figure A.6-30 shows the measured versus calculated pressure at Cell 10 for the low pressure case (~420 kPa), medium pressure cases (~830 kPa), and high pressure case (~1665 kPa), respectively. Typically, the code

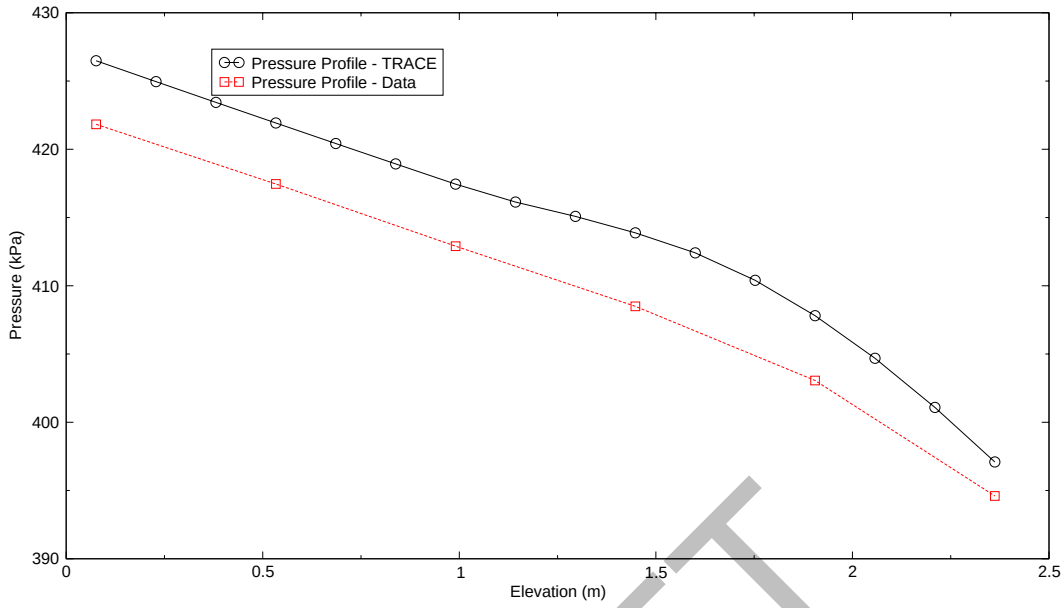

Figure A.6-24. Predicted and Measured Pressure Response Along the Tube Length for a System Pressure of 420 kPa (Test TPF-60) - Heated Tube.

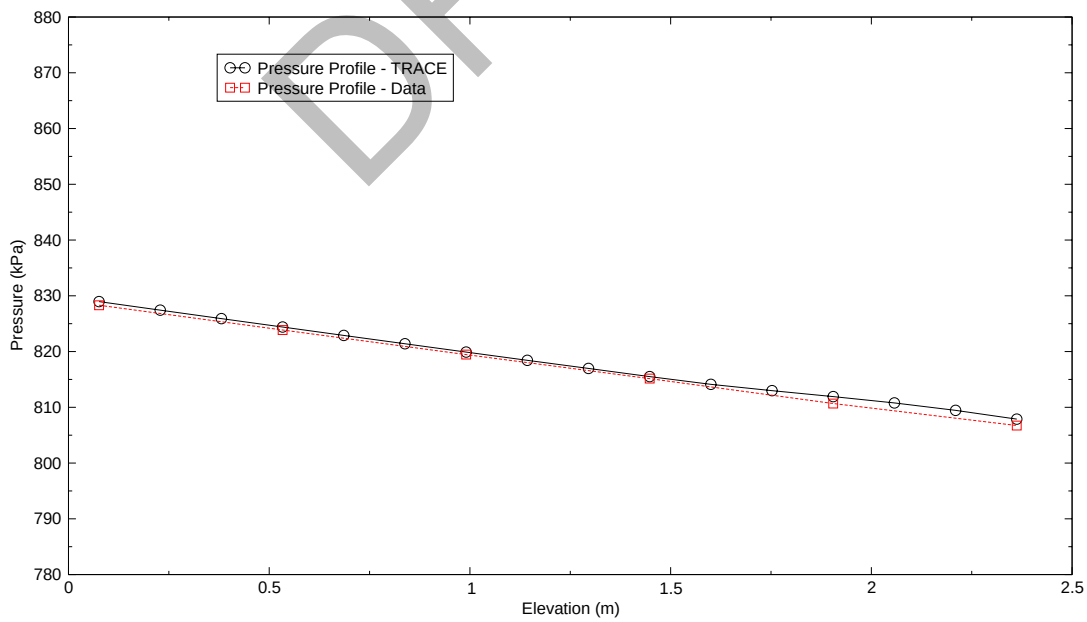

Figure A.6-25. Predicted and Measured Pressure Response Along the Tube Length for a System Pressure of 830 kPa (Test TPF-12) - Heated Tube.

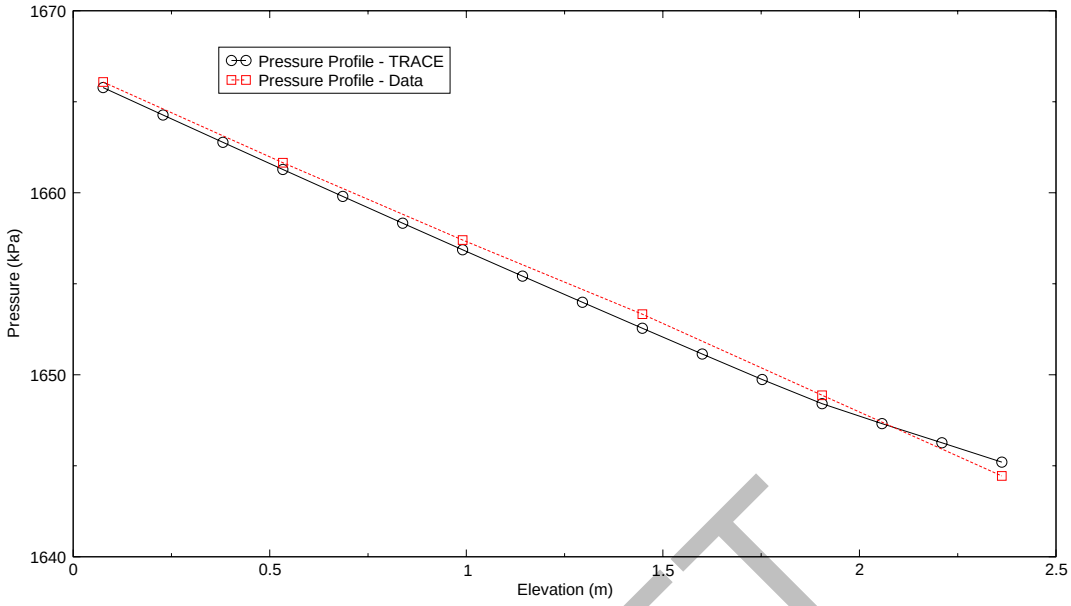

Figure A.6-26. Predicted and Measured Pressure Response Along the Tube Length for a System Pressure of 1665 kPa (Test TPF-76) - Heated Tube

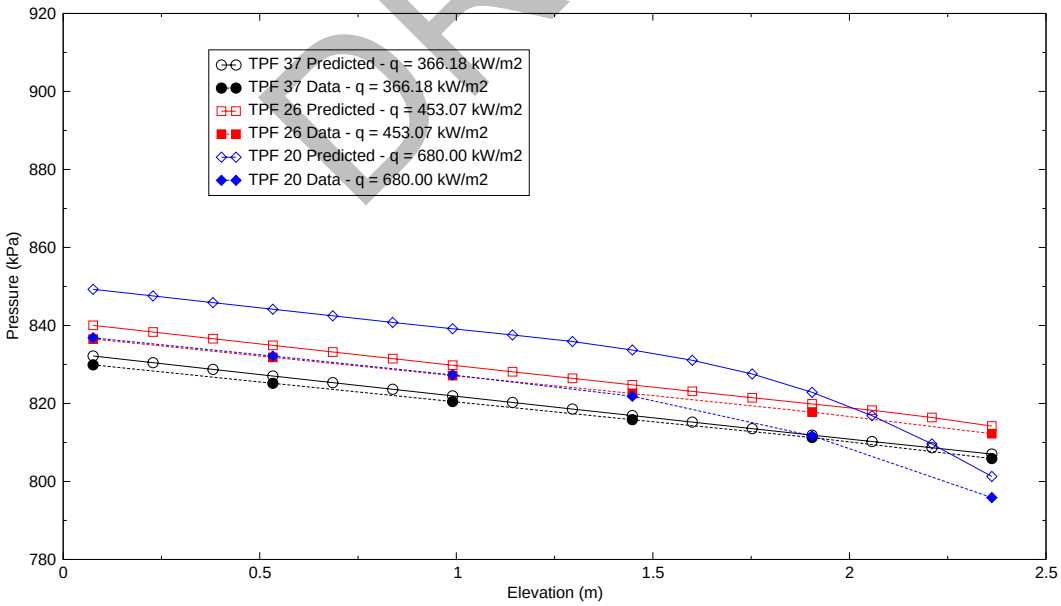

Figure A.6-27. Predicted Versus Measured Pressure Response Along the Tube Length for Different Tube Heat Fluxes - Heated Tube.

slightly over-predicted the measured pressure. However, as shown, the code shows excellent agreement with the data for all cases simulated.

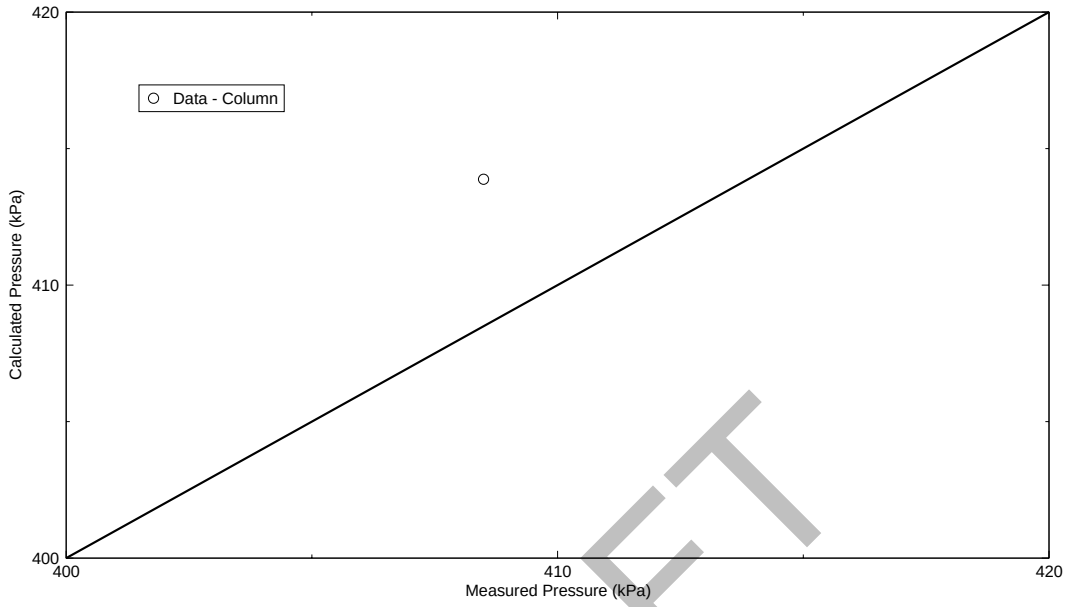

Figure A.6-28. Measured Versus Predicted Pressure at Pressure Tap 3 (Cell 10) for the Heated Tube Test Series Simulated with TRACE - Low Pressure Case.

A.6.7. Assessment Results Summary

Assessment of the single-phase and two-phase wall friction factor models has been performed. Test results of the single-phase liquid wall friction factors showed excellent agreement with the Churchill friction factor correlation except for Reynolds numbers less than 500. A lower limit of 0.001 m/s is placed on the liquid velocity that is used to calculate the Reynolds number used in the friction factor model. Test results of the single-phase vapor also show excellent agreement with the Churchill correlation.

The calculation simulating a falling film in a vertical tube showed excellent agreement with falling film data.

The calculations simulating the two-phase flow experiments for both the non-heated and heated cases showed excellent agreement with the data. The higher pressure cases and the cases with a lower inlet flow rate showed better agreement with the data than those cases with a lower pressure or a higher inlet mass flow rate.

Overall, TRACE has shown it is capable of predicting the wall friction with different thermal/ hydraulic conditions quite well.

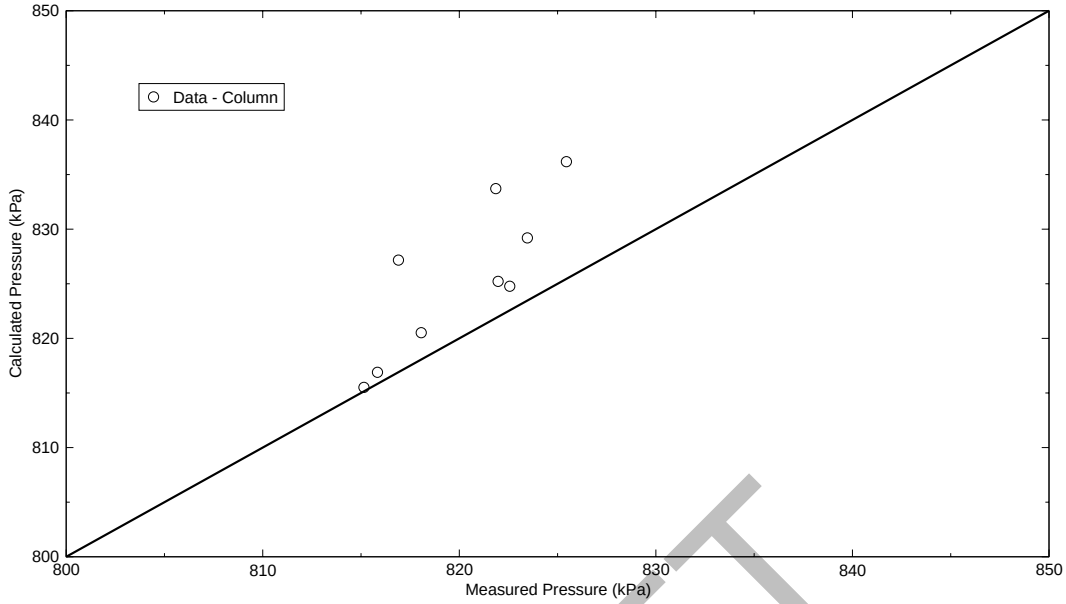

Figure A.6-29. Measured Versus Predicted Pressure at Pressure Tap 3 (Cell 10) for the Heated Tube Test Series Simulated with TRACE - Medium Pressure Cases.

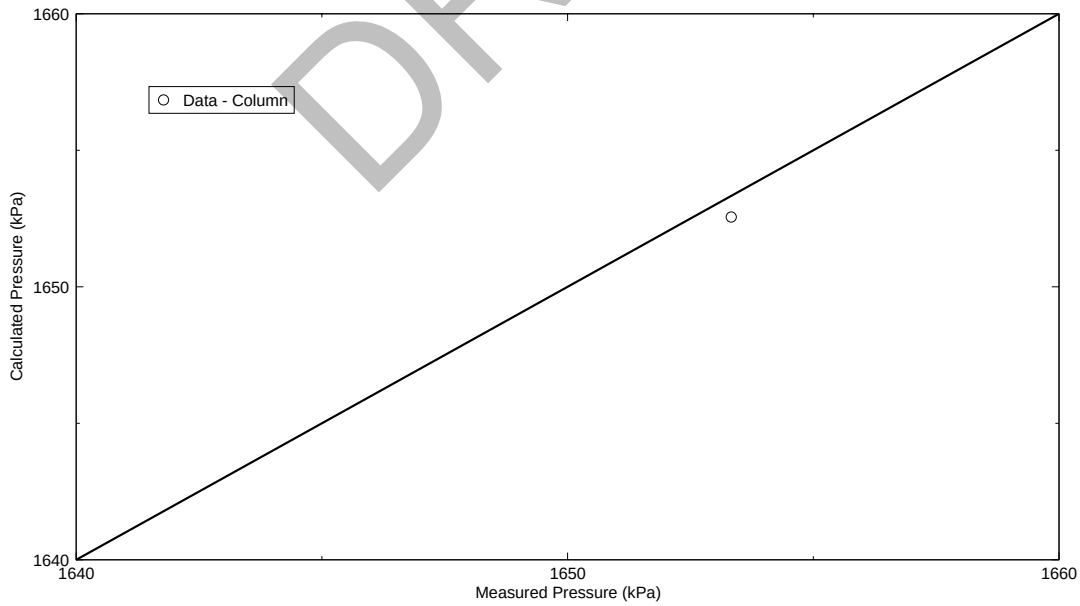

Figure A.6-30. Measured Versus Predicted Pressure at Pressure Tap 3 (Cell 10) for the Heated Tube Test Series Simulated with TRACE - High Pressure Case.

A.6.8. References

1 Churchill, S. W., " Friction-Factor Equation Spans All Fluid-Flow Regimes", Chemical Engineering, 84, No. 24, p. 91 (1977).

2 Weidong Wang, "Two-Phase Wall Friction Model for the TRACE Computer Code", 13th International Conference on Nuclear Engineering (ICONE), Beijing China, May 2005

3 J. K. Ferrell and J. W. McGee, "Final Report Volume III on A Study of Convective Boiling Inside Channels - Two-Phase Flow through Abrupt Expansions and Contractions", TID-23394(Vol.3), USAEC Contract No. AT-(40-1)-2950, N. Carolina State University, Department of Chemical Engineering, Raleigh, NC, June 1966.

4 J. K. Ferrell and D. M. Bylund, "Final Report Volume II on A Study of Convective Boiling Inside Channels - Low Pressure Steam-Water Flow in a Heated Vertical Channel", TID-23394 (Vol. 2), USAEC Contract No. AT-(40-1)-2950, N. Carolina State University, Dept. of Chemical Engineering, Raleigh, NC, June 1966.

5 M. Bolander, "TRACE Calculation Notebook - Single Phase Liquid Wall Friction", May 2006.

6 M. Bolander, "TRACE Calculation Notebook - Single Phase Vapor Wall Friction", May 2006.

7 M. Bolander (ISL), W. Wang (NRC), ""TRACE Calculation Notebook - Falling Film Friction Factors", May 2006.

8 M. Bolander, ""TRACE Calculation Notebook - Two Phase Wall Friction - Non-Heated Wall", May 2006.

9 M. Bolander, ""TRACE Calculation Notebook - Two Phase Wall Friction - With Heated Wall", May 2006.

A.7. Single Tube Flooding - Test of TRACE CCFL Model for Large Pipes

Author(s): Michael B. Rubin

Affiliation: U.S. Nuclear Regulatory Commission

Code Version: TRACE V5.0

Platform and Operating System: Intel x86, Windows XP

A.7.1. Introduction

Counter-current flow limiting (CCFL) is a phenomenon important in several hypothetical accident scenarios. Of particular interest during the reflood period of a large break LOCA, is CCFL and pool formation above the upper core plate following core safety injection. Water that stagnates in the upper plenum and that is held there by CCFL cannot drain into the core and contribute to core cooling. Additionally, CCFL is important in studying flow in steam generator tubes following a small break loss of coolant accident. As the primary system depressurizes steam can condense in the upper part of the steam generator tubes. This flow will utimately be held up at the CCFL point by steam flowing upward.

This section does not compare TRACE results directly to experimental data. Rather, the purpose of the calculations with TRACE is to demonstrate that the TRACE prediction of flooding and CCFL agree with the Wallis correlation for small tubes (one inch diameter) and the Kutateladze correlation for large tubes (eight inch diameter).

The TRACE Theory Manual (Ref. 1) describes the Bankoff CCFL model, and the Wallis and Kutateladze models. Bankoff's form of the CCFL correlation (Ref. 2) was developed using data from eight different plate geometries, including the 15-hole plate used for another assessment (see Appendix B, section B.18.)

A.7.2. CCFL Theory

For a range of plate geometries Bankoff, et al. (Ref. 2) were able to correlate their data using dimensionless superficial gas and liquid velocities H_k^* {k = f (liquid) or g (gas)} scaling as

$$(H_g^*)^{\frac{1}{2}} + (H_f^*)^{\frac{1}{2}} = C \tag{7-1}$$

where

$$H^*_k = j_k \left(\frac{\rho_k}{gw(\rho_f - \rho_g)} \right)^{\frac{1}{2}}, \qquad (k = f, g) \tag{7-2}$$

and

j_k = volumetric flux or superficial velocity

g = acceleration due to gravity

ρ_k = density of phase k

D = hole or pipe diameter constant

n = the number of holes in the plate,

σ = surface tension

w = interpolative reference length between Wallis and Kutateladze scaling

L = Laplace capillary constant used by Kutateladze defined below

L^* = Bond Number defined below

β = empirical parameter defined below

k_c = critical wave number = $2\pi/t_p$

t_p = thickness of plate

γ = ratio of area of holes to area of plate (= 1.0 for a pipe)

The coefficient C is given by:

$$w = D^{(1-\beta)} L^{\beta} \tag{7-3}$$

$$L = \sqrt{\sigma/(g(\rho_f - \rho_g))} \tag{7-4}$$

$$\beta = \tanh(\gamma k_c D) \tag{7-5}$$

When β = 0, the Wallis scaling results and for β = 1 Kutateladze is obtained. For the Wallis Correlation, C should be 0.8 while C = 1.79 for Kutateladze.

A.7.3. TRACE Input Model Description

The TRACE input model to examine single tube flooding consists of 7 components as shown in Figure A.7-1. Two one-dimensional TEEs with four nodes each are connected with a CCFL model turned on at the junction connecting the two TEEs. CCFL correlations can be invoked by TRACE at specific locations as a user option. The lower TEE is connected to a FILL from which steam or air is injected. The upper TEE is connected to a FILL through which water is injected. The lower TEE is connected to a PIPE component that is essentially a large tank to collect liquid, which is connected to a FILL so that water can escape from the system. The upper TEE is connected to a BREAK so that steam or air can escape from the system.

Initial maximum water and steam or air mass flow rates were calculated using an EXCEL spreadsheet that calculates superficial dimensionless velocities for liquid and gas for the CCFL correlation used. This provided the points (1,0) and (0,1) on the flooding or CCFL instability curve for the system pressure used. An example of this curve is Figure A.7-2 from Reference 2. From these points the maximum mass flow rates for the system thermodynamic conditions at which CCFL exists were then determined. Two pressures, 4.13679 MPa (600 psia) and .137892 MPa (20 psia) were studied.

Each case was run as a steady-state calculation with steam or air injected from FILL 41 and water injected from FILL 141. Values of initial water and steam or air mass flow rates to start the TRACE calculations were determined using an EXCEL spreadsheet that calculates superficial dimensionless velocities for liquid and gas for the Wallis and Kutateladze CCFL correlations.

The calculations and analyses were done in two steps. First a calculation was performed to get the steady-state maximum water and steam velocities at the CCFL junction at the ends of the flooding curve. The thermodynamic conditions throughout the system were then retrieved as the starting point for a transient calculation starting with the initial maximum steam or air and liquid flow rates.

The steam or air flow rate was linearly decreased from its maximum initial condition to zero over a substantial time period, which was chosen as 2000 seconds. The liquid flowrate is held constant throughout the transient. With these flowrate conditions there is initially no liquid flowing down the tees and through the CCFL junction because the system is at a CCFL condition. All the liquid

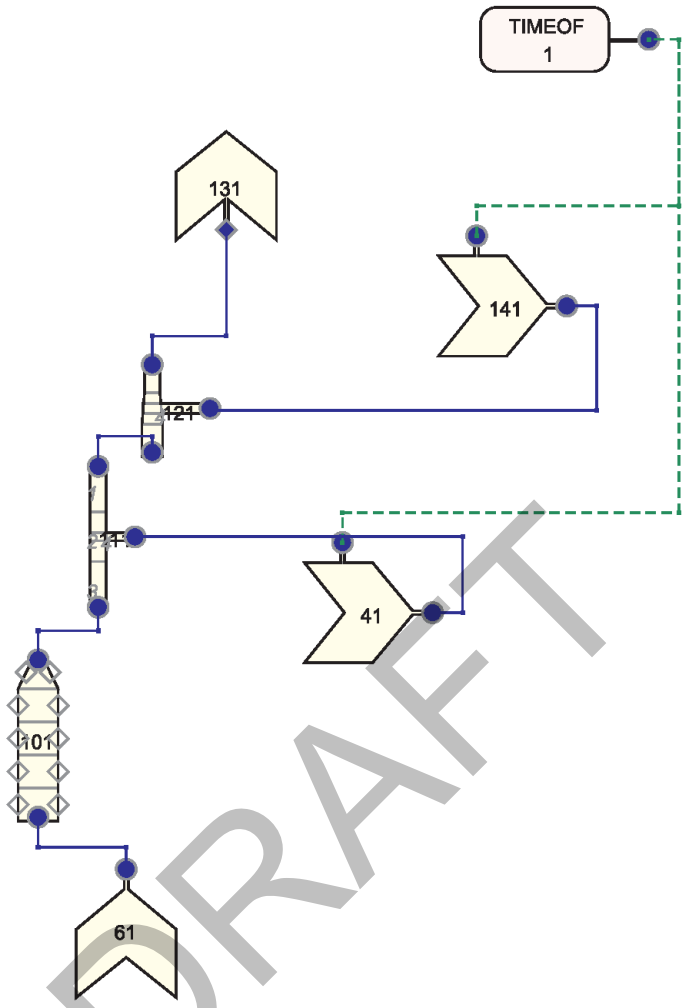

Figure A.7-1. TRACE Noding Diagram for Single Tube Flooding

is being carried up through the system by the steam. As the steam flowrate decreases liquid is able to flow down through the CCFL junction always at the CCFL point for the steam flow going up. The thermodynamic conditions at the CCFL junction versus time are then used to calculate flooding curves using control variables.

The results show that the CCFL model is in general working properly. Figure A.7-3 shows a plot of calculated square root of dimensionless superficial gas velocity divided by C versus the same for the liquid for a 0.0254m (1 inch) pipe with water and steam at 0.137892 MPa (20 psia). The expected Wallis flooding curve is also plotted. The results show that TRACE follows the expected trend, starting at (0,1) and heading towards (1,0) with a slope of 1.0. The TRACE transient was stopped when chugging began in the system, due to the vapor not being able to hold up the liquid any longer.

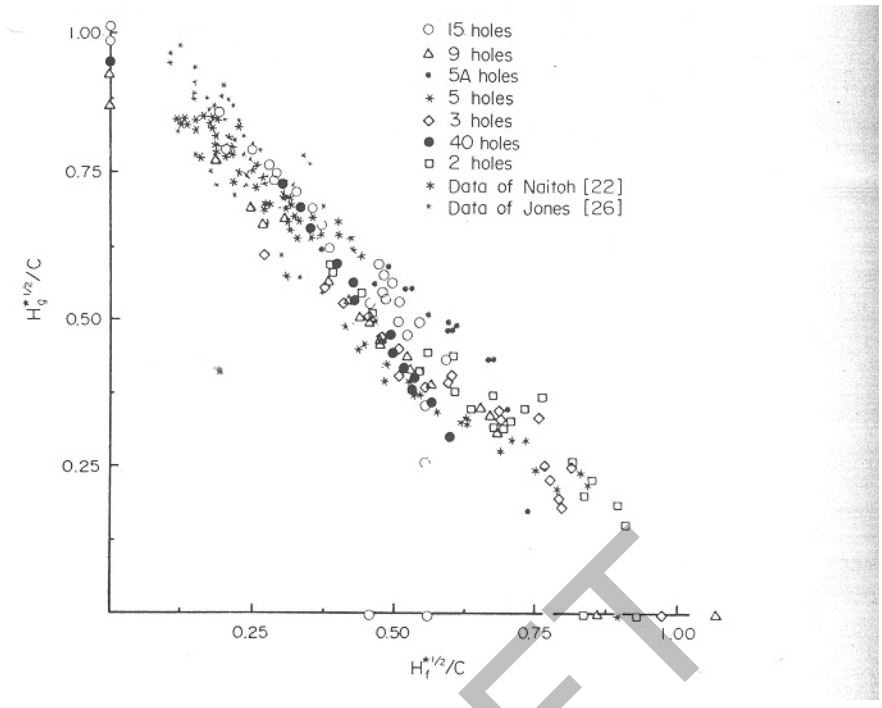

Figure A.7-2. Typical Flooding Curves for Air-Water

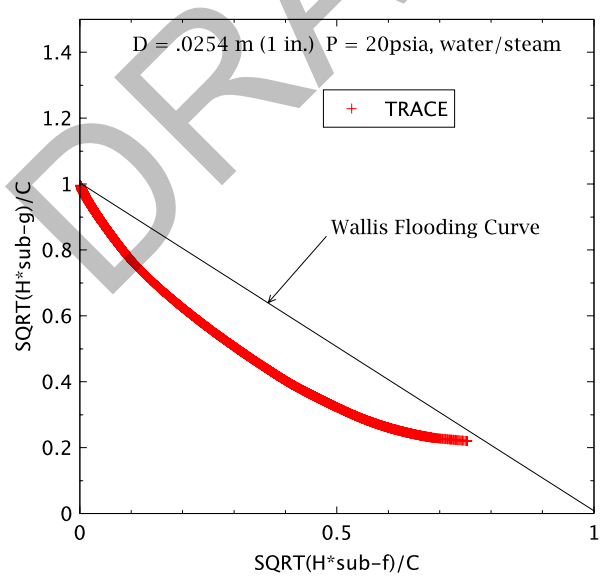

Figure A.7-3. TRACE Gas Versus Liquid Dimensionless Superficial Velocity for a .0254 m (1 in.) Pipe with Water and Steam at .137892 MPa (20 psia)

Figure A.7-4 shows a plot of calculated square root of dimensionless superficial gas velocity divided by C versus the same for the liquid for a 0.0254 m (1 inch) diameter pipe with water and air at 0.137892 MPa (20 psia). The expected Wallis flooding curve is also plotted. The results

show that TRACE follows the expected trend, starting at (0,1) and heading towards (1,0) with a slope of 1.0. The TRACE transient was stopped when chugging began in the system, due to the vapor not being able to hold up the liquid any longer.

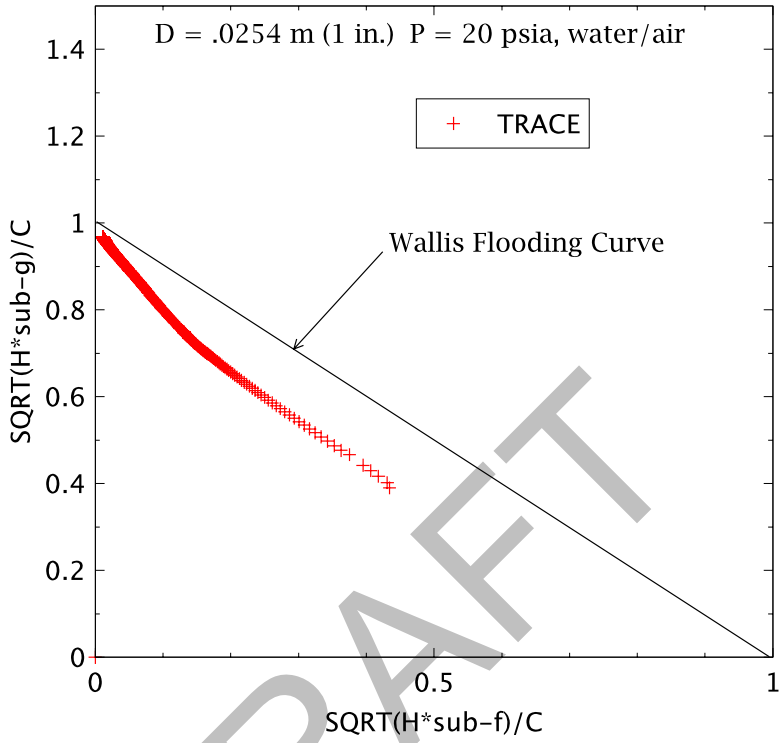

Figure A.7-4. TRACE Gas Versus Liquid Dimensionless Superficial Velocity for a .0254 m (1 in.) Pipe with Water and Air at .137892 MPa (20 psia)

Figure A.7-5 shows a plot of TRACE calculated square root of dimensionless superficial velocity divided by C versus the same for the liquid for a 0.0254 m (1 inch) diameter pipe with water and steam at 4.13679 MPa (600 psia). The expected Wallis flooding curve is also plotted. The results show that TRACE follows the expected trend, starting at (0,1) and heading towards (1,0) with a slope of 1.0. The TRACE transient was stopped when chugging began in the system, due to the vapor not being able to hold up the liquid any longer. Each cross is a point in time. The outliers are most likely due to instability at the CCFL junction at that particular time.

Figure A.7-6 shows a plot of calculated square root of dimensionless superficial gas velocity divided by C versus the same for the liquid for a 0.203 m (8 inch) diameter pipe with water and steam at .137892 MPa (20 psia). The expected Kutateladze flooding curve is also plotted. The results show that TRACE follows the expected trend, starting at (0,1) and heading towards (1,0) with a slope of 1.0. The TRACE transient was stopped when chugging began in the system, due to the vapor not being able to hold up the liquid any longer.

Figure A.7-7 shows a plot of calculated square root of dimensionless superficial gas velocity divided by C versus the same for the liquid for a .203 m (8 inch) pipe with water and air at

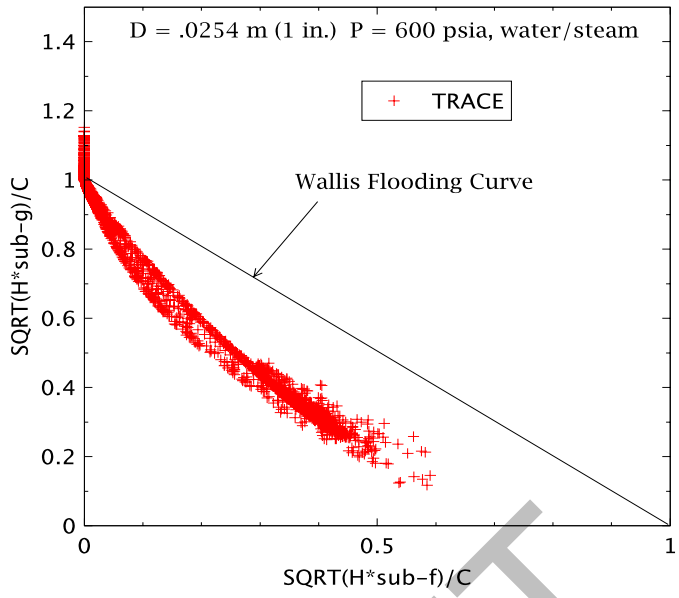

Figure A.7-5. TRACE Gas Versus Liquid Dimensionless Superficial Velocity for a .0254 m (1 in.) Pipe with Water and Steam at 4.13679 MPa (600 psia)

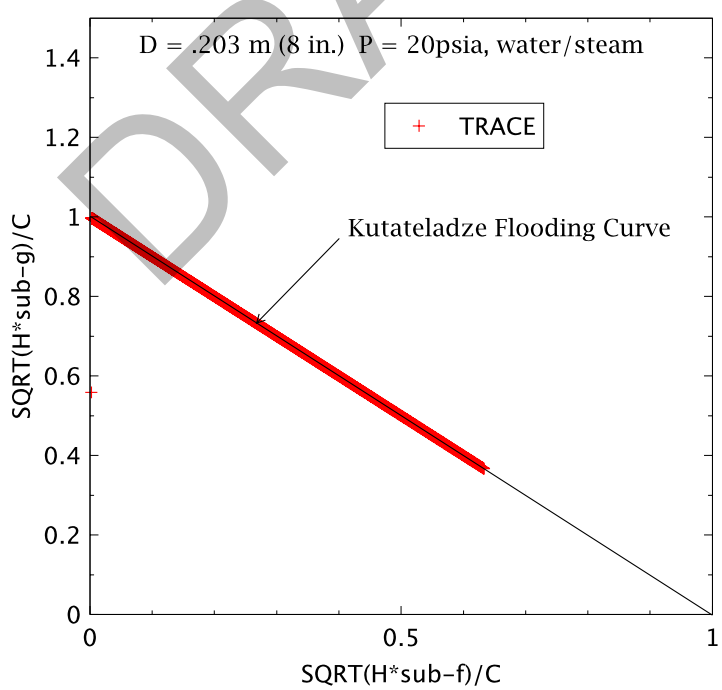

Figure A.7-6. TRACE Gas Versus Liquid Dimensionless Superficial Velocity for an .203 m (8 in.) Pipe with Water and Steam at .137892 MPa (20 psia)

0.137892 MPa (20 psia). The expected Kutateladze flooding curve is also plotted. The results show that TRACE follows the expected trend, starting at (0,1) and heading towards (1,0) with a slope of 1.0. The TRACE transient was stopped when chugging began in the system, due to the vapor not being able to hold up the liquid any longer. Each cross is a point in time. The outliers are most likely due to instability at the CCFL junction at that particular time.

Figure A.7-8 shows a plot of calculated square root of dimensionless superficial gas velocity divided by C versus the same for the liquid for a 0.203 m (8 inch) pipe with water and steam at 4.13679 MPa (600 psia). The expected Kutateladze flooding curve is also plotted. The results show that TRACE follows the expected trend, starting at (0,1) and heading towards (1,0) with a slope of 1.0. The TRACE transient was stopped when chugging began in the system, due to the vapor not being able to hold up the liquid any longer. Each cross is a point in time. The outliers are most likely due to instability at the CCFL junction at that particular time.

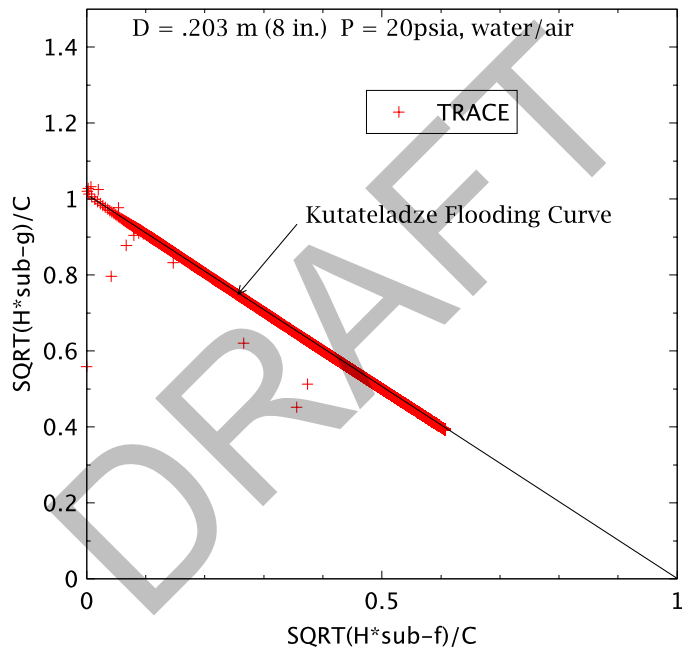

Figure A.7-7. TRACE Gas Versus Liquid Dimensionless Superficial Velocity for a .203 m (8 in.) Pipe with Water and Air at 20 psia

A.7.4. Assessment Results Summary

The assessment shows that TRACE closely calculates the Wallis correlation for a small 0.0254m (1 inch) diameter pipe and the Kutateladze CCFL correlation for a large .203 m (8 inch) diameter pipe for water/steam at low and high pressure, 0.137892 MPa (20 psia) and 4.13679 MPa (600 psia) and for water/air at low pressure, 0.137892 MPa (20 psia). It may be possible to obtain better TRACE results by modifying the input models. This will be done for the next round of assessments.

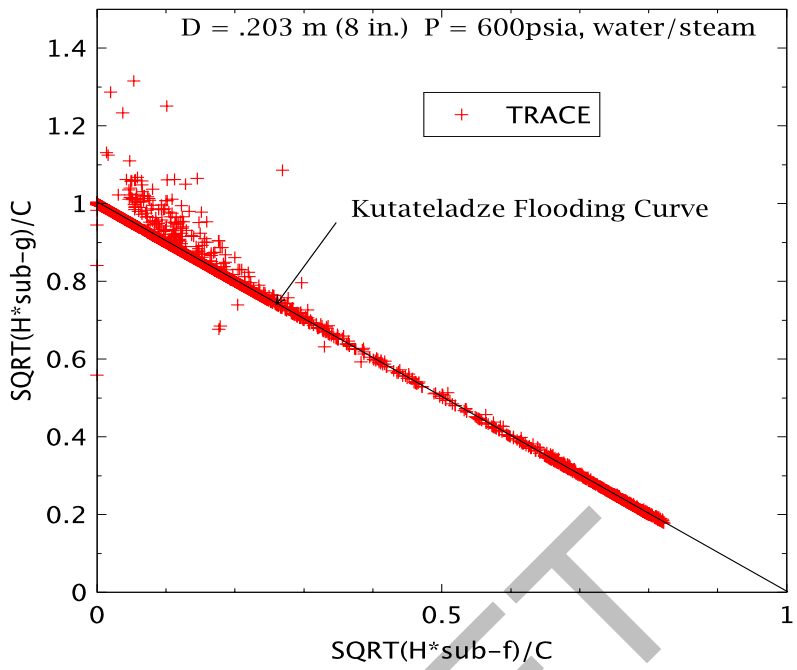

Figure A.7-8. TRACE Gas Versus Liquid Dimensionless Superficial Velocity for an .203 m (8 in.) Pipe with Water and Steam at 4.13679 MPa (600 psia)

A.7.5. References

1 J. W. Spore, et. al., TRAC-M/FORTRAN 90 (Version 3.) Theory Manual, Los Alamos National Laboratory and Pennsylvania State University, LA-UR-00-910, pp 4-5, 4-6, I-66, I-67, I-68, July 2000.

2 2 S. G. Bankoff, R. S. Tankin, M. C. Yuen and C. L. Hsieh, "Countercurrent Flow of Air/Water and Steam/Water Through a Horizontal Perforated Plate", Int. J. Heat Mass Transfer, Vol. 24, No. 8 pp 1381-1395, 1981.

3 S. G. Bankoff and S. C. Lee, "A Brief Review of Countercurrent Flooding Models Applicable to PWR Geometries", Nuclear Safety, Vol. 26, No. 2, pp 139-152, March-April 1985.

4 J. C. Lin, V. Martinez and J. W. Spore, "TRAC-PF1/MOD2 Developmental Assessment Manual", Los Alamos National Laboratory, TRAC DAM-Ver. 5.4, August 20, 1993.

A.8. CISE Adiabatic Tube

Author(s): Michael Kennedy

Affiliation: Information Systems Laboratories, Inc.

Code Version: TRACE V5.0

Platform and Operating System: Intel x86, Windows XP

A.8.1. Introduction

Drag forces between steam and water are determined by the interfacial shear models in TRACE, which are flow regime dependent. The flow regime, and resulting interfacial drag, is primarily a function of the void fraction. The CISE adiabatic pipe tests conducted by Agostini, et. al. (Refs. 1 and 2) are used in this section to assess the TRACE interfacial shear model package. In particular, steady-state adiabatic test R-291 data was simulated with TRACE and the results were compared to data. This same test case had been used previously (Ref. 3) to assess the TRAC-BD1/MOD1 code. The assessment reported in this section shows that the interfacial shear models as implemented in TRACE provide a reasonable prediction of average void fraction in the CISE vertical pipe apparatus for this adiabatic test. The comparison covers a void fraction range of 0.16 to 0.94.

A.8.2. Test Facility Description

The CISE vertical tube is 4.1 meters long and 0.081 meters in diameter. A two-phase mixture of known flowing quality was injected into the bottom of the pipe. After a steady-state condition was reached, isolation valves at the top and bottom of the test section were rapidly closed. The mass of liquid captured was measured and the void fraction determined. This procedure was repeated over a range of inlet steam and liquid flows covering a range of flow quality up to approximately 80%. The experimental data provide a relationship between void fraction and flow quality over a broad range.

A.8.3. TRACE Model Description

The TRACE input model of the CISE test apparatus consists of five components as shown in Figure A.8-1 Liquid FILL 1 and steam FILL 2 connect to TEE component 3. The side tube of the TEE is connected to the inlet of PIPE component 4, which has 11 cells. Discharge from the outlet of the pipe is to BREAK component 5, which controls the test pressure at 4.9 MPa.

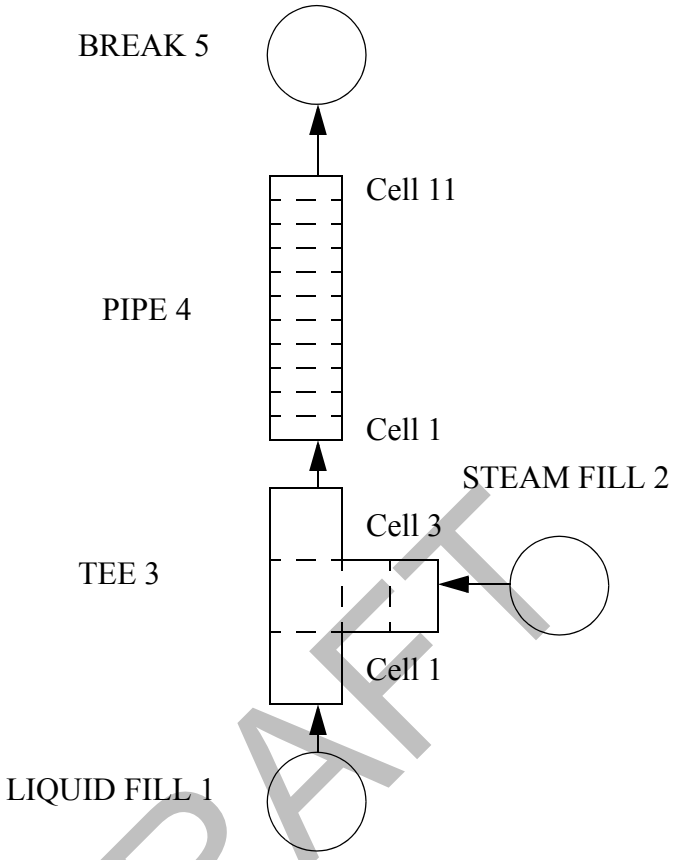

Figure A.8-1. Noding Diagram for CISE Test Apparatus

Inlet steam and liquid flows were specified by tables of inlet mass flow rate versus time to match the experiment boundary conditions. The flows were held at the measured values for nine seconds, then ramped to the next set of experimental conditions over one second. Hence all of the inlet conditions with varying flow quality were simulated in a single run. Initial conditions corresponding to those of the first boundary conditions were input to minimize the startup transient. To assure that a steady-state was reached, a steady-state null transient was run for 30 seconds to initialize the transient model.

Control systems were used to calculate the average void fraction over the 11 nodes in the test section and the flowing quality. Since it was desired to compare to the results that would be obtained with zero slip, control systems were also added to calculate the void fraction that would result in the test section under homogeneous flow conditions.

Flowing quality (x), slip ratio (S) and void fraction (α) in the test section are related by Reference 4:

$$S = \frac{x}{1-x} \cdot \frac{1-\alpha}{\alpha} \cdot \frac{\rho_l}{\rho_g} \tag{8-1}$$

Setting S equal to one and solving for α gives

$$\alpha = \frac{1}{1 + \left(\frac{1-x}{x}\right)\left(\frac{\rho_g}{\rho_l}\right)} \tag{8-2}$$

Control systems were used to calculate the void fraction that would result from homogeneous flow (slip ratio = 1.0). This value was plotted along with the TRACE calculated void fraction to show the departure from homogeneous conditions.

A.8.4. Tests Simulated with TRACE

The steam and liquid flow boundary conditions were input as a function of time to cover the range of flowing quality corresponding to the test data. Figure A.8-2 shows a plot of liquid and steam inlet flows. These inputs are boundary conditions of the analysis and determine the flowing quality. The void fraction averaged over the 11 nodes of the test section is calculated by TRACE, with the averaging done using control systems. Figure A.8-3 shows a plot of the void fraction versus quality. Also included on the plot is the void fraction that corresponds to homogeneous flow. Comparison of this plot with the TRACE results shows that the slip ratio is significantly different from one.

A.8.5. Assessment Results Summary

Experimental data are in the range $0.16 < \alpha < 0.94$. Within this range of void fraction, the assessment shows that TRACE predicts the data to within its error band, estimated to be approximately five percent based on the data scatter. Figure A.8-4 shows a comparison of predicted versus measured void fraction for the 31 data points from References 1 and 2.

This implies that the interphase drag model in TRACE is adequate in this range. The assessment for TRAC-BD1 documented in Reference 3 noted that the slip ratio predicted by TRAC-BD1 was closer to one than it should have been, particularly above 50% steam quality. While there appears to be a slight improvement in the TRACE results compared to TRAC-BD1, this same statement applies to TRACE since the TRACE predictions are above most of the data points. An exception is at low void fractions below 0.3, where the data are sparse and the void fraction is a strong function of quality.

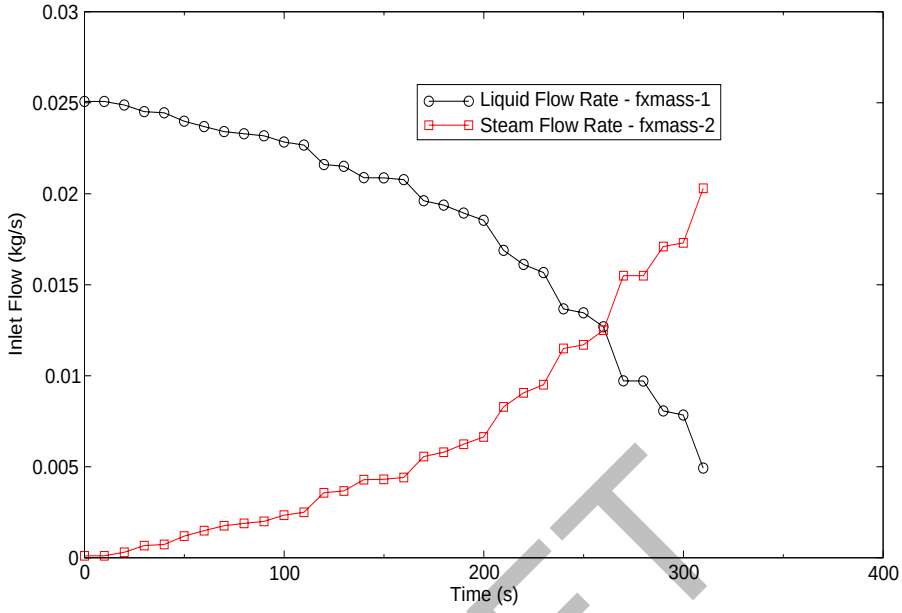

Figure A.8-2. Liquid and Steam Inlet Flows

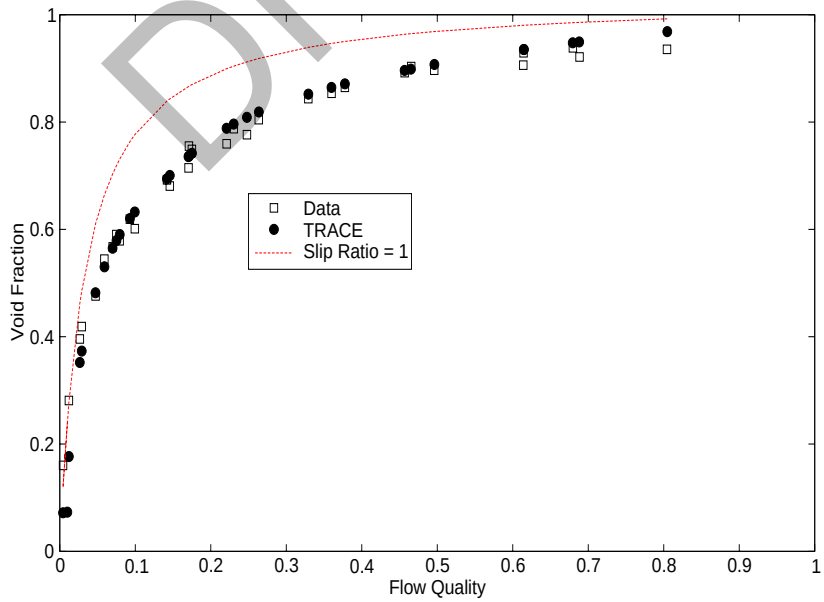

Figure A.8-3. TRACE Calculated Void Fraction Versus Quality

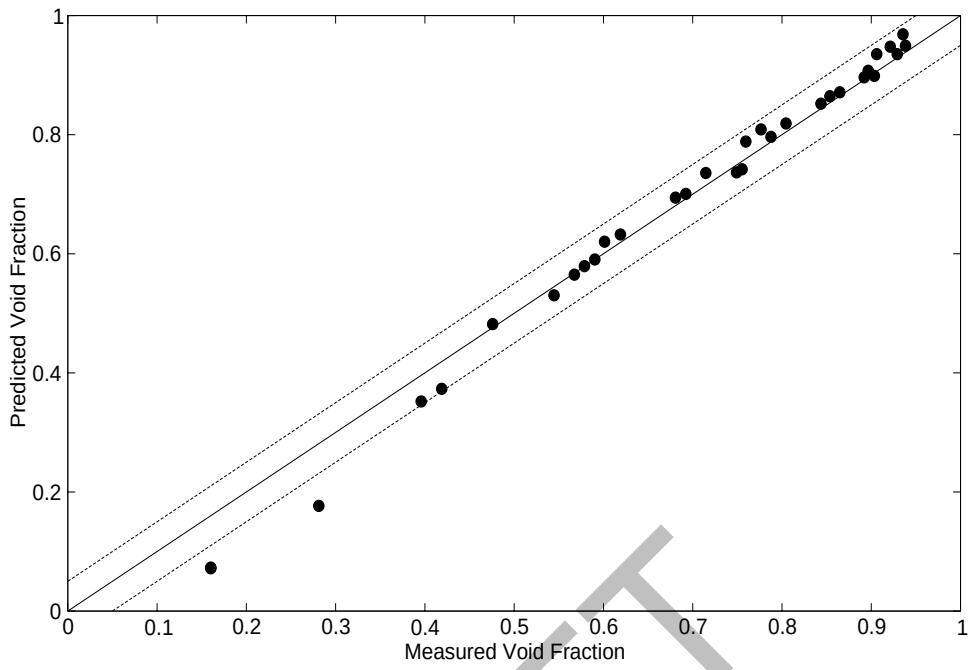

Figure A.8-4. Predicted Versus Measured Void Fraction

A.8.6. References

1 G. Agostini, A. Era and A. Premoli, "Density Measurements of Steam/Water Mixtures Flowing in a Tubular Channel Under Adiabatic and Heated Conditions", CISE-R-291, December 1969.

2 G. Agostini, A. Era and A. Premoli, "Density Measurements of Steam/Water Mixtures Flowing in a Tubular Channel Under Adiabatic and Heated Conditions", energia nucleare, vol. 18, n. 5, 1971.

3 R. W. Shumway, et. al., "TRAC-BD1/MOD1: An Advanced Best Estimate Computer Program for Boiling Water Reactor Transient Analysis, Volume 4: Developmental Assessment", NUREG/CR-3633, EGG-2294, Volume 4, August 1985.

4 L. S. Tong, "Boiling Heat Transfer and Two-Phase Flow", Robert E. Krieger Publishing Company, 1975.